Implementation and Characterization of Dynamic Genetic Networks in Vitro

THÈSE N^O 6617 (2015)

PAR

Henrike Marie NIEDERHOLTMEYER

ÉCOLE POLYTECHNIQUE
FÉDÉRALE DE LAUSANNE

Suisse
2015

Acknowledgements

This thesis would not exist without the help and support of many people.

First of all, I would like to thank Prof. Sebastian Maerkl for being a great advisor during the past 5 years, for always coming up with helpful ideas when I needed them and good discussions.

I would also like to thank my PhD committee for evaluating my work: Prof. Matthias Lütolf, Prof. Esther Amstad, Prof. Sven Panke and Prof. Kobi Benenson.

I am immensely grateful to my colleagues and collaborators who I had the opportunity to work with and learn from in different projects: our collaborators from Caltech, Prof. Richard Murray, Zachary Sun, Yutaka Hori and Enoch Yeung in the cell-free framework project (thanks Zach, Yutaka and Enoch for making this collaboration so much fun!), Viktoria Stepanova who started everything and showed me around during my first weeks at EPFL, Luis Fidalgo and José Garcia who answered endless questions about microfluidics and LabView, Kelli Xu for her work on the binary probes, Lea DeMaddalena for her work on optimizing the *E. coli* RNA polymerase, Amanda Verpoorte for her help with *E. coli* experiments. Thanks also to Matthieu Delincé for the mother machine wafer and Matti Turtola for *E. coli* RNAP proteins. And thank you to all LBNC members for being awesome colleagues and for fun times in the lab and outside the lab: Matt, Francesca, Hannes, Francesco, Ekaterina, Kristina, Luis, José, Marcel, Sylvie, JB, Nicolas, Zoe, Arun, Kelli, Lea, Holly!

And thank you so much to my friends for sharing these past 5 years in Lausanne with me and to my family for their support.

Henrike Niederholtmeyer

Lausanne, June 2, 2015.

Abstract

Transcription and translation (TX-TL) can be performed *in vitro*, outside of cells, allowing the assembly and analysis of genetic networks. This approach to engineering biological networks in a less complex and more controllable environment could one day allow rapid prototyping of network designs before implementing them in living cells. Furthermore, the *in vitro* approach provides insight into how natural biological systems are built and is instructive to define the rules for engineering biological systems from bottom up.

Despite progress in engineering TX-TL mixes for higher yields and longer synthesis times it remains challenging to implement complex genetic networks, such as oscillators, *in vitro*. The reason is that the reactions are usually performed in a batch format, where reaction products accumulate and synthesis rates decline over time.

We addressed the problems associated with batch reactions by developing a microfluidic chip with nanoliter-scale reactors that exchange reagents at dilution rates matching those of dividing bacteria. In these nano-reactors we can run TX-TL reactions in continuous mode keeping synthesis rates at constant steady state levels for more than 30h. The setup allows close control over the reaction conditions such as dilution rates and DNA template concentration, and to monitor mRNA and reporter protein levels in real time. We can test genetic programs of our choice just by adding the DNA templates coding for the desired functions. We implemented diverse regulatory mechanisms on the transcriptional, translational, and posttranslational levels, including RNA polymerases, transcriptional repression, translational activation, and proteolysis.

As a proof of concept for this reactor-based approach to engineering genetic networks we designed and implemented a novel genetic oscillator. Its network architecture consists of a positive feedback loop coupled to delayed negative feedback. Varying dilution rates and DNA template concentrations we mapped its phase diagram showing that steady state conditions were necessary to produce oscillations. The period of oscillations could be tuned by dilution rate.

To demonstrate that *in vitro* synthetic biology is useful for prototyping of dynamic genetic networks, we compared the behavior of biomolecular ring oscillators in a cell-free framework and *Escherichia coli*. Our cell-free framework combines an *E. coli* lysate TX-TL system with the nano-reactor device. We implemented and characterized the "repressilator", a three-node negative feedback oscillator *in vitro*. We then used our cell-free framework to engineer novel three-node, four-node, and five-node negative feedback architectures going from the characterization of circuit components to the rapid analysis of complete networks. We validated our cell-free approach by transferring the three-node and five-node oscillators to *E. coli*, resulting in robust and synchronized oscillations reflecting our *in vitro* observations. Our results demonstrate that comprehensive circuit characterization can be rapidly performed in a cell-free system and that these *in vitro* results have direct applicability *in vivo*.

Enabling a quantitative and more complete characterization of synthetic and natural networks, the reactor-based approach to *in vitro* synthetic biology developed in this thesis will be useful to speed up design-build-test cycles in

genetic circuit design. Furthermore it can be useful to assemble and test subsystems of a future synthetic cell and to explore whether fundamental limits exist to *in vitro* network complexity.

Zusammenfassung

Transkriptions- und Translationsprozesse können aus Zellen isoliert ablaufen. Dieses In-vitro Verfahren erlaubt die Analyse von genetischen Netzwerken in Reaktionsgefäßen unter weniger komplexen und besser kontrollierbaren Bedingungen, wo es eines Tages Forschern erlauben könnte Netzwerkprototypen zu testen, bevor diese in Zellen eingebracht werden. Außerdem bieten in-vitro Verfahren einen Einblick in den Aufbau von natürlichen biologischen Systemen und können zu Erkenntnissen beitragen, wie biologische Systeme aus isolierten Molekülen aufgebaut werden könnten.

Trotz Fortschritten bei der Entwicklung von In-vitro-Translationssystemen, die höhere Ausbeuten und längere Synthesezeiten erlauben, ist es noch immer schwierig komplexe genetische Netzwerke, wie Oszillatoren, in diesen In-vitro-Systemen zu untersuchen. Der Grund dafür ist, dass die Reaktionen meist in einem diskontinuierlichen Prozess durchgeführt werden, wobei sich Reaktionsprodukte ansammeln und Syntheseraten abnehmen.

Um dieses Problem zu lösen haben wir einen miniaturisierten Durchfluss-Reaktor-Chip entwickelt, in dem die In-vitro-Translations-Reagenzien mit Flussraten ausgetauscht werden, die den Verdünnungsraten in sich teilenden Bakterien entsprechen. In diesen Nanoreaktoren können wir Transkriptions- und Translationsreaktionen über 30 Stunden lang unter kontinuierlichen Bedingungen durchführen, welche die Syntheseraten in einem Fließgleichgewicht halten. Dabei erlaubt uns der mikrofluidische Chip die Reaktionsbedingungen genau zu kontrollieren, zum Beispiel die Verdünnungsrate und die Konzentration der Template-DNA. Zudem können wir über Fluoreszenzmikroskopie die Konzentrationen von mRNA und Reporterproteinen in Echtzeit bestimmen. In diesem System können wir genetische Programme unserer Wahl testen indem wir die Template-DNA hinzufügen, auf der die gewünschten Funktionen kodiert sind. So konnten wir verschiedene regulatorische Mechanismen untersuchen, die auf unterschiedlichen Ebenen wirkten. RNA-Polymerasen und Repressorproteine steuerten die Transkription, die Translation konnte mit Hilfe von regulatorischen RNA-Molekülen reguliert werden und posttranslational konnten wir durch gezielte Proteindegradation die Lebensdauer von Proteinen verändern.

Um zu zeigen, dass unser Reaktor für die Charakterisierung von dynamischen genetischen Netzwerken nützlich ist, implementierten wir einen neuartigen genetischen Oszillator. Seine Netzwerkstruktur bestand aus einer positiven Rückkopplung die wir mit einer verzögerten negativen Rückkopplung verknüpften. Wir untersuchten das Phasendiagramm des Oszillators, indem wir Template-DNA-Konzentrationen und Verdünnungsraten veränderten. Dabei konnten wir zeigen, dass kontinuierliche Reaktionsbedingungen notwendig waren um Oszillationen zu beobachten. Die Geschwindigkeit der Oszillationen konnte mit Hilfe der Verdünnungsrate eingestellt werden.

Um einen Nutzen für die Biotechnologie zu haben, müssen In-vitro-Systeme bei der Analyse von biologischen Netzwerken relevante Ergebnisse für zelluläre Systeme liefern. Um dieses zu testen untersuchten wir molekulare Ringoszillatoren in unserem zellfreien System und in *Escherichia coli*. Zuerst charakterisierten wir den „Repressilator", ein Oszillatornetzwerk aus drei Repressorproteinen. Daraufhin entwickelten und testeten wir neue zyklische Netzwerke

mit drei, vier und fünf Knoten aus weiteren Repressoren, die wir zunächst isoliert charakterisierten. Eine Analyse unserer neuen Ringoszillatoren aus drei und fünf Invertern in *E. coli*, wo diese regelmäßige und synchronisierte Oszillationen zeigten, bestätigte unsere in-vitro Beobachtungen. Unsere Ergebnisse zeigen, dass umfassende Analysen von genetischen Netzwerken in zellfreien Systemen möglich sind und dass deren Ergebnisse direkte Relevanz für zelluläre Systeme haben.

In-vitro-Systeme erlauben quantitative und vollständigere Analysen von synthetischen und natürlichen Netzwerken. Der Reaktor-basierte Ansatz für die in-vitro Analyse von biologischen Netzwerken, der in dieser Arbeit entwickelt wurde, wird von Nutzen für die synthetische Biologie sein um Netzwerkprototypen zu erproben. Außerdem könnte er es erlauben die molekularen Grundfunktionen einer zukünftigen künstlichen Zelle aufzubauen und zu testen und zu erforschen wo die Grenzen der Komplexität von biologischen Netzwerken außerhalb von Zellen liegen.

Stichwörter

Zellfreie Transkription und Translation, *In-vitro* synthetische Biologie, Genetische Netzwerke, Oszillatoren, Mikrofluidik, Fluoreszenzmarker für mRNA

Contents

List of Figures

Chapter 1 Introduction

1.1 *In vitro* synthetic biology

Synthetic biology uses engineering principles to facilitate the creation of novel biological functions and systems. The field has been rapidly growing since 15 years when the first artificial genetic devices, the toggle switch[1] and the repressilator[2], were constructed in the bacterium *Escherichia coli*. Since then, many more potentially useful genetic circuits have been built such as switches, oscillators, logic gates, filters, sensors and devices for cell-cell communication[3]. Facilitated by DNA synthesis technologies, progress in parts characterization, standardization and modularization, and growing databases of sequences coding for novel biosynthesis pathways and genetic regulators, synthetic biology has the potential to have a major impact on human health, energy and the way we interact with our environment. However, despite many promising achievements, the complexity of synthetic systems is still far from that of natural biological systems and the engineering process remains challenging[4]. Many parts are not sufficiently well characterized, behave unpredictably under changed conditions and depend strongly on their host because of unintended interactions with natural cellular processes. Even when parts are well characterized and function reliably separately, they often do not behave in the expected way when they are assembled into larger devices or systems requiring laborious tweaking of expression strengths to achieve the desired behavior. This not very rational testing and construction process can become prohibitively time-consuming and expensive for more complex systems. *In silico* models can help to identify targets that will have the greatest effects on the system's performance but are often incomplete and provide only qualitative insights. Another problem is that functioning of the synthetic circuits is linked to viability of their cellular host. Toxicity and loading effects are common and lead to failure of the synthetic circuit or unpredictable results [5]. In short, many problems of synthetic circuits arise because their cellular hosts are insufficiently characterized and interactions are far too complex to be quantitatively modeled.

In vitro, cell-free systems have the advantage that this complexity is reduced facilitating a thorough and quantitative characterization of the system. In fact, a large portion of the knowledge about the molecular mechanisms of processes in cells, such as metabolism, replication, transcription and translation derives from biochemistry studies looking at single enzymes or larger molecular assemblies in isolation. Similarly, *in vitro* synthetic biology aims at isolating specific biological phenomena of interest or to re-create them from natural or unnatural parts in a test tube.

This is interesting from a fundamental research point of view because it allows testing if one's knowledge about the necessary components of a system is complete. Examples of this idea include reconstitution of the bacterial Min system self-organizing into surface waves on membranes *in vitro*[6] and reconstitution of the bacterial transcription[7] and translation [8] machineries. *In vitro*, hypotheses can be tested more rapidly because measurements and perturbations are easier in cell-free systems. *In vitro* systems allow experiments that would be difficult or impossible *in vivo* as they do not require host viability and are not confined in cellular boundaries. For example, the optimization of a metabolic network for synthesis of a fine chemical showed how extensive measurements and perturbations can lead to enhanced understanding of a system and ultimately to improved yields[9]. In addition to facilitating measurements and

perturbations, *in vitro* systems can be sufficiently simple to allow complete and quantitative models, for example of the transcription and translation reactions[10,11], and of dynamic reaction networks [12-15]. Re-creating systems from unnatural building blocks can provide insights on how the architecture of a network influences system behavior un-obscured by the specific properties of the natural components. Examples for this included implementation of a genetic network emulating embryonic pattern formation in an artificial spatially structured environment[16], predator-prey dynamics re-created from a DNA-based reaction network[14] and the study of genetic regulatory networks by constructing oscillators and switches in simplified environments, which will be discussed in more detail below.

One ambitious long-term goal of *in vitro* synthetic biology is to assemble an artificial cell-like structure from the bottom-up using well-characterized building blocks, which would be a major advance in elucidating the fundamental mechanisms of life. As progress in this direction many studies have shown interactions between cytoskeletal proteins and membranes, which may be harnessed to reconstitute a division machinery of an artificial cell. For example, the bacterial Min system self-organizes on membranes [6], actin bundles could be anchored to the membranes of vesicles [17], contractile FtsZ rings were reconstituted in liposomes [18], and microtubules and molecular motors induce shape changes of lipid vesicles [19]. Although a combination of all fundamental processes an artificial cell would need to perform[20] is still far out of reach, progress has been made towards reconstituting other sub-systems like DNA replication[21], the transcription[7] and translation machinery[8], and a simple metabolism[22].

Although a well-understood cell-like hybrid of biological and synthetic materials might have applications for interfacing between living and non-living materials, as a biosensor, for therapeutics or synthesis of biopolymers [20,23], *in vitro* systems also have other, more immediate applications. They can, for example, be used to synthesize fine chemicals that are difficult to produce synthetically [24-27]. They can also be used to produce proteins that are difficult to produce in living cells such as proteins that contain non-natural amino acids[28] or that are medically relevant [29,30] or libraries of proteins for screening purposes[31,32]. Recently, *in vitro* systems have also begun to attract attention for rapid prototyping of genetic parts[33,34], simple genetic networks[35] and metabolic pathways[9] for *in vivo* implementation.

1.2   Genetic networks *in vitro*

In vitro systems provide a simplified environment to study genetic networks, which allows analysis of network architectures and parameter spaces that give rise to certain dynamic phenomena. Of interest are for example bistable switches and molecular memory, sensory systems such as fold-change detectors, and networks that generate spatial patterns or oscillations. These phenomena are interesting from a purely theoretical point of view and because they are important in biology. Bistability for example allows switching between states in the life cycle of the phage lambda, in the *E. coli lac* operon and in cell cycle progression[36]. Fold-change detection can be found in the molecular mechanism for bacterial chemotaxis[37]. Pattern formation is important in development [14,38] and oscillating networks control the circadian rhythm, cell divisions, signaling and metabolic systems[39].

All the above-mentioned dynamic phenomena have been re-created in biochemically simple *in vitro* systems relying on the synthesis, hybridization and degradation of nucleic acids. The *in vitro* transcriptional circuits developed by Erik Winfree's group use synthetic DNA molecules that undergo hybridization reactions and can be transcribed into short RNA sequences, which then in turn activate or inactivate switches by hybridizing with complementary DNA strands. This system has been used to build transcriptional oscillators[12,40], a bistable circuit[41] and a fold-change detector [37]. Another, similarly simple system is the DNA toolbox[42], which uses DNA hybridization, polymerization and degradation reactions to construct dynamic reaction networks generating oscillations[13], switchable memories[15] and

spatio-temporal patterns[14,38]. The above examples show that these simple, artificial systems based on nucleic acid chemistry can be used to study wide varieties of dynamic reaction networks. The reactions are sufficiently simple to allow quantitative models and to allow the reactions to remain in a far-from-equilibrium state for hours, allowing complex dynamics.

Despite the advantages of their simplicity purely nucleic acid based systems are too artificial for some questions. For more immediate relevance for *in vivo* systems it is advantageous to study true genetic networks that are based on transcription and translation reactions and involve natural genetic regulators. *In vitro* transcription and translation (TX-TL) reaction mixes have been developed for cell-free protein synthesis and can produce large amounts of product. Depending on the application or the protein of interest one can choose between lysates from different origins (the most popular ones are *E. coli*, wheat germ and rabbit reticulocytes) containing the native biosynthetic machinery of that organism[43]. A different interesting system in the commercially available PURE system, a minimal, defined reaction mix, which consists of the reconstituted translation machinery of *E. coli*[8]. The PURE system has the advantage that all its components and their concentrations are known. This makes it interesting for bottom-up synthetic biology because it is not a "black box" unlike a lysate system, which essentially contains all the proteins present in the cytoplasm of the strain that was used to prepare the extract. Use of this defined, minimal system also eliminates unwanted side reactions that consume energy and precursors. Disadvantages of the PURE system are its rather high cost, lower yields and shorter synthesis times compared to many extract systems. For efficient transcription most TX-TL reaction mixes contain a phage RNA polymerase but lysates can also be prepared by methods preserving the activity of the native *E. coli* polymerase[44], which makes them interesting for *in vitro* synthetic biology and rapid prototyping[33,45]. In order to achieve transcription from native *E. coli* promoters in the PURE system it is possible to supplement the reaction with a purified *E. coli* RNA polymerase holoenzyme [7] but this generally results in low transcription rates. Quantitative models of the transcription and translation processes exist for both lysate-based systems[10] and the PURE system[11].

More than ten years ago, Noireaux and Libchaber built the first cell-free genetic networks [46]. Their networks were mainly activation cascades, where the output of one stage acted on the expression of the next stage. This study showed that it was generally possible to build genetic networks of considerable size (up to three expressed genes) but also showed important limitations of the system. The authors observed that each new stage decreased the output by at least an order of magnitude and pointed out loading effects on the translational machinery due to the accumulation of transcripts[46]. Other early examples of *in vitro* genetic networks were a short cascading network in lioposomes[47] and a simplified network emulating pattern formation in *Drosophila* development[16]. Later cell-free genetic networks also incorporated specialized genetic control such as RNAi to build a two-input logic gate[48]. With advances in the preparation of efficient TX-TL reagents network sizes became larger [45] but examples of positive and negative feedback remained basic. Simple negative feedback was achieved with TetR and LacI repressors reducing their own expression and by sigma factor 28 competition for the *E. coli* RNA polymerase core enzyme [35,45]. A simple positive feedback loop was constructed from T7 RNA polymerase activating its own transcription[49]. *In vitro* genetic networks have been limited in circuit size and capabilities in feedback regulation because transcription and translation rates decline over time as reaction products accumulate and precursors are consumed. Especially the accumulation of reaction products makes it difficult to implement dynamic genetic networks such oscillators and switches that rely on negative feedback because regulators from earlier stages in the network will never be removed. In order to increase mRNA and protein turnover in TX-TL reactions active degradation mechanisms have been implemented[50] and reaction times could be increased by placing the reaction in specialized reactors and "feeding" it with precursor molecules [51-55]. A continuous

reaction would simultaneously solve both problems associated with genetic networks in TX-TL reactions, deceasing synthesis rates and accumulation of reaction products, but requires specialized technology.

1.3   Aims and overview of this thesis

Motivated by the power of cell-free systems for quantitative and extensive analyses of biological systems we aimed to study dynamic genetic networks *in vitro*. In the beginning of this research project, no dynamic genetic network, such as an oscillator, had been implemented in a cell-free environment. This thesis aimed to develop technologies for the implementation and quantitative characterization of dynamic genetic networks *in vitro*, and to demonstrate how these tools can be used for basic and applied research.

Most regulators used to build genetic networks act on the initiation of transcription. Frequently, however, the mRNA intermediate of the TX-TL reaction is not determined. For a quantitative understanding and rational engineering of genetic networks we needed a method to measure and follow mRNA concentrations during TX-TL reactions. Chapter 2 describes the development of binary FRET probes and a complementary mRNA target site for real-time measurement of mRNA concentrations *in vitro*. We used this method to characterize transcription and mRNA degradation rates, resulting in a quantitative description of mRNA dynamics in the PURE system.

Chapter 3 describes how we addressed the issues of performing TX-TL reactions in batch format, where reaction products accumulate and synthesis rates decline over time. We developed a microfluidic nano-reactor device that exchanges reagents at dilution rates matching those of dividing bacteria to keep TX-TL reactions at steady state. I will show how we used this reactor-based approach to characterize diverse genetic regulatory mechanisms, and to implement the first genetic oscillator in a TX-TL reaction demonstrating that continuous conditions allow the analysis of the operating regimes of dynamic genetic networks *in vitro*.

To be of significance to biological engineering for the prototyping of genetic networks, it is critical that synthetic circuits behave similarly in cells and in cell-free environments. Chapter 4 will describe a cell-free framework for biological systems engineering, and demonstrate that genetic networks can be rapidly characterized and engineered *in vitro* with direct relevance for *in vivo* systems. We characterized the repressilator network[2] *in vitro* and engineered novel three-node, four-node, and five-node negative feedback architectures. We then transferred the novel three- and five-node oscillators to *E. coli*, where we observed similar robust oscillations like in the *in vitro* system showing that cell-free synthetic biology has the potential to drastically speed up design-build-test cycles in biological engineering.

Finally, in chapter 5 I will briefly summarize and discuss the results of this work pointing out limitations and how those could be addressed in the future. An outlook will describe possible applications of the technologies developed in this thesis.

Chapter 2 Real-Time mRNA Measurement during an *in Vitro* Transcription and Translation Reaction Using Binary Probes

2.1   Abstract

In vitro transcription and translation reactions have become popular for a bottom-up approach to synthetic biology. Concentrations of the mRNA intermediate are rarely determined although knowledge of synthesis and degradation rates could facilitate rational engineering of *in vitro* systems. We designed binary probes to measure mRNA dynamics during cell-free protein synthesis by fluorescence resonance energy transfer. We tested different mRNA variants and show that the location and sequence environment of the probe target sites are important parameters for probe association kinetics and output signal. Best suited for sensitive real-time quantitation of mRNA was a target site located in the 3' untranslated region, which we designed to reduce secondary structure. We used this probe – target pair to refine our knowledge of mRNA dynamics in the commercially available PURE cell-free protein synthesis system and characterized the effect of TetR repressor on mRNA synthesis rates from a T7 promoter.

2.2   Introduction

In vitro transcription and translation (ITT) reactions have been widely used and optimized for protein synthesis and screening purposes [31,52]. More recently, those *in vitro* systems have become popular for a bottom-up approach to synthetic biology [46]. Fundamental molecular processes of life were reconstituted *in vitro*, such as the *E. coli* translation machinery from purified components [8] and the *E. coli* RNA polymerase holoenzyme, which was synthesized by adding the DNA templates for the subunits of the enzyme complex into an ITT reaction [7]. Examples for structural self-organization that could be reconstituted in ITT reactions programmed with DNA templates include the synthesis and assembly of the T7 bacteriophage [56], the self-assembly of cytoskeletal structures in liposomes [57] and emulating embryonic pattern formation [16]. The dynamics and behavior of synthetic gene networks have also been studied in ITT reactions. Multi-stage cascades, where the gene product of one stage is the input for the next stage, AND gates, and negative feedback loops have been assembled [35,45-47]. All genetic regulators, activators, and repressors, employed in these genetic networks acted on the initiation of mRNA synthesis. Furthermore, Shin and Noireaux have established a method to increase mRNA turnover and propose that active mRNA degradation might facilitate the engineering of dynamic genetic networks [50]. Despite their focus on regulation of mRNA synthesis and mRNA degradation these studies only used reporter protein production as their readout. To rationally assemble and characterize *in vitro* genetic networks it would be helpful to directly quantitate mRNA dynamics and synthesis rates. After all, it is this intermediate

that regulation acts upon most often and whose concentration determines protein output, often in a non-linear fashion as the translation machinery becomes saturated at high concentrations of mRNA [46].

RNA concentrations can be determined by different techniques *in vivo* and *in vitro*. Potential real-time methods that can detect a specific mRNA employ fluorophores that bind to a region of the mRNA of interest, which changes their emission properties. Examples include "spinach" [58] and oligonucleotide probes like molecular beacons and binary probes [59,60]. Binary probes consist of two DNA oligonucleotides that hybridize to adjacent locations on a target sequence. Each carries a fluorophore of a fluorescence resonance energy transfer (FRET) donor – acceptor pair. When both probes are bound to the target sequence the fluorophores are brought in close proximity so that FRET can occur. This technique has been used to measure mRNA synthesis during *in vitro* transcription [61]. Models of the transcription and translation processes during GFP synthesis were important steps towards a more quantitative understanding of the dynamics of protein synthesis in cell-free systems [10,11]. These studies also measured mRNA levels over time to take into account synthesis and degradation of mRNA for their models. Stögbauer et al. [11] used a molecular beacon, which bound to a sequence in the GFP coding region on the mRNA.

In this work we designed binary probes, which we tested in combination with different mRNA target designs in order to derive a probe – target pair that allows sensitive real-time quantitation in ITT reactions and could be used for other genes without the need for sequence re-design. We demonstrate the value of the probes as a tool for *in vitro* synthetic biology by refining our understanding of RNA dynamics in the PURE ITT system [8] and measuring the effect of the TetR repressor on mRNA synthesis from a T7$_{tet}$ promoter.

2.3   Results and discussion

We decided to place the probe target site, the nucleotide sequence to which the binary probes bind, outside of the protein coding region, either in the 5' or 3' un-translated region (UTR), in order to avoid interference between probe binding and translating ribosomes. This has the additional advantage that the same probe – target combination could be used for other genes without requiring a different set of costly FRET probes and re-optimization of the target sequence. Similar to previous probe designs [61,62], we chose a sequence of 30 bp as the target for the two probes, which consisted of 15 bp each. We chose Cy3 and Cy5 fluorophores as our FRET pair, with a spacing of 4 nucleotides, or about 1.65 nm, for optimal FRET efficiency [59] (Figure 2.1).
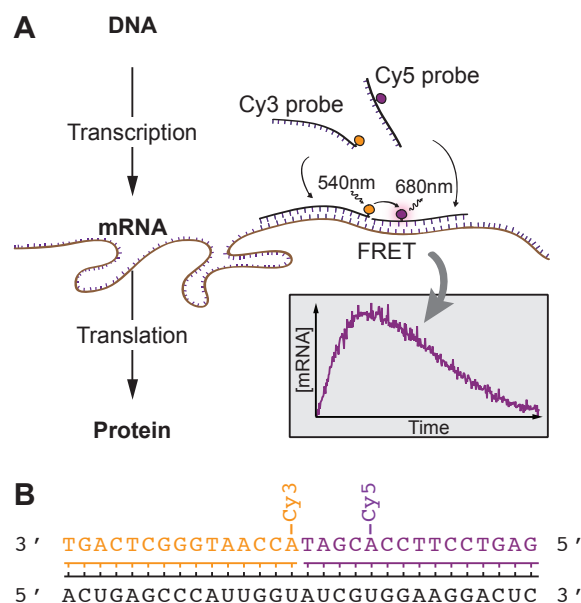
Figure 2.1 Design of the binary probes and their target sequence.
(A) Real-time measurement of mRNA during *in vitro* transcription and translation. A mRNA with the target site for the binary probes and the coding region for the protein is produced from a DNA template. The binary probes carrying either a Cy3 or Cy5 fluorophore are present in the ITT mix and hybridize to the RNA. This brings the donor and acceptor fluorophores in close proximity so that FRET can occur. The FRET fluorescence allows quantification of mRNA concentration over time. (B) Sequences of the RNA target (black) and the bound probes with positions of the fluorophores.

We found that the sequence environment of the target site on the mRNA has a strong influence on the observed FRET signal. We thus synthesized different mRNAs *in vitro*, purified them and compared binding of the binary probes to identical target concentrations. In the different mRNAs tested the probe target site was placed either in the 5' or the 3' UTR (Figure 2.2**a**). We tested one mRNA with the target site in the 5' UTR and three mRNAs with the target site in the 3'UTR. Those differed in the distance of the target site to the stop codon (3' target version 1 compared to versions 2 and 3) and the stability of the secondary structure that could be formed by the nucleotides surrounding the target sequence, which was minimized in version 3 by adding stretches of adenines around the target site (see **Table S2.1**).

We observed a stable FRET signal over 12h when the probes were added to a DNA target in buffer (Figure 2.2**b**), showing that no photo-bleaching occurred under the imaging conditions employed. All mRNAs, except for the negative control without a target sequence, produced measureable FRET signals and EGFP protein, when added to ITT mix (Figure 2.2**d**). The binding kinetics and the maximal FRET signals differed considerably for the different target variants tested in both buffer (Figure 2.2**b**) and ITT mix (Figure 2.2**c**), which we attribute to mRNA secondary structure and degradation. When the target site was located on mRNA, hybridization of the probes was slower than to the DNA target. The 5'UTR target gave rise to the slowest binding kinetics and lowest FRET signal. The mRNAs with the target site in the 3'UTR exhibited faster association kinetics and higher FRET signals, indicating that mRNA secondary structure and target site location are important parameters (see **Table S2.1**). The fastest binding kinetics and highest FRET signal was observed for the 3'UTR with the sequence that was specifically optimized to reduce secondary structure in the nucleotides surrounding the 30bp target sequence. It was our goal to have a sensitive real-time measurement of mRNA during *in vitro* protein synthesis, so for all subsequent experiments we used the 3' UTR version 3. In addition, this 3'UTR also increased protein production probably by altering the secondary structure of the mRNA (Figure 2.2**d, Table S2.1**).
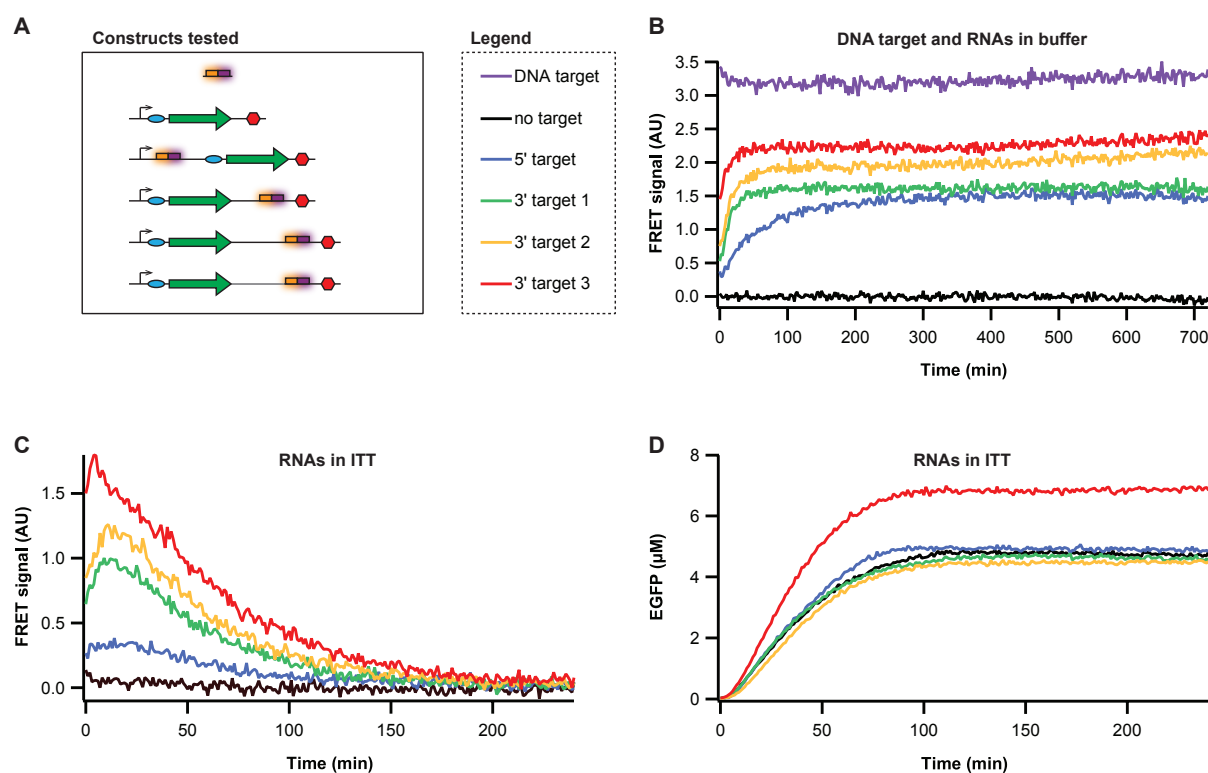
Figure 2.2 Effect of the sequence environment of the target site on hybridization kinetics and FRET signal.
(A) Schematics of the different DNAs and RNAs that were compared for probe binding. The DNA target was the 30 bp complementary sequence to the probes. The mRNAs were produced by *in vitro* transcription with T7 RNA polymerase and all contained the same EGFP coding region and ribosomal binding site (RBS). They differed in the position and the sequence around the target site located in the 5' or 3' UTR. The colored lines representing the bound probes indicate position of the target site. (B,C) Hybridization of the binary probes (each at 1µM) to DNA or mRNA target (all at 480nM) in buffer (B) or ITT mix (C). FRET signal was calculated by normalizing the FRET fluorescence to the Cy5 fluorescence and subtracting the FRET background from a reaction containing no RNA or DNA (see Methods for details). (D) EGFP signal produced by the reaction in (C).

During synthesis of mRNA from the different DNA templates (Figure 2.2**a**), the 3' target 3 also gave rise to the highest FRET signal when tested in a transcription reaction (**Figure S2.1**) as well as in an ITT reaction (**Figure S2.2**). Although different concentrations of mRNA were synthesized, these differences could not explain the differences in signal. When the FRET signal in a transcription or an ITT reaction was normalized by mRNA concentration, 3' target 3 showed the highest signal (**Figures S2.1 and S2.2**), which shows that during synthesis of mRNA, probe hybridization kinetics are important for sensitivity. When identical concentrations of purified mRNA were added into an ITT reaction we observed the same dependence of hybridization kinetics and FRET signal on target site position as in buffer, but here the FRET signal declined exponentially after reaching a peak at about 20 min (Figure 2.2**c**). We attributed this decline to mRNA degradation. We verified by qRT-PCR that mRNA degradation was indeed occurring at a comparable rate as determined by our FRET probes (Figure 2.3). Degradation of mRNA follows first order kinetics [10,50]. This exponential decay can be described by the following function:

$$(1) \qquad m(t) = m_0 \cdot e^{-\deg_m \cdot t},$$

where m_0 is the initial mRNA concentration and $\deg_m$ the mRNA degradation rate.

Known amounts of mRNA were added to ITT mix containing an excess amount of binary probes (1µM). The decreasing FRET signals of different initial mRNA concentrations (250 to 900 nM, starting at 40 min, see **Figure S2.3**)

were fitted to equation (1) and the RNA degradation rate was determined to be 0.0085 ± 0.0019 min^{-1}, which is 10-fold greater than the value reported for the PURE system in a previous study [11], where mRNA degradation had not been observed experimentally but was determined by fitting a model with eight free parameters to the experimental data.
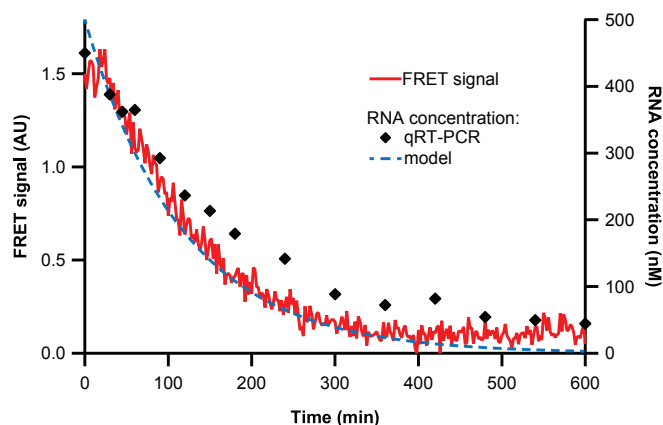
Figure 2.3 Degradation of mRNA in the PURE ITT mix.
Degradation of 500 nM mRNA in ITT mix as observed by qRT-PCR and FRET signal. The experimental results are compared to the predicted RNA concentration for a degradation rate of 0.0085 min^{-1}.

In order to calibrate the FRET signal to mRNA concentration we used the peak FRET signal of different mRNA concentrations (average of signal from 10 to 30 min) and plotted this against the mRNA concentration at 20 min, which was calculated from the known initial concentration and the RNA degradation rate. The FRET signal increased linearly with mRNA concentration until mRNA concentration exceeded probe concentration (Figure 2.4). At a probe concentration of 1 µM we could detect mRNA concentrations ranging from 50 to 900 nM. At mRNA concentrations below 50 nM the signal to noise ratio was too low to allow a reliable quantitation under our experimental conditions.
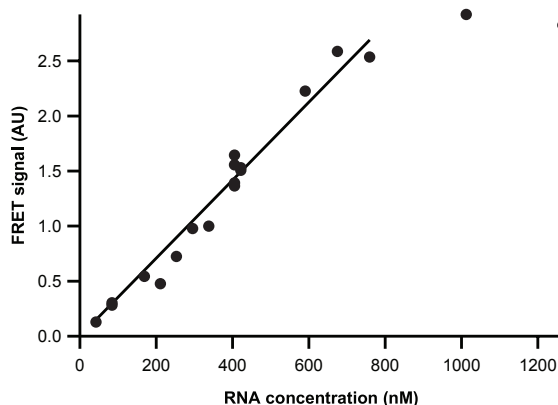
Figure 2.4 Calibration of the FRET signal to mRNA concentration.
The peak FRET signal around 20 min (average of signal between 10 and 30 min) was plotted against the RNA concentration at 20 min, which was calculated from the known initial mRNA concentration using the determined degradation rate. For mRNA concentrations smaller than probe concentration (1µM) the FRET signal increased linearly with a slope of 0.0035 nM^{-1}.

Using the calibration of the FRET signal we could quantitate mRNA synthesis from a DNA template. The mRNA synthesis rate depended on the DNA template concentration used in the ITT reaction (Figure 2.5**a**). Although the mRNA concentrations differed more than threefold over the range of DNA template concentration tested, the effect on

EGFP concentration was low, showing that the translation machinery became saturated above 200 nM of mRNA (see **Figures S2.3b** and **S2.4b**). The mRNA measurement determined from the FRET signal was confirmed by qRT-PCR for the highest DNA template concentration (Figure 2.5**a**).

The change in mRNA concentration, m, can be described by the following differential equation:

(2) $\qquad m'(t) = syn(d) - \deg_m \cdot m(t)$

The transcriptional activity, syn(d), is a function of the DNA concentration, d. We assume DNA concentration to be constant, which is a fair approximation as the DNA template decays very slowly and retains full functionality until up to 6h into the ITT reaction (**Figure S2.7**). The degradation rate of mRNA, deg$_m$, we previously determined. With m(0)=0, the solution of equation (2) for a given DNA template concentration is:

(3) $\qquad m(t) = \dfrac{syn(d)}{\deg_m} \cdot (1 - e^{-\deg_m \cdot t})$

To determine initial transcription rates the mRNA concentrations of the different DNA template concentrations during the first 100 min of the reaction were fitted to equation 3 (**Figure S4a**) and plotted against DNA concentration (Figure 2.5**b**). Transcription can be described by Michaelis-Menten kinetics:

(4) $\qquad syn(d) = \dfrac{v_{max} \cdot d}{K_{TS} + d}$

By fitting equation 4 the maximum transcription rate, v$_{max}$, was determined to be 10.4 nM/min and the DNA concentration for half-maximal transcription rate, K$_{TS}$, was 4.4 nM (Figure 2.5**b**). Both values were in good agreement with values reported by Stögbauer et al. using the same ITT mix [11].

To be able to describe the complete reaction, we have to take into account a decrease of transcriptional activity because the process consumes substrates and enzymes can degrade. If there was no decrease of transcriptional activity, the mRNA concentration would reach a steady state when mRNA synthesis and degradation are balanced (**Figure S2.5**). The fact that mRNA concentration decreases after reaching a maximum at about two to three hours suggests that the transcriptional activity decreases. In contrast to Stögbauer et al. [11], we did not observe a clear dependence of the time when RNA synthesis ceases on the DNA concentration (Figure 2.5**a**). At this point we did not want to make any assumptions on the mode by which transcriptional activity decreases, so we introduced the relative activity, act(t), as the fraction of initial transcriptional activity at time t.

(5) $\qquad m'(t) = act(t) \cdot syn(d) - \deg_m \cdot m(t)$

Using Euler's method mRNA concentration over time can be approximated with:

(6) $\qquad m(t + \Delta t) = m(t) + \big(act(t) \cdot syn(d) - \deg_m \cdot m(t) \big) \cdot \Delta t$

(7) $\qquad act(t) = \dfrac{m(t + \Delta t) - m(t) + \deg_m \cdot m(t) \cdot \Delta t}{\Delta t \cdot syn(d)}$

Using equation 7 and the experimental results for mRNA concentration, we calculated the relative transcriptional activity comparing two time points with a fixed time increment of Δt over the course of the ITT reaction (Figure 2.5c). For all DNA template concentrations the relative transcriptional activity followed a sigmoidal curve. For the first hour it remained at its initial rate and then decreased to 0 after about eight hours (Figure 2.5c, **Figure S2.6**). Interestingly, the transcription rate started to decrease when EGFP synthesis started to plateau. It has been shown that a decrease in energy charge caused by the hydrolysis of nucleoside tri- and diphosphates is the limiting factor for cell-free protein synthesis reactions [8,46]. Translation is the main contributor to this decrease in energy charge [63]. Transcription, however, also requires nucleoside triphosphates, which could explain why protein and mRNA synthesis cease at the same time. The relative mRNA synthesis activities were fitted by a Hill function:

$$(8) \qquad act(t) = 1 - \frac{1}{1 + \left(\dfrac{t_{half}}{t}\right)^n}$$

For neither the time of half-maximal activity, t_{half}, or the Hill coefficient, n, which determines the steepness of the activity decline, a dependence on DNA concentration could be observed (**Figure S2.6**). The average of t_{half} was 203±13 min and 2.9±0.7 for n (black line in Figure 2.5c). With this, equation 5 could predict mRNA concentration over the complete reaction time of 12 hours for different DNA template concentrations (Figure 2.5d). We also show that the decrease in transcriptional activity could not be explained by a degradation of the DNA templates, which degrade at a much slower rate (**Figure S2.7**).
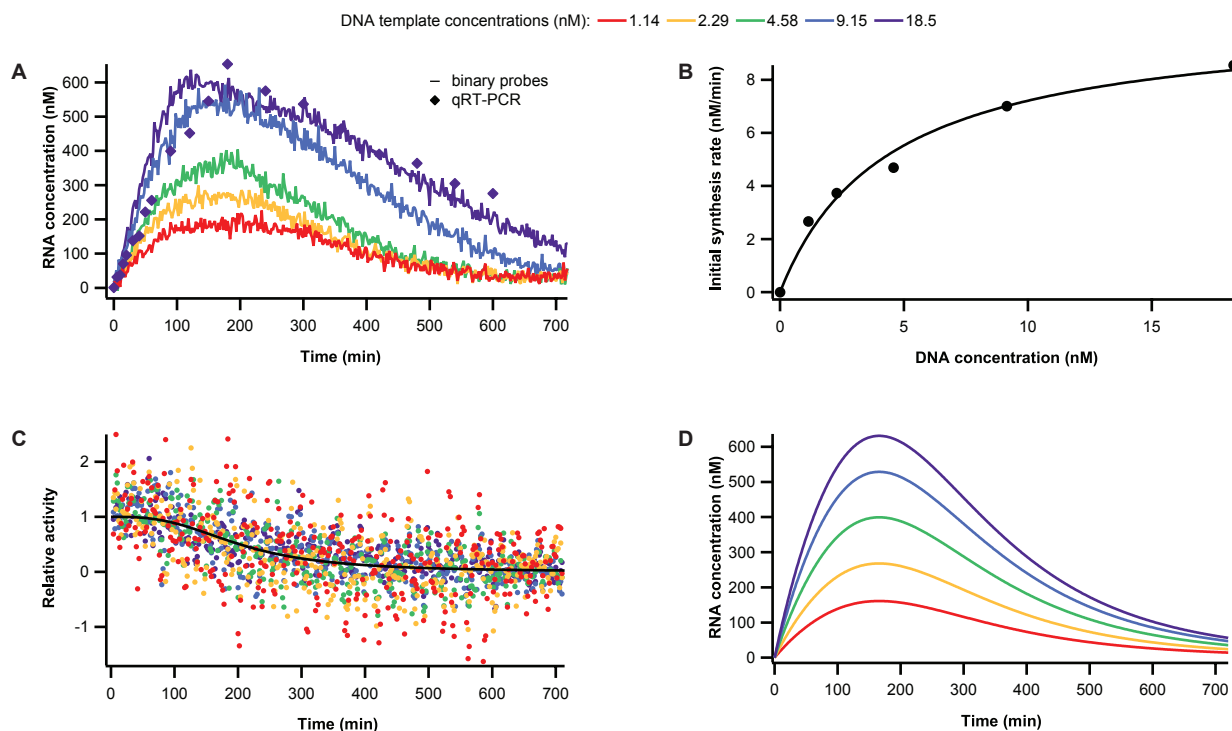
Figure 2.5 RNA synthesis from different DNA template concentrations during ITT.
(A) RNA concentrations during synthesis from different template concentrations in ITT, measured by binary probes and qRT-PCR. (B) Initial mRNA synthesis rates for different DNA template concentrations. Initial rates were determined from the first 100 min of synthesis assuming no decline of transcriptional activity. (C) Relative transcriptional activity over time during synthesis from different DNA template concentrations. Relative activity was determined with equation 7 from the concentration change during a time increment of 6 min. To reduce the noise we used the average of 3 measurements (corresponding to 6 min) around each time point. With the known mRNA degradation and initial synthesis rate we could calculate what fraction of initial activity was left at each time point. The black line is the Hill function (equation 8), which was used to fit the results (see Supporting Figure S4). (D) Results of our model of mRNA dynamics in ITT at different DNA template concentrations. The model took into account mRNA degradation and a transcription rate, which is dependent on the DNA template concentration (B) and time (C).

Regulators in genetic networks often act by modulating transcription. A number of transcriptional activators and repressors have been used to build *in vitro* networks [35,45-47]. In ITT reactions their effect has, to our knowledge, only been studied as output of a reporter protein product. For a rational design of *in vitro* networks it would however be useful to study the effect on mRNA synthesis directly. We applied our method of real-time mRNA measurement to the repression of a T7 promoter by TetR. Instead of the standard T7 promoter used to drive expression in the previous experiments, the $T7_{tet}$ promoter included the TetR operator sequence downstream of the T7 promoter. This promoter had been previously shown to be repressible by TetR in *Leishmania* [64]. Purified TetR protein was added at different concentrations to the ITT reaction and a dependence of mRNA synthesis rate and EGFP output on TetR concentration was observed (Figure 2.6 and **Figure S2.8**). 1000 nM of TetR inhibited transcription almost 5-fold while the control reactions with the standard T7 promoter without a TetR binding site remained unaffected (Figure 2.6**c**). The maximum transcription rate syn_{max} (4.9 nM/min), the TetR concentration for half-maximal repression (368 nM), Km, and the Hill coefficient (1.2) were determined by fitting a Hill function (Figure 2.6**c**):

$$(9) \qquad syn([\text{TetR}]) = \frac{syn_{max} \cdot Km^n}{Km^n + [\text{TetR}]^n}$$

The Km we observed is substantially higher than the affinity of TetR to its operator, which was determined to be 5.6nM[65]. This discrepancy can be explained by the fact that repressor and polymerase do not exclude each other from the promoter, as has been found for inhibition of T7 RNA polymerase by the *lac* repressor bound at a similar distance downstream of the promoter [66]. Operator placement in respect to the T7 promoter is important for the repression characteristics [67,68] and it seems that there is a tradeoff between maximal expression strength and efficient repression depending on the distance of the operator to the transcriptional start site [35]. With the first base of the *tet* operator at +9 relative to the T7 promoter we measured an intermediate Km of about 370 nM in respect to the values determined by Karig et al. [35], which were 73 nM for the operator starting at +4 and 3000 nM for the operator starting at +10. We would like to stress however that Karig et al. determined repression via protein output, which might have masked a repression of transcription rate in the case of the latter, stronger promoter due to saturation of the translational machinery with mRNA. We observed this effect for EGFP output (Figure 2.5**d**), where half-maximal repression is obtained at a higher TetR concentration (845 nM).

For a thorough characterization of genetic parts and devices in ITT reactions it will be useful to determine transcription rates directly and in real-time. In this regard the 3' UTR target – binary probe pair we described in this work will be a useful tool for *in vitro* synthetic biology to quantitate mRNA concentrations in ITT reactions. Our probe - target pair has been optimized for fast binding kinetics to provide sensitive real-time measurements and can be used for other genes of interest. It could also be useful for *in vitro* transcriptional circuits, where a number of different RNA molecules are synthesized [12]. We applied the method to refine our knowledge of mRNA dynamics in the PURE system, where we found that mRNA degradation plays a more important role than had been previously suggested [11] and we characterized the repression of a T7$_{tet}$ promoter [64] by TetR in the same cell-free protein synthesis kit.
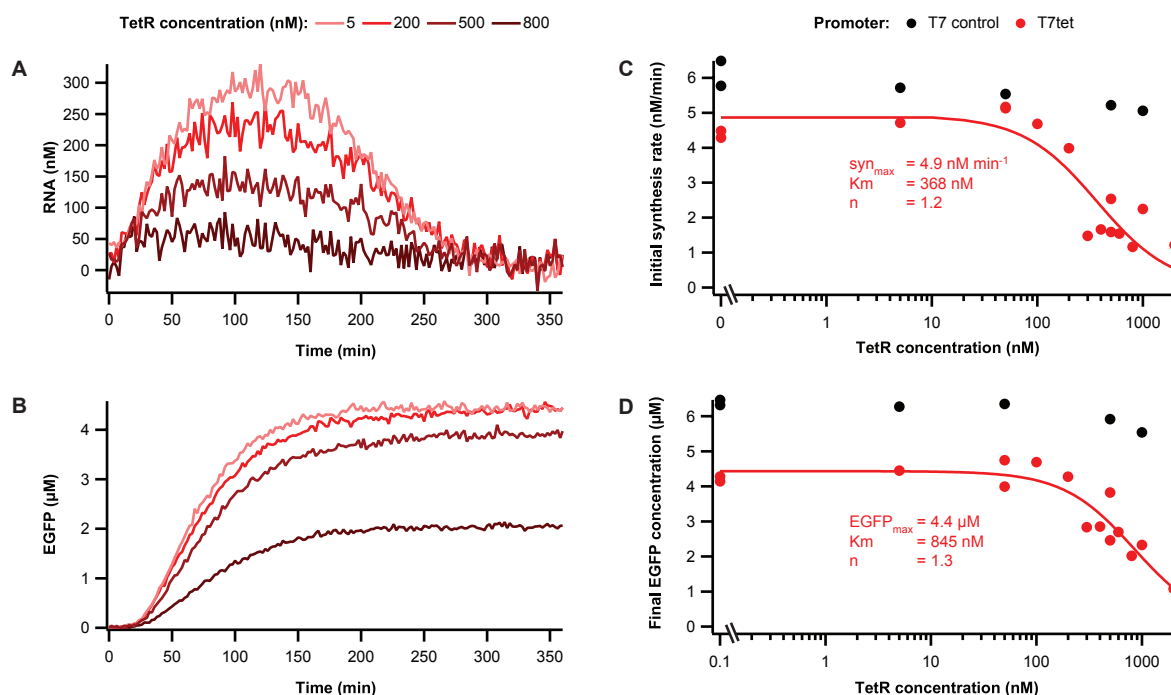
Figure 2.6 Repression of transcription from the T7tet promoter by TetR.
Examples of mRNA (A) and EGFP (B) synthesis driven by the T7$_{tet}$ promoter at different concentrations of TetR repressor. DNA template concentration was 10 nM. (C) Initial mRNA synthesis rates versus TetR concentration for the T7$_{tet}$ promoter and the constitutive T7 promoter control. (D) Endpoint EGFP signals for T7$_{tet}$ and constitutive T7 promoter at different TetR concentrations. The RNA synthesis rates and final EGFP signal of the repressed promoter were fitted to a Hill function (equation 9) to determine maximal activity, concentration of TetR for half-maximal activity and Hill coefficient[65].

2.4 Methods

DNA linear template preparation and sequences

DNA templates for ITT or *in vitro* RNA synthesis reactions were prepared by two-step PCR [69].. The EGFP coding region was amplified from pKT127 [70] with gene specific primers, which also introduced a strong ribosomal binding site. T7 promoter and terminator, as well as the respective 5' and 3' UTRs, which contained the target sites were added in the second step of the PCR by the 3' and 5' extension primers (see Supporting **Table S2.2**). PCR products were purified before use and concentrations determined with a Nanodrop spectrophotometer. Oligonucleotides used as primers and the binary probes were purchased from IDT DNA. The binary probes had the following sequences: 5'-/Cy3/ACCAATGGGCTCAGT-3' and 5'-GAGTCCTTCC/Cy5/ACGAT-3'.

Reaction setup and RNA and EGFP measurements

RNA and DNA targets were tested in Buffer 4 (New England Biolabs) supplemented with 200µg/ml BSA and 1µM probes. For ITT reactions the commercial kit PURExpress (New England Biolabs) was used following the manufacturers instructions. Reactions were supplemented with Protector RNase Inhibitor (Roche), 1µM of each probe, DNA or mRNA and TetR repressor (obtained from Imgen Biosciences Inc.) at the indicated concentrations. Reaction volume was 5µl, which was centrifuged to the bottom of wells in optical 384-well polystyrene plates (Nunc) and covered with 35µl of Chill-Out Liquid wax (Biorad) to avoid evaporation. Reactions were performed at 37°C in a Biotek SynergyMx plate reader at 37°C without shaking. Every 2min for 12 hours EGFP fluorescence (excitation 485±9nm, emission 515±9nm at a sensitivity of 70), Cy5 fluorescence (650±9nm, 680±9nm, sensitivity 100) and Cy3/Cy5 FRET fluorescence (540±20nm, 680±20nm, sensitivity 100) were measured. Fluorescence of technical repeats varied substantially due to the small reaction volume. We found that we could significantly reduce this variability by normalizing to the Cy5 fluorescence, which is unaffected from probe binding. EGFP and FRET signals were determined by dividing with Cy5 fluorescence of the respective well. For FRET signals we additionally subtracted the background fluorescence of a reaction that contained water instead of DNA or mRNA template over time. EGFP signal was calibrated to known concentrations of purified protein (BioVison) (**Figure S2.9**).

Preparation of pure mRNA and qRT-PCR

RNA was prepared with the MEGAscript T7 kit (Ambion) and purified with the MEGAclear kit (Ambion) following the manufacturers instructions. Concentrations were determined spectrophotometrically. As a control, mRNA concentrations during ITT reactions were measured by qRT-PCR. For this, 1µl samples were taken at different time points from a tube containing ITT mix at 37°C and diluted 50-fold in H_2O. These samples were stored at -80°C until used. If necessary a DNase treatment was performed using the TURBO DNA-free kit (Life Technologies). Afterwards the samples were further diluted to a final dilution of 1:10,000. 2µl of sample were analyzed in 10µl reactions of the Power SYBR Green RNA-to-CT 1-Step kit (Life Technologies) in the 7500 Fast Real-Time PCR System (Applied Biosystems). Primers amplified a region of the EGFP gene (see **Table S2.2**) and were used at 0.6µM for the forward and at 0.3µM for the reverse primer. These conditions resulted in PCR efficiencies between 96 and 98%. Concentrations were determined from a standard curve of dilutions of purified mRNA synthesized from the T7-EGFP 3' target version 3 template in a range from 0.3 to 36.3pM mRNA per PCR reaction.

2.5   Supplementary Information

Table S2.1: Secondary structure and position of target site. Distance to ribosomal binding site (for 5' target) or stop codon (for 3' targets). Stability of mRNA secondary structure was calculated for the sequence surrounding the target site (± 35 bp) using mfold[71] (http://mfold.rna.albany.edu/?q=mfold/RNA-Folding-Form) with default settings. If multiple structures were possible, the free energies, ΔG, of all of them are listed. The FRET signals in buffer (main text Figure 2b) were fitted with the exponential saturation function f(x) = S(1−e^{-bx}). The observed association rate, b, and the FRET signal at saturation, S, are listed.

mRNA	ΔG (kcal/mol)	Distance	Association rate (min^{-1})	FRET signal at saturation
5' target	-25.0, -24.0	56 bp	0.02	1.4
3' target 1	-16.7	46 bp	0.09	1.6
3' target 2	-17.1	62 bp	0.09	1.9
3' target 3	-5.1, -4.9	62 bp	0.34	2.2

Table S2.2: Oligonucleotide primers used in the study.

Use and primer name	Sequence
EGFP gene specific PCR:	
EGFP-fwd	CCTCTAGAAATAATTTTGTTTAACTTAAGAAGGAGGAAAAAAAA ATGTCTAAAGGTGAAGAATTATTCAC
EGFP-rev	GTAGCAGCCTGAGTCGTTATTATTTGTACAATTCATCCATACCAT GG
5' extension primers:	
5'ext-T7_no-tgt	GATCTTAAGGCTAGAGTACTAATACGACTCACTATAGGGAGACC ACAACGGTTTCCCTCTAGAAATAATTTTGTTTAAC
5'ext-T7_5'tgt	GATCTTAAGGCTAGAGTACTAATACGACTCACTATAGGGAGACC ACAACGGTTTCACTGAGCCCATTGGTATCGTGGAAGGACTCGCC TGTTTTCGCTTGTGTAGAGTTCTTCCTCTAGAAATAATTTTGTTT AAC
5'ext-T7tet	GATCTTAAGGCTAGAGTACTAATACGACTCACTATAGGGAGATC TCCCTATCAGTGATAGACCTCTAGAAATAATTTTGTTTAAC
3' extension primers:	
3'ext_no-tgt	CAAAAAACCCCTCAAGACCCGTTTAGAGGCCCCAAGGGGTTATG CTAGTTTTTTTTTTTTTTTTTTTTTTTTTTTTTGTAGCAGCCTGAG TCG
3'ext_3'tgt-1	CAAAAAACCCCTCAAGACCCGTTTAGAGGCCCCAAGGGGTTATG CTAGTTTTTTTTTTTTTTTTTTTTTTTTTTTTTGATCGAGTCCTTC CACGATACCAATGGGCTCAGTAAGAACTCTACACAAGCGAAAA CAGGCGTAGCAGCCTGAGTCG
3'ext_3'tgt-2	CAAAAAACCCCTCAAGACCCGTTTAGAGGCCCCAAGGGGTTATG CTAGTTTTTTTTTTTTTTTTTTTTTTTTTTTTTGATCGAGTCCTTC CACGATACCAATGGGCTCAGTAAGAACTCTACACAAGCGAAAC TGACATCTGGAGTACACAGGCGTAGCAGCCTGAGTCG
3'ext_3'tgt-3	CAAAAAACCCCTCAAGACCCGTTTAGAGGCCCCAAGGGGTTATG CTAGTTTTTTTTTTTTTTTTTTTTTTTTTTTTTGATAGAGTCCTTC CACGATACCAATGGGCTCAGTTTTTTGTTTTTTGGGTTTTGGTTT TGTTTTCCAGTACACAGGCGTAGCAGCCTGAGTCG
Final amplification primers:	
5'final	GATCTTAAGGCTAGAGTAC
3'final	CAAAAAACCCCTCAAGAC
qRT-PCR:	
EGFP-qPCR-fwd	GGTGAAGGTGAAGGTGATGC
EGFP-qPCR-rev	TAAGGTTGGCCATGGAACTG
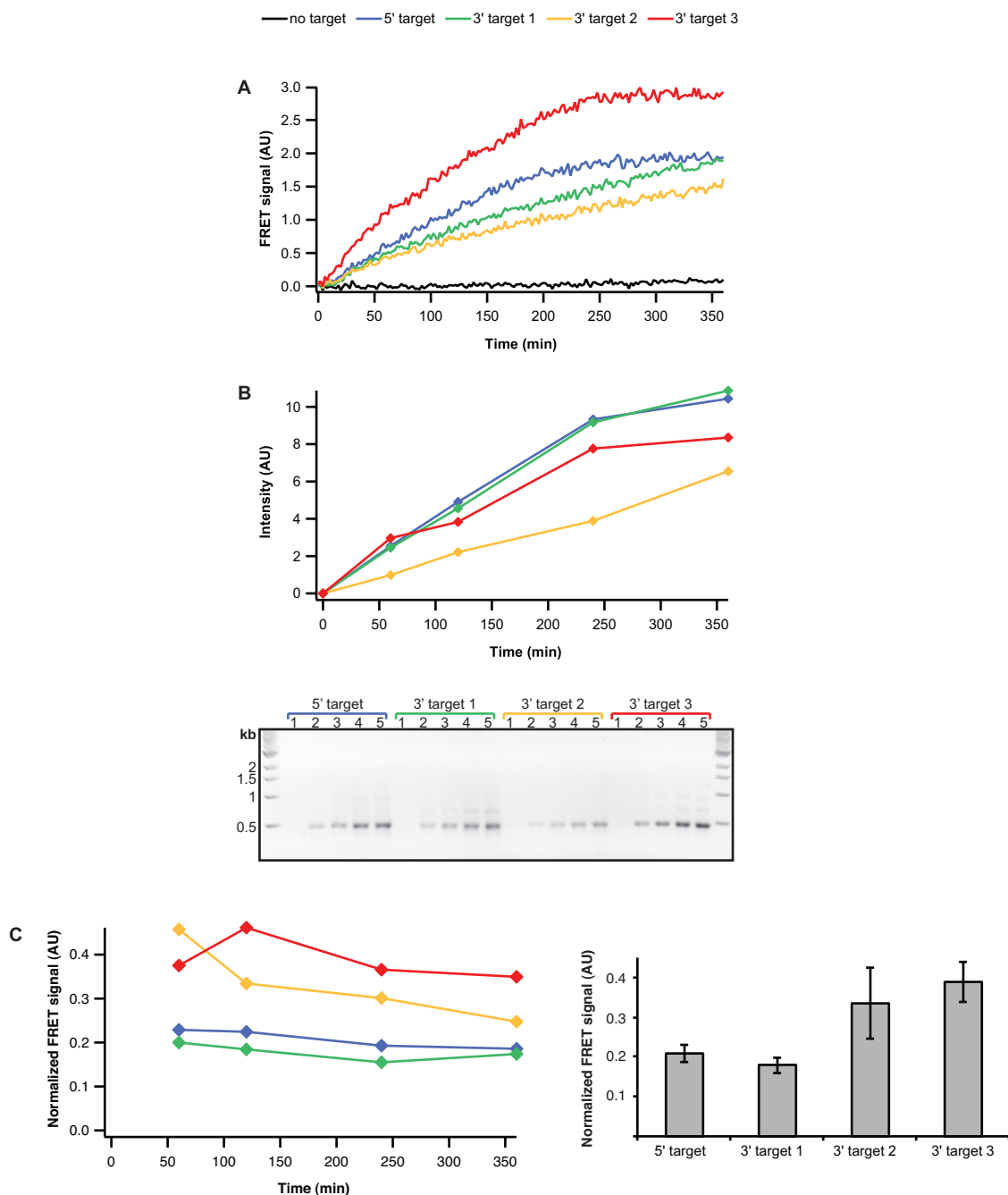
Figure S2.1: Comparison of FRET signal during mRNA synthesis of mRNAs with different target sites in a transcription reaction. Despite RNA concentration differences, 3' target 3 was most sensitive also in a transcription reaction. (A) FRET signal over time. (B) RNA concentration determined by quantification from a gel. Lanes 1-5 are the different time points in the graph. The ladder is a DNA ladder and cannot be used to estimate the size of the RNA molecules. 1μl of a 1:10 dilution of the reaction was loaded on the gel. DNA template was present at a concentration of 18.5nM in the reactions and was not visible on the gel. Transcription reactions were performed in 40mM Tris-HCl pH 7.9, 6mM $MgCl_2$, 10mM DTT, 10mM NaCl, 2mM spermidine, 2mM NTPs and with 1:100 of T7RNAP enzyme mix of the MEGAscript kit (Ambion). The gel was prepared as described in [72] and stained with GelRed (Biotium). (C) FRET signal normalized by RNA concentration determined in (B). Shown is on the left the normalized FRET signal over time and on the left the averages of all time points with their standard deviation. 3' target 3 has the highest FRET signal per mRNA molecule.
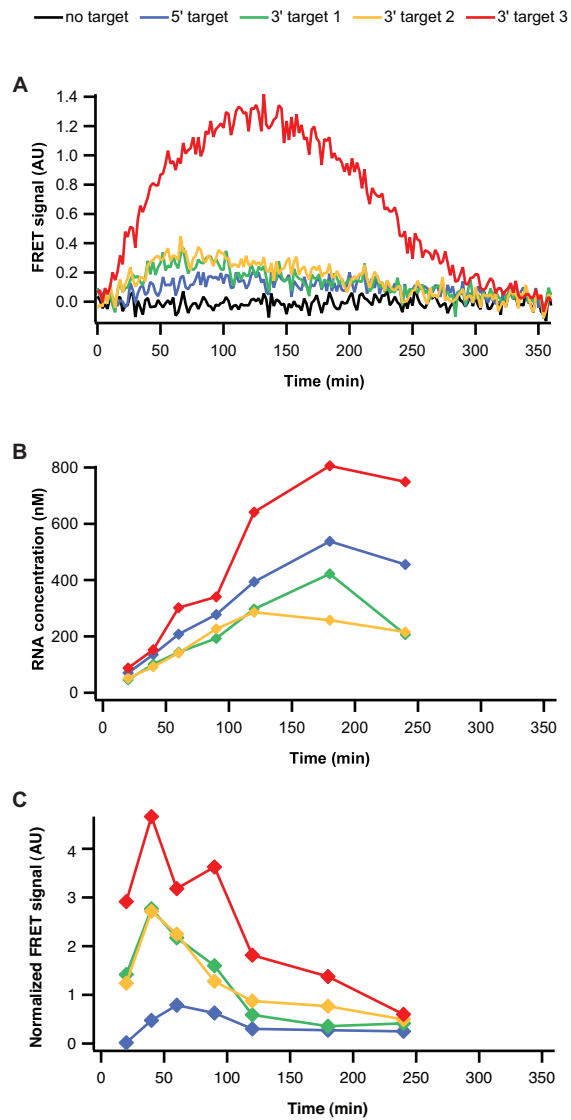
Figure S2.2: Comparison of FRET signal during mRNA synthesis of mRNAs with different target sites in an ITT reaction. Despite RNA concentration differences, 3' target 3 was most sensitive during RNA synthesis in an ITT reaction. (A) FRET signal over time. (B) RNA concentration determined by qRT-PCR. Reactions were performed at a DNA template concentration of 18.5nM. FRET signal of the 3' target 3 mRNA was higher than the signal from the other target mRNAs to an extend, which cannot be explained by their differences in concentration. (C) FRET signal normalized by RNA concentration determined in (B). 3' target 3 has the highest FRET signal per mRNA molecule. The normalized FRET signals varied over time, which is could be due to hybridization kinetics or the fact that qRT-PCR primers were located in the middle of the mRNA, while the FRET target is at the 3' or 5' end of the mRNA, where the mRNA is probably degraded earlier.
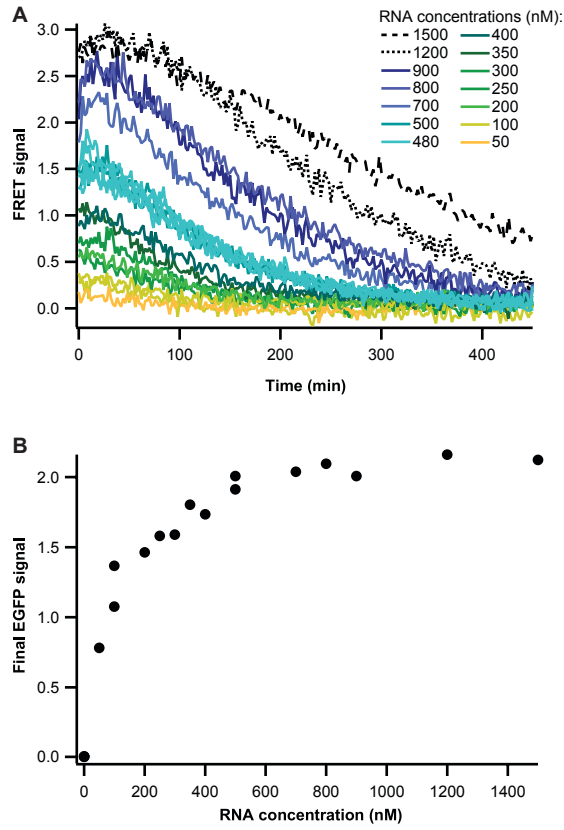
Figure S2.3: Addition of different concentrations of pure mRNA with 3' target version 3 into ITT mix. (A) FRET signals. The traces of the concentrations between 250 and 900 nM, starting at 40 min, were fitted to a function of exponential decay to determine the mRNA degradation rate. (B) Final EGFP signal reached in the reactions in (A).
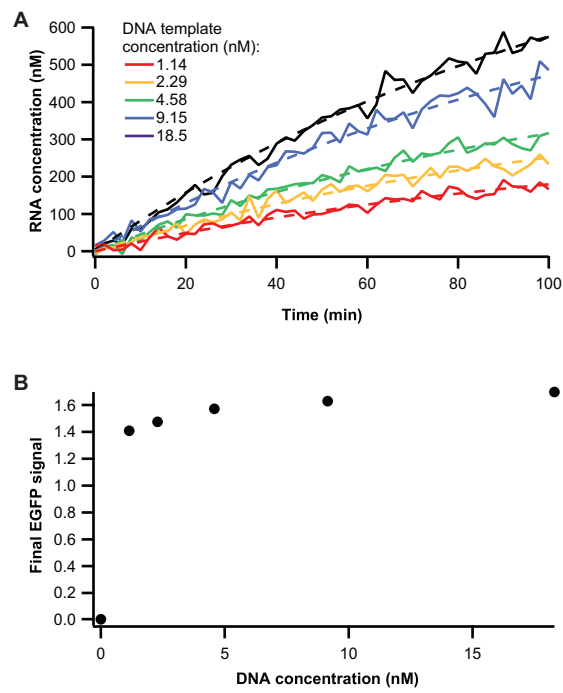
Figure S2.4: RNA and EGFP synthesis from different DNA template concentrations. (A) Initial RNA synthesis rate was determined by fitting RNA concentration during the first 100 min of the reaction to equation 3 (see main text). (B) Final EGFP signal reached in the reactions in (A) from different DNA template concentrations.
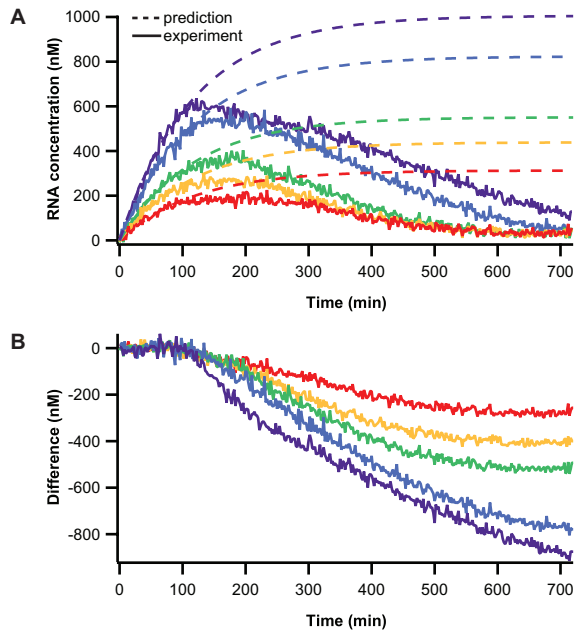
Figure S2.5: Degradation of transcriptional activity. (A) Comparison of mRNA concentration predicted from our model for an mRNA degradation rate of 0.0085 min^{-1} and a constant transcriptional activity (values shown in Figure 5b) to experimental results for different DNA concentrations. (B) Differences between experimental results and the prediction for constant transcription rates (A). For all DNA template concentrations there is a significant difference starting after 120 min.

A

Fit function: $$act(t) = 1 - \frac{1}{1 + \left(\dfrac{t_{half}}{t}\right)^{n}}$$

Fit results:

DNA template concentration (nM)	Time of half maximal activity t_{half} (min)	Hill coefficient n
18.5	209.77	1.97
9.15	219.55	2.97
4.58	196.01	3.95
2.29	185.65	3.21
1.14	202.31	2.56

B

C

D

E

F
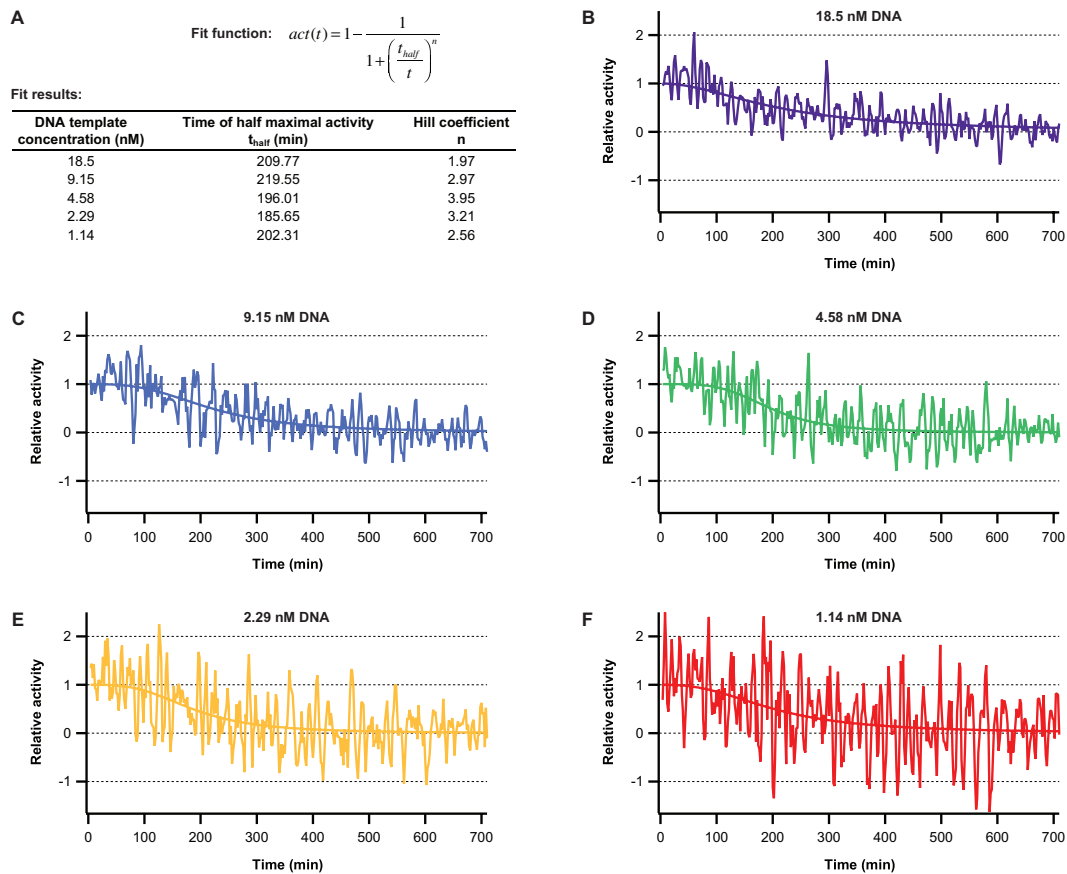
Figure S2.6: Relative transcriptional activity over time in ITT reactions containing different DNA template concentrations. (A) Summary of fit results for different template concentrations. We found no dependence on DNA template concentration. (B-F) Fraction of initial mRNA synthesis rate left at each time point of the reactions containing different DNA template concentrations calculated as described in the main text. Shown is also the fit to the Hill function in (A).

34

A Quantification from gel

B qRT-PCR

C Functional test
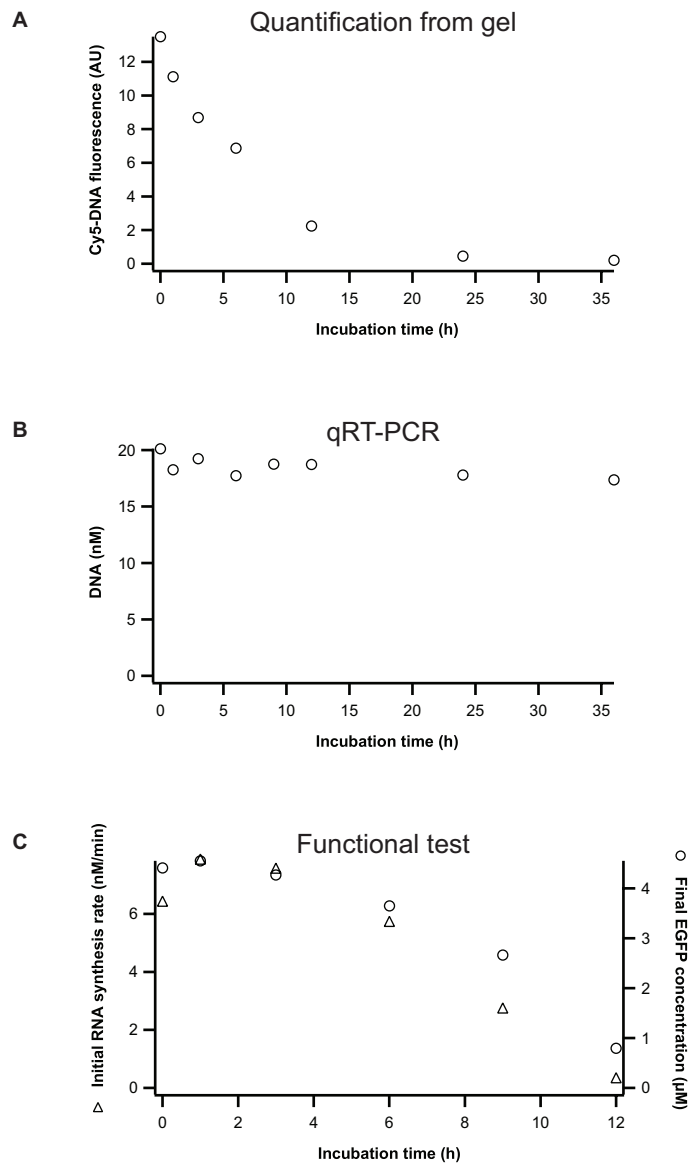
Figure S2.7: DNA stability in an ITT reaction. 18.5nM of DNA template were incubated at 37°C in an ITT reaction. Samples were taken at different time points and analyzed by different methods. (A) DNA template was labeled on both ends with a Cy5 fluorophore, which was introduced by the final primers. For each time point, 1µl of ITT mix was run on a gel and imaged on a Typhoon Scanner (GE) for Cy5 fluorescence. The intensity of the bands was analyzed. The graph shows the average band intensities of 3 replicates. This method overestimates DNA degradation because the DNA template is still functional if some terminal bases are missing. (B) DNA concentration in ITT mix was also measured by qRT-PCR, which amplified a 90bp region in the EGFP coding region. This method underestimates DNA degradation because only a short stretch of template from the middle of the molecule has to be present to produce a signal. (C) For a functional test of DNA stability, a DNA template with the 3' target 3 and a T3 promoter instead of the T7 promoter, which is not transcribed by the T7 RNA polymerase in the ITT reaction, was used. Subsequently, 1µl of a 1:2 dilution of the samples was added to a 5µl ITT reaction containing 200nM T3 RNA polymerase. The reaction for time point 0 therefore contained 1.85nM of DNA template. Initial RNA synthesis rate and final EGFP concentration were determined as described in the main text. In combination the experiments show that DNA is degraded starting at the ends of the molecule. The functional test shows that the promoter and the 3' target are hardly affected by degradation until 6h.
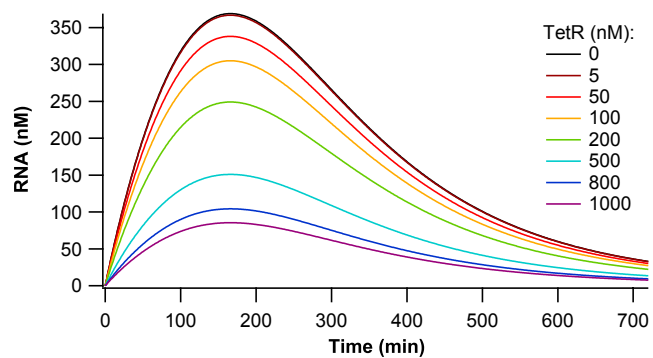
Figure S2.8: Model predictions of mRNA synthesis from TetR repressed T7 promoter at different TetR concentrations. Initial mRNA synthesis rates given by Figure 6C were used in the model presented in Figure 5 to predict mRNA concentration over time in an ITT reaction containing different concentrations of TetR repressor.
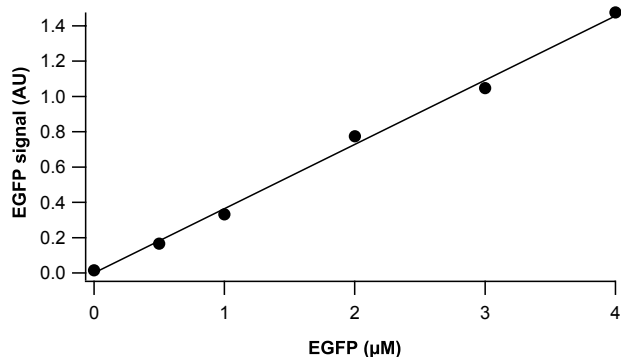
Figure S2.9: Calibration of EGFP fluorescence signal to EGFP concentration. Different concentrations of purified EGFP protein (BioVision) were added to ITT reactions and imaged under standard conditions.

Chapter 3 Implementation of cell-free biological networks at steady state

3.1   Abstract

Living cells maintain a steady state of biochemical reaction rates by exchanging energy and matter with the environment. These exchanges usually do not occur in *in vitro* systems, which consequently go to chemical equilibrium. This in turn has severely constrained the complexity of biological networks that can be implemented *in vitro*. We developed nanoliter-scale microfluidic reactors that exchange reagents at dilution rates matching those of dividing bacteria. In these reactors we achieved transcription and translation at steady state for 30 hours and implemented diverse regulatory mechanisms on the transcriptional, translational, and post-translational level, including RNA polymerases, transcriptional repression, translational activation, and proteolysis. We constructed and implemented an *in vitro* genetic oscillator and mapped its phase diagram showing that steady state conditions were necessary to produce oscillations. This reactor-based approach will allow testing whether fundamental limits exist to *in vitro* network complexity.

3.2   Significance

Transcription and translation can be performed *in vitro*, outside of cells, allowing the assembly of artificial genetic networks. This bottom-up approach to engineering biological networks in a completely defined and minimal environment is instructive to define the rules and limitations of network construction. It is, however, still challenging to implement complex genetic networks *in vitro* because the reactions are usually performed in a batch format, where reaction products accumulate and synthesis rates decline over time. Here, we addressed this problem by developing a microfluidic device to perform in vitro transcription and translation reactions in continuous mode, where synthesis rates stay constant. This allowed us to build and implement a genetic oscillator that showed sustained oscillations for extended periods of times.

3.3   Introduction

Instead of complex and ill-characterized cellular hosts, *in vitro* systems have recently become popular alternatives for implementing synthetic networks. *In vitro* systems can be completely defined, easily manipulated, interrogated, and have been used to study a number of biological phenomena. For example, periodic temporal patterns were observed in systems based on nucleic acid synthesis and degradation [12,13], and ordered spatial patterns were created from purified cell division regulators [6]. *In vitro* transcription and translation (ITT) based systems should, in principle, be able to employ all regulatory functionalities found in living cells. Reconstituted, defined ITT systems like the PURE mix [8], are

particularly appealing for bottom-up synthetic biology. A number of recent examples show that various genetic [16,35,45-47] and metabolic [22] networks can be implemented in ITT systems. Complexity of genetic networks has, however, been limited to genetic cascades, where the output of one stage acts on the next stage, while examples of positive and negative feedback have been basic [35,45,49]. The main limitation to network complexity *in vitro* derives from its batch reaction format. In batch, synthesis rates decrease as pre-cursors are consumed, enzymatic activities degrade, and reaction products accumulate. This rapid approach to chemical equilibrium severely limits network size. In addition, negative feedback is particularly difficult to implement, because regulators from earlier stages are not removed. Partial solutions to these problems included systems that supplied small molecule precursors by diffusion [45,55], implementation of active degradation mechanisms for RNA and proteins [50], or the use of simpler biochemical systems that consume less energy and can therefore run for a longer time [12,13].

3.4 Results

Steady state transcription and translation in microfluidic nano-reactors

To enable the implementation of complex genetic networks *in vitro* we developed a microfluidic device in which ITT proceeds at steady state for extended periods of time. Our microfluidic device contains eight independent 33nL reactors (SOM), and functions similarly to previous devices [73-75]. Dilutions occurred in discrete steps, where each dilution step added fresh ITT mix and template DNA, displacing part of the old reaction volume (Figure 3.1**A**). Dilution rates could be precisely tuned by changing the volume displaced per dilution step in a range of 10-40% of reactor volume. The time interval between dilution steps was kept at 15min (SOM). These exchanges resulted in dilution rates of 0.4-2 h^{-1}. To enable long-term reactions, we cooled the ITT mix off-chip to 6°C, while keeping the on-chip reaction temperature at 37°C. Fluorescent reporters allowed us to determine DNA, mRNA, and protein concentrations in real-time [76] and a computer program controlled all device and imaging operations (Figure 3.1**B**, Section 3.7)

We used a reaction rate model to describe the process of transcription and translation [10,11,76]. We measured the reaction rate parameters that characterize an ITT batch reaction, and added the dilution steps that replace fractions of the reactor volume by reaction mix with full synthesis activity (Figure 3.1**C** and Section 3.8). During continuous reaction, synthesis rates reach a steady state, where the rate at which activity decrease is balanced by the inflow rate of fresh reaction mix. Consequently, RNA and protein concentrations also reach steady-state levels (Figure 3.1**D**). On the basis of our model (see Supplementary Information), a genetic system like the repressilator [2] would not oscillate in a batch reaction. Improvements like degradation mechanisms for mRNA and protein, as well as elongated synthesis times [45,50,55] could possibly lead to a few damped oscillations in batch, whereas sustained oscillations can only be obtained under continuous conditions (Figure 3.1**E**).
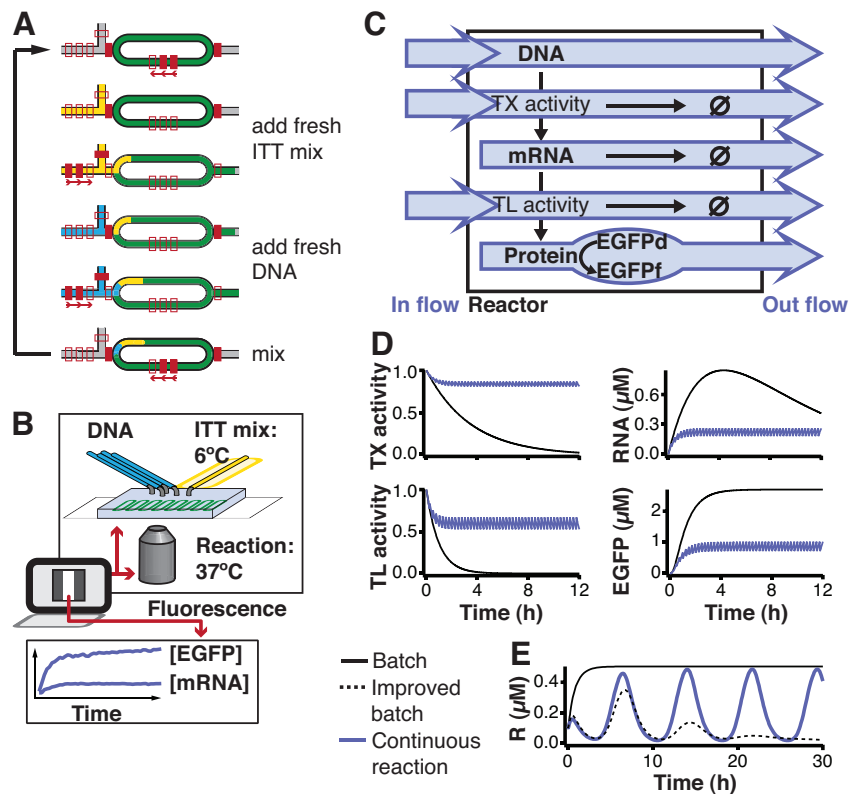
Figure 3.1 ITT under steady state conditions.
(**A**) Function of a microfluidic nano-reactor for continuous ITT. At each dilution step, the supply channel is flushed with fresh reagent. A peristaltic pump meters a specific volume into the reaction ring. After both ITT mix and DNA have been added, another peristaltic pump mixes the reaction. (**B**) Experimental setup and analysis. (**C**) Model of EGFP synthesis in the reactor. Relative transcriptional (TX) and translational (TL) activities decrease at constant rates. In the continuous reaction (blue arrows), all modeled species are diluted at a constant rate, and DNA as well as relative TX and TL activities are replaced at the same rate. (**D**) Model predictions for a batch and a continuous reaction. Predictions were for 18.3nM DNA and dilutions of 32% every 15min. (**E**) Model of the repressilator[2] under three reaction conditions (SOM). We show the concentration of one of the repressor proteins, R.

We performed protein synthesis reactions *in vitro*, generating EGFP from a linear DNA template regulated by a T7 promoter at dilution rates comparable to bacterial doubling times between 20 and 104min (Figure 3.2**A**). We achieved dilution dependent steady state mRNA and protein levels for 30h (Figure 3.2**B**). Independent of dilution rate, DNA template concentration remained constant in all conditions (**Figure S3.1**). When we momentarily stopped the flow of fresh reagents, RNA and protein concentrations increased, and returned to their previous steady state levels when dilution was resumed (Figure 3.2**C**). To demonstrate the dynamic nature of synthesis and dilution we switched between periods where DNA template or water was added (Figure 3.2**D**). This led to continuously changing DNA template concentrations with RNA and protein concentrations oscillating with a slight delay. Our model accurately captured these dynamic changes.
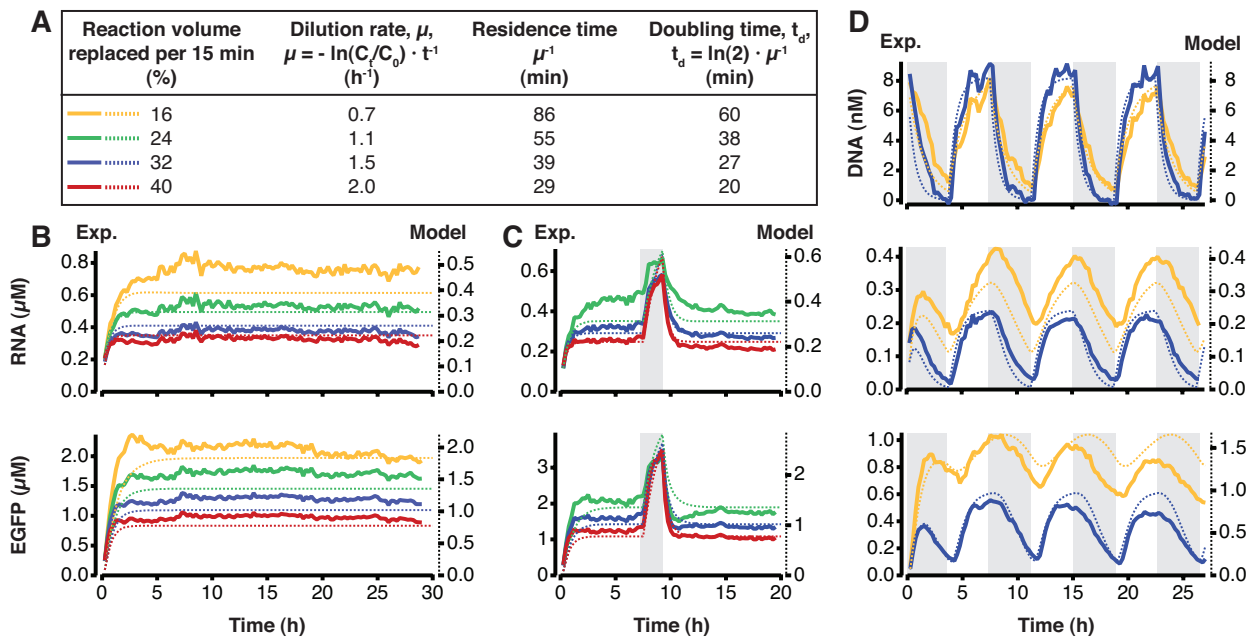
Figure 3.2 Steady state ITT.
(**A**) Dilution conditions for the experiments in this figure. Experimental RNA and protein concentrations (solid lines, left axes) and model prediction (dashed lines, right axes) for (**B**) long-term ITT at different dilution rates, (**C**) a transient switch to batch conditions and (**D**) oscillating DNA template concentrations (shaded area: water added; white area: DNA added).

Implementation of regulatory mechanisms

We implemented a number of regulators, acting transcriptionally, translationally, and post-translationally, under steady state conditions. We transiently expressed the regulators to allow comparison of RNA and protein concentration of the reporter in the presence and absence of the regulator in one experiment (Figure 3.3). We implemented transcriptional activation by expressing T3 RNA polymerase (T3RNAP) or sigma factor 70 (σ^{70}) in the presence of the *Escherichia coli* RNAP core enzyme, and EGFP under control of their respective promoters. Expression of either protein increased RNA concentration from undetectable levels to ~150 and 18nM for T3RNAP and *E. coli* RNAP, respectively, and also increased EGFP concentration in the expected manner (Figure 3.3**A**). Transcriptional repression by TetR reduced transcription of promoters expressed by three different polymerases (T3, T7, and *E. coli* RNAP). Co-expression of *tetR* reduced RNA levels to 30, 50 and 40% of their unrepressed levels for T3, T7 and *E. coli* RNAP, respectively. These changes of mRNA concentration consequently led to a decrease in EGFP levels (Figure 3.3**B**). We implemented translational activation using two regulator RNAs that were previously used *in vivo* to induce mRNA translation by trans-activation and stop codon suppression (Figure 3.3**C**) [77,78]. In trans-activation a trans-activator RNA modifies mRNA secondary structure of a cis-repressed RNA making the ribosomal binding site accessible [77]. For stop codon suppression we used the amber suppressor tRNA encoded by *supD* allowing read-through of a UAG stop codon [78], which was located immediately after the start codon of the EGFP gene. Aminoacylation of the tRNA with serine required no additives to the ITT system as both enzyme and amino acid are present. These mechanisms led to an increase in EGFP concentration from undetectable levels to 14 and 35nM, while RNA concentrations remained high in

the presence and absence of the regulator RNA (expression of *supD* reduced RNA concentration by about 10-20%, Figure 3.3**B**). To quantify the effect of both activators on translation of their respective reporter mRNAs, which were synthesized at different concentrations, we used the model of EGFP ITT to determine the ratio of observed to expected EGFP concentration for the measured mRNA concentration. According to this analysis, translation efficiency was 1.4% for trans-activation and 2.8% for stop codon suppression (**Figure S3.2**). Finally, we successfully implemented protein degradation by reconstituting the AAA+ protease ClpXP (a large 700-800kDa multisubunit complex [79]). Degradation of GFP targeted for recognition by AAA+ proteases has been shown in cell extracts, where these proteases were naturally present [50]. Here, we functionally expressed the protease *in vitro* expressing from two separate DNA templates for the two subunits of the protease and showed that it specifically degraded ssrA tagged EGFP. In the presence of ClpXP steady state EGFPssrA concentration decreased by about 80% (Figure 3.3**D**). Again, we calculated expected EGFP concentrations from the measured mRNA concentrations, which decreased when ClpX and ClpP were expressed, to determine if EGFP decrease was indeed caused by protein degradation. Only in the case of ssrA-tagged EGFP did we observe a significant decrease of observed to expected EGFP when both protease subunits were expressed (**Figure S3.2**).
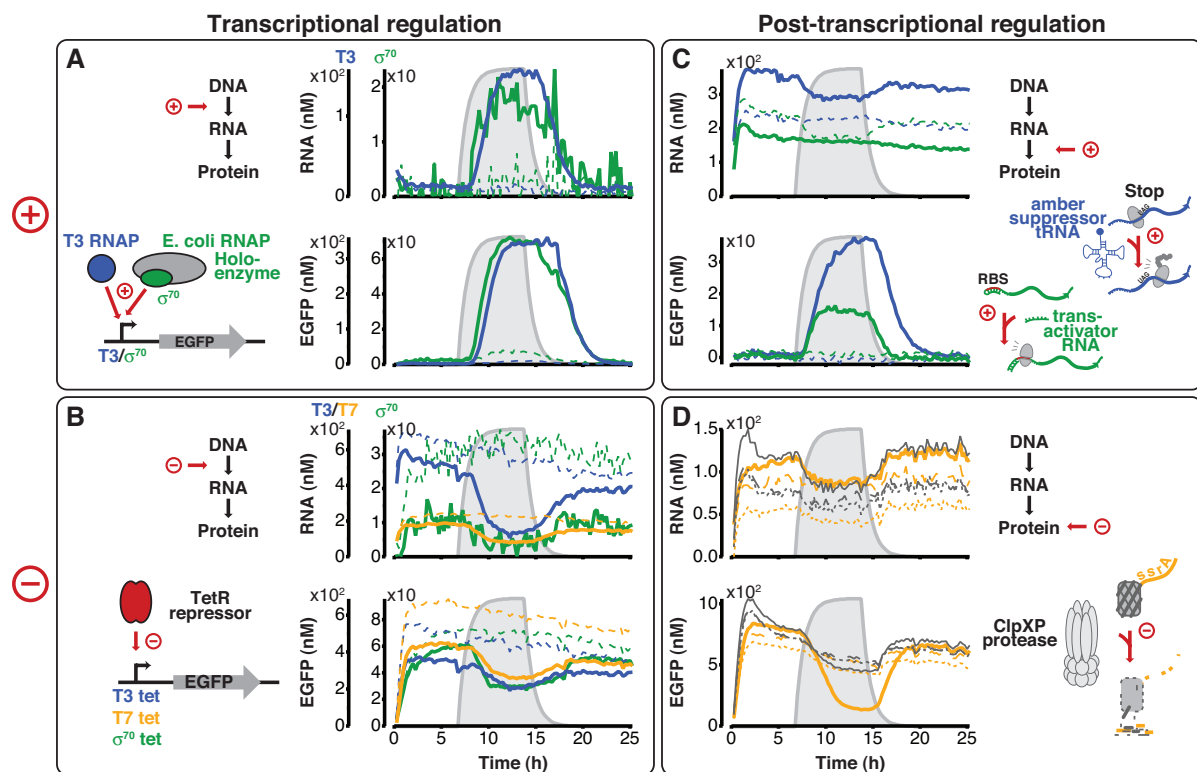
Figure 3.3 Regulation at the transcriptional, translational, and post-translational level.
Solid lines: experimental data, dashed lines: controls. DNA template of the regulator was transiently present (grey shaded area, concentration calculated for dilution rate set in the nano-reactor experiment). Reporter (EGFP) DNA template was present at constant concentration. Detailed summary of concentrations and controls in table S2. (**A**) Transcriptional activation by T3RNAP and σ70. *E. coli* RNAP core enzyme was present in the reaction mix. Controls: wrong activator. (**B**) Transcriptional repression by TetR. Promoters transcribed by three different RNA polymerases were tested in the presence of their respective polymerase. Controls: promoter without repressor binding site. (**C**) Activation of translation by RNA molecules. Controls: wrong activator. (**D**) Protein degradation by ClpXP protease. Controls: no degradation tag (ssrA): grey lines; only one protease subunit expressed: broken lines.

An *in vitro* genetic oscillator

Using three regulators from this toolbox we built a genetic oscillator based on a positive feedback and delayed negative feedback architecture [12,13] (Figure 3.4**A**). In our oscillator network T3RNAP induces its own expression, which constitutes the positive feedback loop. The same polymerase also transcribes the *supD* and *tetR* genes to produce amber suppressor tRNA and *tetR* mRNA, which can only be translated when the suppressor tRNA concentration is sufficiently high. TetR then represses transcription of the T3RNAP gene, which eventually stops its own synthesis. Citrine and cerulean fluorescent proteins allowed us to simultaneously monitor expression from the two promoters in the system. Steady state conditions were necessary to produce oscillations, which we only observed in a narrow range of dilution rates (Figure 3.4**B**). The range of dilution rates that gave rise to oscillations increased with decreasing *supD* template concentration; *supD* was, however, necessary, as well as the other two components (**Figure S3.3**). Oscillation period increased linearly in a range of 4-16h as a function of residence time (**Figure S3.4**). These residence times correspond to cellular doubling times between 20 and 58min. A similar dependence of period on dilution rate has been found for bacterial growth rates [80]. Apart from oscillations or damped oscillations two other general behaviors were observed: at high residence times reporter concentrations peaked once and then went to a low stable steady state, and at low residence times or when *supD* template was absent they immediately approached a stable steady state (Figure 3.4**C**).
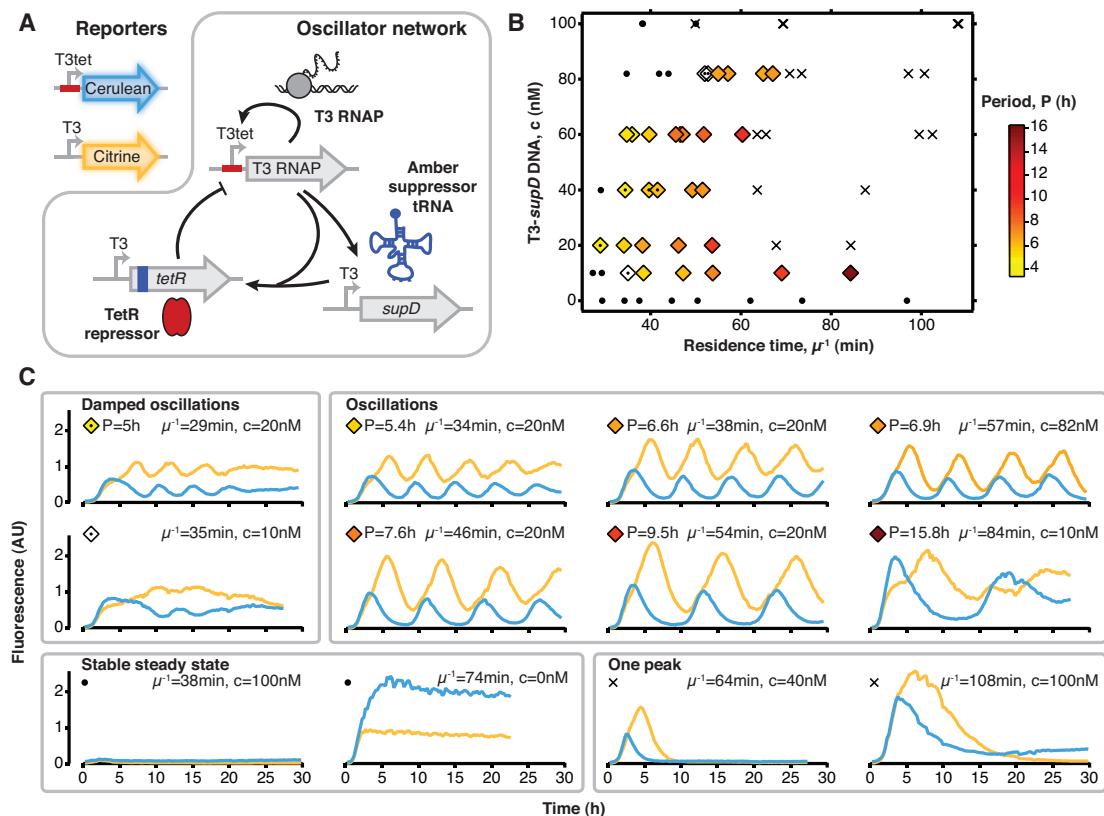
Figure 3.4 Steady state ITT conditions allow implementation of a genetic oscillator.
(**A**) The oscillator consists of three DNA templates: T3RNAP, *supD* amber suppressor tRNA, and TetR repressor; and reporters for the two promoters in the network: yellow fluorescent protein (Citrine) and cyan fluorescent protein (Cerulean). (**B**) Phase diagram of the oscillator at different *supD* DNA template concentrations and different dilution rates. Oscillations (diamond symbols) occurred over a narrow range of dilution rates, which also determined the period of oscillations (fill color). Two other general behaviors were observed: one fluorescence peak and then low fluorescence (cross) or the system immediately reached a stable steady state (circles). (**C**) Cerulean (blue) and citrine (yellow) example traces.

3.5 Discussion

Biological *in vitro* oscillations were previously only achieved in biochemically simple reactions, such as oligonucleotide-based systems containing an active degradation mechanism [12,13]. Our genetic oscillator shows that continuous reaction conditions allow complex dynamics to occur in cell-free protein synthesis reactions, and in a sustained fashion. We observed that oscillations occurred in a narrow range of physiological dilution rates, which is important information for the implementation of *in vivo* oscillators, where dilution rates cannot be tuned as easily.

The examples of regulators we implemented in this study show that there appear to be no major limitations in the control mechanisms that can be implemented *in vitro*. Nonetheless, there are still many mechanisms to be tested including different transcriptional repressors, transcriptional activators such as LuxR or protein phosphorylation. It may moreover be possible to use systems that could not be implemented *in vivo* because of interference with vital processes in the host. In the course of characterizing different regulators with the goal of identifying suitable candidates to assemble a genetic oscillator we found that *E. coli* RNA polymerase promoters recognized by σ^{70} often exhibited very low transcription rates. A recent report suggests that circular DNA might be a better template than linear DNA to reproduce *in vivo* transcription rates from *E. coli* promoters [34]. In order to achieve tight repression of a strong promoter, we included two TetR operator sites into the T3 promoter, which explains its higher repression efficiency than the T7tet promoter. The TetR repressed version of the *E. coli* promoter featured two operator sites but the considerably lower activity in the unrepressed state made it less suitable for our oscillator design. The combination of transcriptional strength and tight repression are desirable features of promoters in many synthetic networks and often not trivial to engineer [2,77]. To achieve tighter control of the *tetR* gene in our oscillator network than transcriptional control could provide we added stop codon suppression as a second regulatory level.

The reactor-based approach presented here allows bottom-up synthetic biology experiments to be performed in a completely defined and controlled environment. It differs from earlier designs of reactors for continuous ITT reactions [52,54] in that it is not based on a size-exclusion membrane for exchange of molecules. In our microfluidic reactor based approach all molecules, including RNA polymerase, translation machinery and DNA template, are constantly exchanged. While the exchange of enzymes involved in the reaction ensures that synthesis rates stay at a constant steady state even if they degrade over time, it could be interesting to immobilize the DNA templates in the reactor, or to organize specific protein products in a spatial manner [81]. Although our DNA template concentrations were in the range of low copy number plasmid concentrations in *E. coli*, RNA and protein concentrations were higher than average cellular concentrations. Due to the relatively large size of our nano-reactors (two orders of magnitude larger than the giant bacterium *Epulopiscium* [82]), stochastic processes may be difficult to study at the moment [83]. It should however be feasible to scale down the 33nL reactors by 1-2 orders of magnitude with existing microfabrication approaches [84] and to use *E. coil* RNAP instead of a phage RNAP. Down-scaling reactor volume would also permit hundreds to possibly thousands of reactors to be integrated on a single device [85,86]. Combined with high-throughput DNA synthesis methods [87] this approach would allow the rapid characterization of many synthetic network variants. Due to the fact that ITT reactions only require linear DNA templates, which were exclusively used in this study, such an *in vitro* screen would require no laborious cloning steps.

It will be exciting to determine whether any fundamental limits exist to the complexity of systems attainable *in vitro*. The examples of regulator mechanisms implemented here show that there appear to be no major limitations in the control mechanisms that can be used. We were able to implement a genetic oscillator *in vitro* similar in complexity to synthetic gene networks achieved *in vivo* a few years ago [2]. Our nano-reactor may prove to be a viable system to study

processes that would interfere with vital processes *in vivo* or processes that occur in organisms that are un-culturable. Furthermore, the system could be used to boot-up and test the biochemical subsystems of a minimal artificial cell including DNA-replication [21], the translation machinery, or biosynthesis of precursors [20].

3.6   Methods

Preparation of DNA templates

PCR for linear DNA templates was performed as previously described [76]. Primer sequences are listed in Table S3.1. PCR templates were pKT127 for EGFP [70], pKT211 for Citrine [70], pBS10 for Cerulean (Yeast resource center), BBa_K346000 (Registry of Standard Biological parts) for T3 RNA polymerase, repressilator plasmid [2] for *tetR*, *E. coli* DH5α genomic DNA for *rpoD*. Short DNA templates for *supD* (Registry of Standard Biological parts Part:BBa_K228001) and taR12 [77] were created by PCR using overlapping oligonucleotides. Regulatory sequences such as promoter, ribosomal binding site, terminator and ssrA tag were included in the oligonucleotide primers. To monitor mRNA concentration, the EGFP template contained a target site for binary probes in its 3' untranslated region [76]. To monitor DNA concentration, the DNA template contained two Cy5 labels introduced by the 3' and 5' final primers.

Reaction setup

We used the commercial PURExpress ITT kit (New England Biolabs) and added water to a volume of 80% of the final reaction volume. The remaining 20% of the reaction volume consisted of DNA template at 5x of its final concentration. ITT and DNA fractions were combined on the microfluidic chip. If necessary, the ITT mix was supplemented with binary probes [76] at a final concentration of 1μM, *E. coli* RNA polymerase core- or holoenzyme (Epicenter) at 35 and 25ng/μl respectively or 100nM T3 RNAP polymerase (Fermentas). For a steady state ITT reaction, ITT mix and DNA were combined in the reactors on the microfluidic chip in a 5:1 ratio. Every 15 min, the reactor was imaged and a fraction of the reactor volume was replaced with fresh ITT mix and DNA at 5:1 ratio. Details on operation and characterization of the microfluidic chip can be found in the SI Appendix. Final concentrations of DNA templates in the genetic oscillator were 5nM T3tet-T3RNAP, 10nM T3-amber-tetR, and variable T3-supD concentration (between 0 and 100nM). The reporter template DNAs for T3-Citrine and T3-Cerulean were at 2.5nM each. Concentrations of DNA templates for the experiment with transcriptional and post-transcriptional regulators are summarized in Table S3.2.

Data acquisition and analysis

We used an inverted microscope with an automated stage to image the eight reactors on the chip. Fluorescence was determined by imaging the reactor channel using a 20x magnification and fluorescence filters for GFP, Cy3-Cy5 FRET, Cy5, YFP and CFP. Background fluorescence of a position next to the channel was subtracted from channel fluorescence. Concentrations of mRNA and EGFP were calculated from calibrations of FRET and EGFP fluorescence using purified molecules [76]. To determine mRNA concentrations we performed a blank reaction without DNA template in one of the reactors and subtracted FRET background fluorescence. Additionally, we normalized to average blank FRET fluorescence. To determine the period of sustained and damped oscillations of the genetic oscillator we measured the time between the first and the second fluorescence maximum for both CFP and YFP fluorescence and used the average. Data was analyzed using IgorPro and MATLAB software.

3.7   Fabrication, design and operation of the nano-reactor device

Design and fabrication

We designed a two-layer microfluidic chip to perform ITT reactions at steady state (Figure 3.5). The design of the microfluidic chip is similar to previous devices [73-75]. One chip contains eight reaction rings to simultaneously run eight independent experiments. Different reagents can be connected to nine fluid inlets, which can be addressed by a multiplexer. Fluid bypasses allow rapid flushing of channels leading to the reaction rings. The inlet of each reaction ring can be opened and closed independently from the others. A peristaltic pump in front of the rings is used to meter reagents into the reaction rings. A second peristaltic pump is used to mix the contents inside the rings. The design allowed us to use, different dilution rates or different template DNAs in each of the nanoreactors. Each nanoreactor had a volume of 33nL.

Molds for the control and the flow layer were fabricated on separate wafers by standard photolithography techniques and patterned with photoresist to produce channels with the heights stated in Figure 3.5. To ensure a homogenous film of photoresist on the mold for the flow layer, we applied the thinner AZ9260 first, and developed, before we spin-coated the thicker SU8 layer. The microfluidic chips were fabricated from PDMS by standard multilayer soft lithography[88]. The control layer was located at the bottom of the chip and plasma bonded to a glass slide.
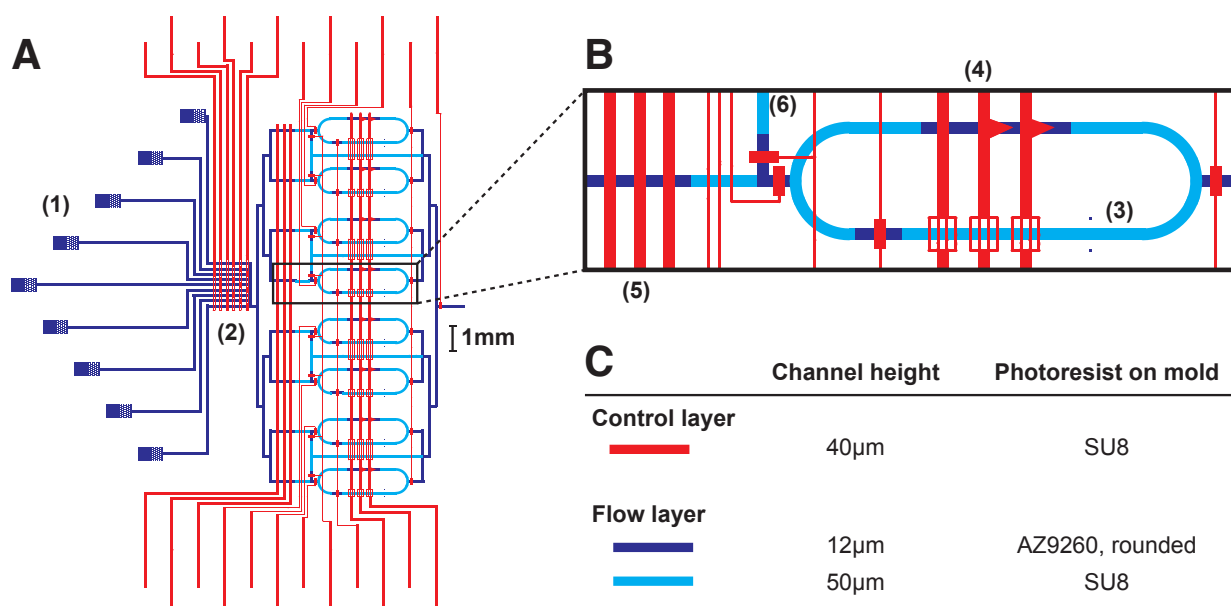
Figure 3.5 Design of the microfluidic chip.
(**A**) Design of the full microfluidic device. (**B**) Close-up of a reaction ring. The control layer is shown in red and the flow layer in two shades of blue. The width of a flow channel or a control valve is 100µm. (1) Reagent inlets, (2) multiplexer, (3) reaction ring and imaging position, (4) peristaltic pump for mixing of reagents in the reaction ring, (5) peristaltic pump to add reagents into the reaction ring, (6) bypass channel. (**C**) Channel heights and photoresists used.

Operation of the nano-reactor device

Pressure of microfluidic flow and control was regulated by a custom pneumatic setup. Control lines were set to 40psi, except the three lines, which controlled the peristaltic mixing pump, which were set to 20 psi using a separate pressure gauge and were additionally connected to a vacuum pump. Microfluidic valves were actuated by computer-controlled solenoid valves operated by a custom written LabView program. Depending on the experiment, flow pressure was regulated between 5 and 9psi to achieve additions between 0.4 and 1% of the ring volume per pump cycle. Usually, the flow pressure was set to the value, where one pump cycle of the peristaltic input pump corresponded to 0.8% of the reactor volume.

The device was placed on an automated microscope in an opaque, temperature controlled incubation chamber, which allowed fluorescent imaging and a constant reaction temperature set to 37°C. One critical feature enabling long-term reaction conditions, was cooling of the ITT mixture before it enters the microfluidic chip, which was accomplished with a combination of a peltier element and water cooled heat sink (Figure 3.6). The volume of ITT mixture for the entire experiment was aspirated into a FEP (fluorinated ethylene propylene) tube, for storage on the peltier element. This tube was then connected to the microfluidic chip via a PEEK (polyether ether ketone) tube (Vici) with a thin inner diameter (180µm) to reduce the volume of un-cooled ITT reagent. For all other reagents we used tygon tubing without cooling.
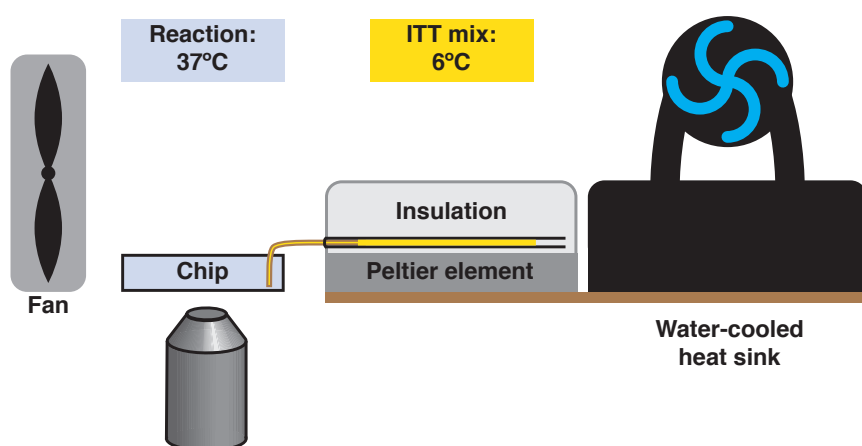
Figure 3.6 Cooling of the ITT mix.
Schematic of the custom-built cooling system for the ITT mix. The FEP tube holding the ITT mix for the experiment is held on top of a peltier element (Laird Technologies), it is connected to the microfluidic chip via a PEEK tube with a thin inner diameter (180µm). The heat sink for the peltier element is a copper plate cooled by a CPU cooler (EK waterblocks) connected to a water pump regulated to 8°C (Solid State cooling systems). In order to prevent condensation and ice formation on the edge of the peltier element facing the microfluidic chip, we placed a fan on the opposite site of the device. This temperature control system kept the ITT mix in the storage tube at approximately 6°C while the on-chip reaction temperature was 37°C, the temperature in the incubation chamber enclosing the setup.

Characterization of the nano-reactor device

The volume added into the reaction rings per pump cycle of the peristaltic input pump was consistent across the eight reactors on the chip and increased linearly with the number of pump cycles (Figure 3.7**A**). Before each experiment, the dilution rate was determined by measuring the washout rate of EGFP fluorescence (Figure 3.7**B**).

We measured the speed at which reagents inside the reactions rings were mixed by adding a plug of fluorescent EGFP solution into the rings. One position of the channel was imaged while the peristaltic pump started moving the fluorescent plug in a circle, which leads to mixing (Figure 3.8). Within less than 2 min mixing was completed.
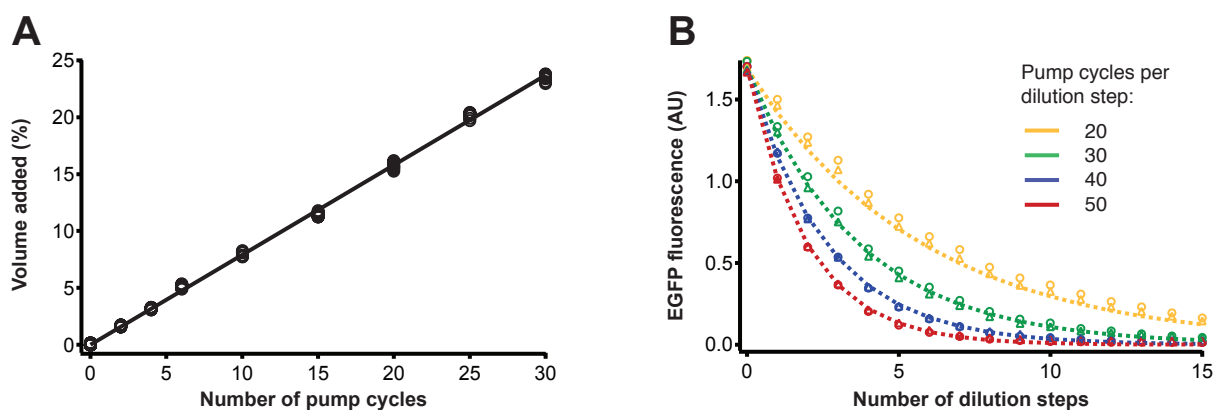
Figure 3.7 Characterization of the peristaltic input pump.
(**A**) Volume added into the reactors depends linearly on the number of pump cycles. Shown are the results from eight reactors of the same device. (**B**) Washout from the reactor at different dilution rates. Shown are the results of eight reactors from one device, with two repeats of each dilution rate (markers), and the prediction for a washout of 16, 24, 32 and 40% of reactor volume per dilution step (dashed lines). In both panels one pump cycle displaced 0.8% of the reactor volume.
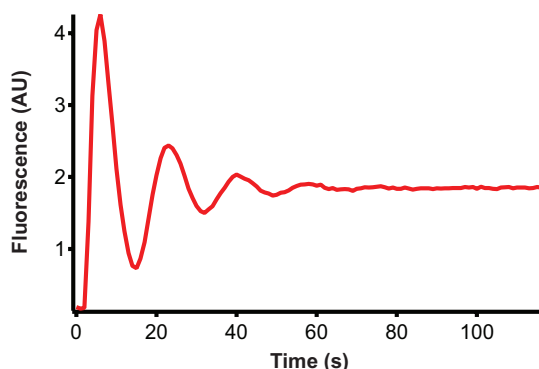
Figure 3.8 Mixing of reagents in the reaction rings.
To reaction rings filled with 2% BSA in PBS a plug of 7% of the reactor volume of 100µg/ml EGFP was added with the peristaltic input pump. The reactor channel was imaged while the peristaltic mixing pump moved the EGFP plug in a circle, causing the solutions to mix.

Experimental procedure

Priming and calibration

At the beginning of each experiment the device was primed with a solution of 2% BSA in PBS. Then, the dilution rates were calibrated as shown in Figure 3.7B. This ensured correct functioning of the device before start of the experiment and to adjust the dilution rates to the desired value.

Steady state ITT reaction

Operation of the microfluidic chip and imaging during steady state ITT reactions was fully automated with a custom written LabView program. The sequence of operations was as follows:

Step	Operation
0	Initial fill: - flush reactors with ITT mixture - meter 20% reactor volume of template DNA into the reactors - mix
	Repeat the following steps every 15min:
1	Image each reactor
2	Flush the bypass channels with buffer
3	Addition of fresh ITT mix: - flush the bypasses channels with ITT mixture - add 4*n pump cycles of ITT mixture into the reactors - flush the bypass channels with buffer
4	Addition of DNA: - flush the bypasses channels with DNA solution - add n pump cycles of DNA into the reactors - flush the bypass channels with buffer
5	Mix
6	Repeat from step 1

Flushing of the bypass channels with costly reagents like ITT mixture and DNA solutions was done with the peristaltic input pump in order to reduce reagent consumption. For a complete experiment of 30h, only 6.25µl of ITT mixture were required per reactor. The buffer used for flushing was 5mM Tris-HCl pH8.5. The peristaltic mixing pump was actuated with a frequency of 8.3Hz. The input pump was actuated with a frequency of 1.7Hz for flushing the bypass channel, and with a frequency of 0.3Hz to add reagents into the reactions rings.

3.8 Model of an ITT reaction in the nano-reactor device

Model of a batch ITT reaction

We describe the ITT reaction in batch with a set of six differential equations

DNA, d:

(1) $d'(t) = 0$

mRNA, m:

(2) $m'(t) = TX(d) \cdot act_{TX}(t) - \deg_m \cdot m(t)$

dark (immature) EGFP, p_d:

(3) $p_d'(t) = TL(m) \cdot act_{TL}(t) - mat \cdot p_d(t)$

fluorescent (mature) EGFP, p_f:

(4) $p_f'(t) = mat \cdot p_d(t)$

Relative transcriptional activity, act_{TX}:

(5) $act_{TX}'(t) = -\deg_{TX} \cdot act_{TX}(t)$

Relative translational activity, act_{TL}:

(6) $act_{TL}'(t) = -\deg_{TL} \cdot act_{TL}(t)$

We determined each parameter of this model in separate experiments. TX is the initial transcription rate that depends on DNA template concentration. TL is the initial translation rate that depends on mRNA concentration. We assume an unspecific decrease of those activities as a function of time and use act_{TX} and act_{TL} as the relative activities left at a given time. RNA, transcriptional activity and translational activity degrade/decrease with rates $\deg_m$, $\deg_{TX}$, $\deg_{TL}$ respectively. Dark EGFP matures to fluorescent EGFP with the rate mat. We did not observe any degradation of fluorescent EGFP.

Degradation of mRNA

The rate of mRNA degradation was determined as in[76] by monitoring the decrease of a known concentration of purified mRNA, m_0, in an on-chip batch reaction (Figure 3.9). The decreasing RNA concentration was fit to the solution of equation (2), with TX=0:

(7) $m(t) = m_0 \cdot e^{-\deg_m \cdot t}$

In different experiments and at different initial RNA concentrations we measured degradation rates between 0.003 and 0.008 min^{-1}. For the model, we used a RNA degradation rate $\deg_m$ of 0.003 min^{-1}.
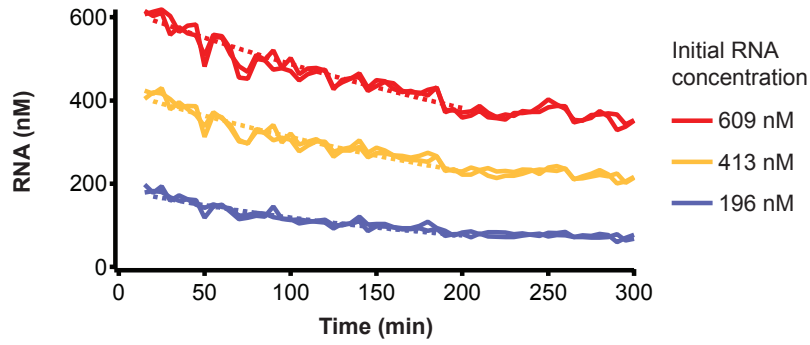
Figure 3.9 On-chip measurement of mRNA degradation rate.
Different concentrations of purified mRNA were added to an ITT reaction on chip. Concentration of mRNA was monitored over time and fit to equation (7) (dashed lines).

Initial rate of transcription

We determined the initial transcription rate as a function of DNA in an on-chip batch reaction as in [76]. The initial change in mRNA concentration can be described by equation (8) and we fit RNA concentration during the initial phase of the reaction to the solution, equation (9) (Figure 3.10**A**).

$$(8)\ m'(t) = TX(d) - \deg_m \cdot m(t)$$

$$(9)\ m(t) = \frac{TX(d)}{\deg_m} \cdot (1 - e^{-\deg_m \cdot t})$$

Transcription can be described by Michaelis-Menten kinetics:

$$(10)\ TX(d) = \frac{TX_{max} \cdot d}{K_{TX} + d}$$

The maximal initial transcription rate, TX_{max}, was 11.5 nM/min and the DNA concentration for half maximal activity, K_{TX}, was 5.5nM (Figure 3.10**B**).

Figure 3.10 On-chip measurement of initial transcription rate.
(**A**) RNA synthesis from different DNA template concentrations was monitored and the concentration during the initial 50 min of the reaction was fit to equation (9) using a fixed mRNA degradation rate, $\deg_m$, of 0.003 min^{-1} (dashed lines) to determine TX(d). (**B**) Initial transcription rates as determined in (A) and fit to Michaelis-Menten kinetics (equation 10).

Relative transcriptional activity over time

The relative transcriptional activity of an on-chip batch reaction over time was determined for RNA synthesis from different template DNA concentrations as in[76] using Euler's method (Figure 3.11):

(11) $m(t + \Delta t) = m(t) + (TX(d) \cdot act_{TX}(t) - \deg_m \cdot m(t)) \cdot \Delta t$

(12) $act_{TX}(t) = \dfrac{m(t + \Delta t) - m(t) + \deg_m \cdot m(t) \cdot \Delta t}{TX(d) \cdot \Delta t}$.

We approximated the mode of transcriptional activity decrease by exponential decay (see equation 5). The rate of the decrease in relative transcriptional activity, $\deg_{TX}$, was on average 0.005 min⁻¹.
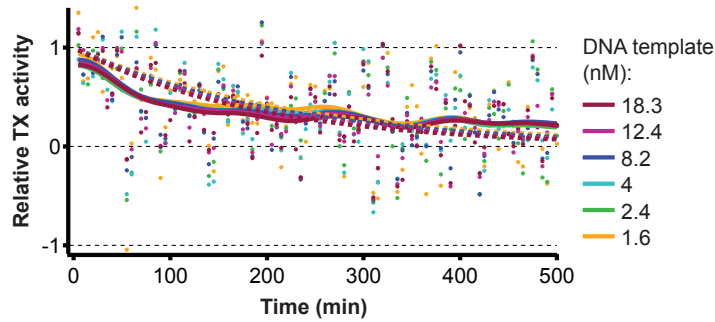
Figure 3.11 On-chip relative transcriptional activity over time.
The relative transcriptional activity with respect to its initial value was calculated for RNA synthesis from different DNA template concentrations using equation (12) (dots) and the previously determined rates. These traces were smoothed for visualization (lines) and fit to an exponential decay function to determine the rate of decrease (dashed lines).

Maturation of EGFP

To determine the maturation rate of EGFP in our experimental conditions an ITT reaction producing EGFP was stopped by adding RNase, which immediately stops translation. Any increase of EGFP after this addition was therefore due to maturation of dark EGFP to fluorescent EGFP. This simplifies equation (3) to

(13) $p_d{}'(t) = -mat \cdot p_d(t)$

With this, the solution of equation (4) is:

(14) $p_f(t) = p_0 + \Delta p \cdot (1 - e^{-mat \cdot t})$

p_0 is the concentration of fluorescent EGFP when translation is stopped and Δp is the increase in its concentration when all dark EGFP is completely converted to fluorescent EGFP. EGFP maturation rate was determined to be 0.1 min⁻¹ (Figure 3.12).
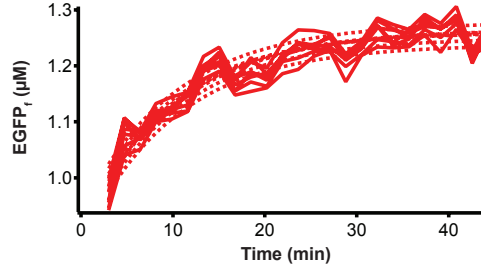
Figure 3.12 On-chip maturation of EGFP.
After 25 min of an on-chip ITT reaction from a DNA template, translation was stopped by adding 0.6µM RNase. Concentration of fluorescent EGFP after RNase addition (lines) was fit to equation (14) to determine the maturation rate.

Initial rate of translation

We measured EGFP synthesis from different concentrations of purified mRNA. In the initial phase of this reaction, not taking into account a decrease of translational activity over time, this simplifies equations (2) and (3) to

(15) $m'(t) = -\deg_m \cdot m(t)$

(16) $p_d'(t) = TL(m) - mat \cdot p_d(t)$

With $TL(m) = \alpha_{TL} \cdot m(t)$ and $p_f(0) = p_d(0) = 0$, the solution of equations (15), (16) and (4):

(17) $p_f(t) = \dfrac{\alpha_{TL} \cdot m_0}{\deg_m \cdot (\deg_m - mat)} \cdot (mat \cdot (e^{-\deg_m \cdot t} - 1) + \deg_m \cdot (1 - e^{-mat \cdot t}))$.

Concentration of fluorescent EGFP of the initial phase of the reaction was fit to equation (17) to determine α_{TL} (Figure 3.13**A**). Translation follows Michaelis-Menten kinetics:

(18) $TL(m) = \dfrac{TL_{max} \cdot m}{K_{TL} + m}$.

K_{TL}, the mRNA concentration at half-maximal translation rate, was determined from multiple benchtop experiments to be 150.2 nM. This K_{TL} was used to determine the average TL_{max} of two independent on-chip reactions. The TL_{max} on-chip was lower than in a benchtop reaction and also more variable (Figure 3.13**B**). For the model we used an average value of 76.4 nM/min.
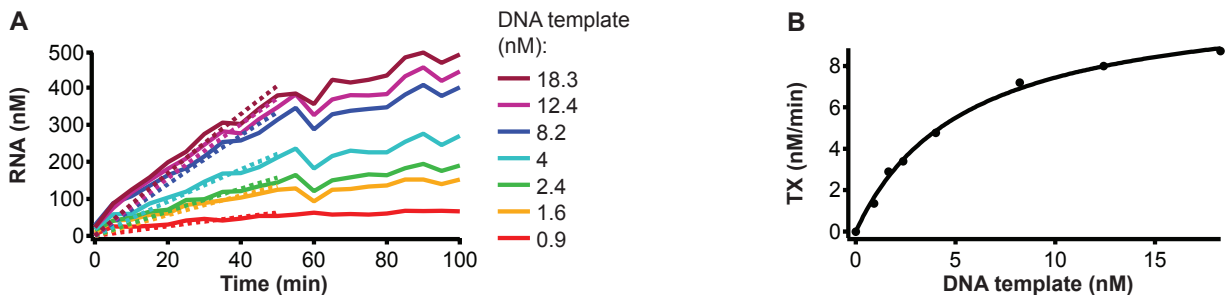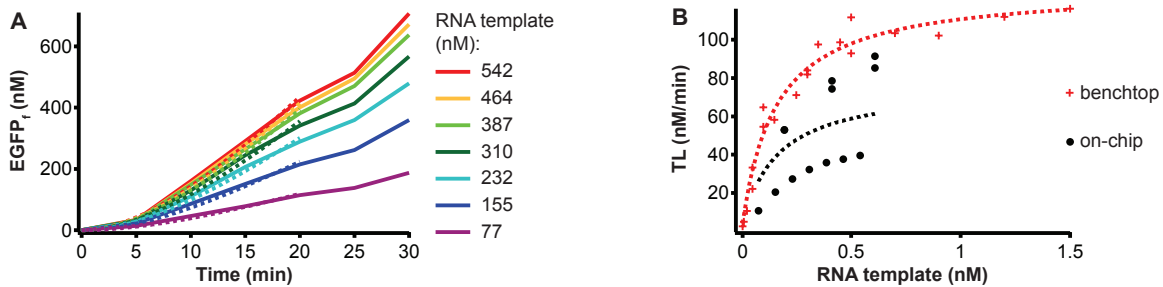

Figure 3.13 On-chip measurement of initial translation rate.
(**A**) On-chip EGFP synthesis from different mRNA template concentrations was monitored and the concentration during the initial 20 min of the reaction was fit to equation (17) using the known initial mRNA concentration m_0 and the previously determined rates, $\deg_m$ and *mat* (dashed lines) to determine α_{TL}. (**B**) Initial transcription rates, TL, in a benchtop reaction (red crosses) and in two independent on-chip experiments (black circles) as determined in (A) were fit to Michaelis-Menten kinetics (equation 18) (dashed lines).

52

Translational activity over time

Translational activity over time was determined by Euler's method. Equations (15), (3) and (4) can be written as

(19) $m(t + \Delta t) = m(t) - \deg_m \cdot m(t) \cdot \Delta t$

(20) $p_d(t + \Delta t) = p_d(t) + \Delta t \cdot (act_{TL}(t) \cdot TL(m) - mat \cdot p_d(t))$

(21) $p_f(t + \Delta t) = p_f(t) + \Delta t \cdot mat \cdot p_d(t)$.

From the known initial mRNA concentration, we calculated the mRNA concentration at each later time point. We had measured the concentration of fluorescent EGFP, p_f. Using smoothed p_f values we determined the concentration of dark EGFP, from equation (21):

(22) $p_d(t) = \dfrac{p_f(t + \Delta t) - p_f(t)}{\Delta t \cdot mat}$.

This allowed us to calculate the relative translational activity, act_{TL} at each time point, which is the fraction of the initial activity left.

(23) $act_{TL}(t) = \dfrac{p_d(t + \Delta t) - p_d(t) + mat \cdot p_d(t) \cdot \Delta t}{\Delta t \cdot TL(m)}$.

Within one experiment the rate of decrease of translational activity was very consistent and did not depend on the mRNA concentration used (Figure 3.14). The average rate of activity decrease determined from two independent on-chip experiments was 0.017min^{-1}.
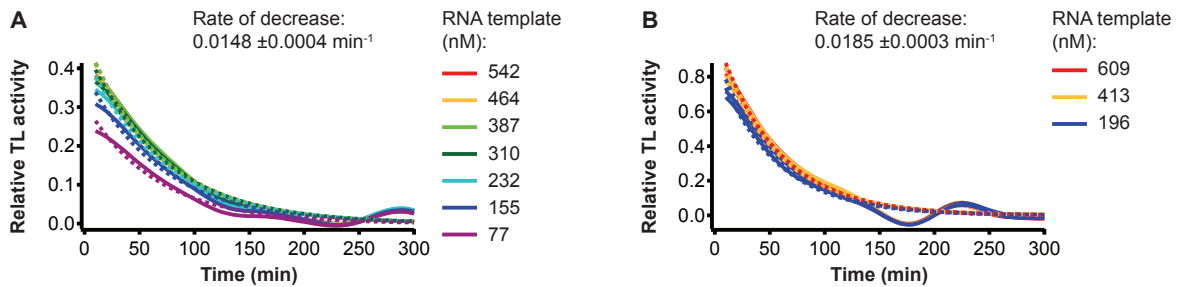
Figure 3.14 Relative translational activity over time.
In two independent on-chip experiments (**A** and **B**) EGFP was synthesized from different initial concentrations of purified mRNA. The relative translational activity with respect to its initial value was calculated using equations (19), (22), (23) and smoothed EGFP$_f$ measurement traces. The relative activities over time were then fit to an exponential decay function to determine the rate of decrease (dashed lines).

Summary of rates

The rates we measured here for a batch reaction on chip compared well with rates that were previously determined for the same ITT reaction mixture for bench-top reaction with larger volumes[11,76]. The following table summarizes all the rates we determined in the sections above that describe a batch reaction on chip, and that we used in our model:

Rate	Value
RNA degradation rate, $\deg_m$	0.003 min^{-1}
Initial transcription rate, $TX(d)$	$TX(d) \dfrac{11.5 \frac{nM}{min} \cdot d}{5.5nM + d}$
Rate of relative transcriptional activity decrease, $\deg_{TX}$	0.005 min^{-1}
EGFP maturation rate, mat	0.1 min^{-1}
Initial translation rate, $TL(m)$	$TL(m) \dfrac{76.4 \frac{nM}{min} \cdot m}{150.2nM + m}$
Rate of relative translational activity decrease, $\deg_{TX}$	0.017 min^{-1}

Model of a continuous reaction with dilutions

To describe the continuous reaction in the microfluidic reactor we modeled the processes of the batch ITT reaction in discrete time intervals, Δt, of one minute. Every 15min a dilution fraction, dil (between 0.16 and 0.4, depending on the dilution conditions), was removed from the concentrations of the modeled molecules and the transcription and translation activities, which constitutes the washout. Also every 15min, full transcription and translation activities and DNA concentration, all scaled by fraction dil, were added:

		Every 15 min
DNA	$d(t + \Delta t) = d(t)$	$-dil \cdot d(t) + c \cdot dil \cdot d(t)$
mRNA	$m(t + \Delta t) = m(t) + \Delta t \cdot (TX(d) \cdot act_{TX}(t) - \deg_m \cdot m(t))$	$-dil \cdot m(t)$
EGFP$_d$	$p_d(t + \Delta t) = p_d(t) + \Delta t \cdot (TL(m) \cdot act_{TL}(t) - mat \cdot p_d(t))$	$-dil \cdot p_d(t)$
EGFP$_f$	$p_f(t + \Delta t) = p_f(t) + \Delta t \cdot mat \cdot p_d(t)$	$-dil \cdot p_f(t)$
Rel. TX act	$act_{TX}(t + \Delta t) = act_{TX}(t) - \Delta t \cdot \deg_{TX} \cdot act_{TX}(t)$	$-dil \cdot act_{TX}(t) + dil$
Rel. TL act	$act_{TL}(t + \Delta t) = act_{TL}(t) - \Delta t \cdot \deg_{TL} \cdot act_{TL}(t)$	$-dil \cdot act_{TL}(t) + dil$

Concentration, c, of DNA is usually equal to the initial DNA concentration d(0), in which case DNA concentration is constant. In special cases c can change transiently during the experiment, which leads to a new steady state DNA concentration, c.

Initial conditions

d(0) varied from experiment to experiment. In continuous ITT reactions $m(0)=p_d(0)=p_f(0)=0$ and $act_{TX}(0)=act_{TL}(0)=1$.

Prediction of transcriptional and translational activities at different dilution rates

The predicted relative transcriptional and translational steady state activities depended on the dilution rate. The higher the dilution rate, the higher was the steady state activity. Figure 3.15 shows the predicted relative transcriptional and translational activities for the experiments of Figure 3.2.
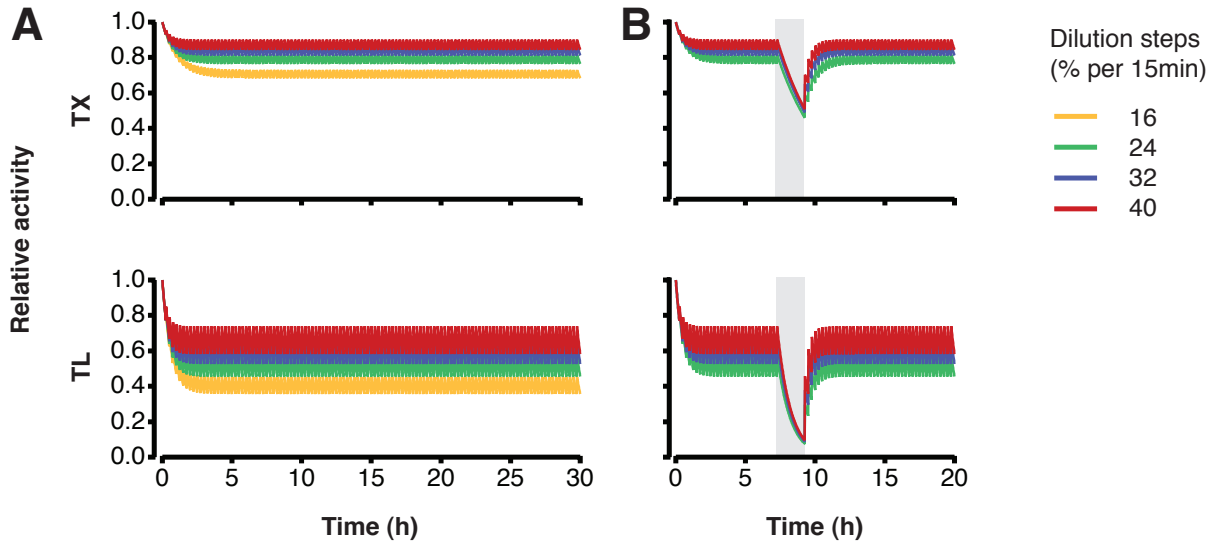
Figure 3.15 Predicted relative transcriptional and translational activities at different reaction conditions.
(**A**) Long-term steady state ITT at different dilution rates. The predicted relative transcriptional and translational activities shown here correspond to the experiment and predictions in Figure 3.2B. (**B**) Transient switch to batch conditions. No dilutions occurred in the shaded time span. The predicted relative transcriptional and translational activities shown here correspond to the experiment and predictions in Figure 3.2C. Relative activities were modeled with discrete dilution steps every 15min, which cause the teeth-like fluctuations.

Model of the repressilator in batch and continuous reaction

The repressilator consists of three transcriptional repressors, which each inhibit the expression of the preceding gene in the network [2]. We modeled the repressilator as a symmetric system, where all repressors are identical except for their DNA-binding specificities, using the following differential equations for mRNA and protein concentration of the three repressors, R1-3 (i = R2, R3, R1 and j = R1, R2, R3):

$$m_i{}'(t) = act_{TX}(t) \cdot \frac{TX \cdot Km^n}{Km^n + p_j^n} - \deg_m \cdot m_i(t) - dil \cdot m_i(t),$$

$$p_i{}'(t) = act_{TL}(t) \cdot \frac{m_i(t)}{m_{total}(t)} \cdot TL(m_{total}(t)) - \deg_p \cdot m_i(t) - dil \cdot m_i(t).$$

We set the transcription rate at the unrepressed state, TX, of each promoter to 3nM/min, the Michaelis constant, Km, to 40nM and the Hill coefficient, n, to 2. The translation rate, TL, was calculated from equation 18. To take into account

55

saturation of the translation machinery at high mRNA concentration we determined the translation rate for total mRNA concentration, m_{total}, and scaled by the fraction of mRNA concentration of the repressor modeled in that case.

Transcription and translation activities were modeled as above, using the following differential equations:

$$act_{TX}{}'(t) = -\deg_{TX} \cdot act_{TX}(t) - dil \cdot act_{TX}(t) + dil \ ,$$

$$act_{TL}{}'(t) = -\deg_{TL} \cdot act_{TL}(t) - dil \cdot act_{TL}(t) + dil \ .$$

We compared behavior of the oscillator under batch and continuous reaction conditions. Additionally we modeled an "improved" batch reaction, where mRNA degradation and protein degradation rates are increased to *in vivo* levels of *E. coli*[50,89], and where the rates of activity decrease of transcription and translation were a 10th of the rates we measured. These improvements seem experimentally feasible, if mRNA and protein degradation mechanisms [50] and feeding of the ITT reaction by diffusion of small molecules [45,55] were combined. The values of the following parameters were varied as follows in the three different reaction conditions:

Parameter	Reaction conditions		
	Batch	**Improved batch**	**Continuous**
Dilution rate, *dil*	0	0	$1.54h^{-1}$
mRNA degradation, $\deg_m$	$0.003min^{-1}$	$0.053min^{-1}$	$0.003min^{-1}$
Protein degradation, $\deg_p$	0	$0.017min^{-1}$	0
Decrease of transcriptional activity, $\deg_{TX}$	$0.005min^{-1}$	$0.0005min^{-1}$	$0.005min^{-1}$
Decrease of translational activity, $\deg_{TL}$	$0.017min^{-1}$	$0.0017min^{-1}$	$0.017min^{-1}$

Initial conditions were 1nM for all mRNA species, 0 for protein concentrations of R1 and R2 and 100nM of protein R3. Initial relative transcriptional and translational activities were 1. We show concentration of repressor protein R3 in Figure 3.1E.

3.9 Supplementary Information

Table S1. Oligonucleotide primers used in the study.

Use and primer name	Sequence

Gene specific primers
Color annotations: Ribosomal binding site   Amber stop codon   ssrA tag

EGFP/Citrine-fwd	CCTCTAGAAATAATTTTGTTTAACTTAAGAAGGAGGAAAAAAAAATGTCTAAAGGTGAAGAATTATTCAC
amber-EGFP-fwd	CCTCTAGAAATAATTTTGTTTAACTTAAGAAGGAGGAAAAAAAAATGTAGAAAGGTGAAGAATTATTCACTG
EGFP/Citrine-rev	GTAGCAGCCTGAGTCGTTATTATTTGTACAATTCATCCATACCATGG
EGFP-ssrA-rev	GTAGCAGCCTGAGTCGTTATTAAGCAGCCAGAGCGTAGTTTTCGTCGTTAGCAGCTTTGTACAATTCATCCATACCATGG
T3RNAP-fwd	CCTCTAGAAATAATTTTGTTTAACTTAAGAAGGAGGAAAAAAAAATGAACATCATCGAAAACATCG
T3RNAP-rev	GTAGCAGCCTGAGTCGTTA TTATGCAAAGGCAAAGTCAGAC
rpoD-fwd	CCTCTAGAAATAATTTTGTTTAACTTAAGAAGGAGGAAAAAAAAATGGAGCAAAACCCGCAG
rpoD-rev	GTAGCAGCCTGAGTCGTTATTATTAATCGTCCAGGAAGCTACGC
tetR-fwd	CCTCTAGAAATAATTTTGTTTAACTTAAGAAGGAGGAAAAAAAAATGTCCAGATTAGATAAAAGTAAAG
amber-tetR-fwd	CCTCTAGAAATAATTTTGTTTAACTTAAGAAGGAGGAAAAAAAAATGTAGAGATTAGATAAAAGTAAAG
tetR-rev	GTAGCAGCCTGAGTCGTTATTAAGACCCACTTTCACATTTAAG
clpX-fwd	CCTCTAGAAATAATTTTGTTTAACTTAAGAAGGAGGAAAAAAAAATGACAGATAAACGCAAAGATG
clpX-rev	GTAGCAGCCTGAGTCGTTATTA TTCACCAGATGCCTGTTG
clpP-fwd	CCTCTAGAAATAATTTTGTTTAACTTAAGAAGGAGGAAAAAAAAATGTCATACAGCGGCGAAC
clpP-rev	GTAGCAGCCTGAGTCGTTATTAATTACGATGGGTCAGAATCGAATC
Cerulean-fwd	CCTCTAGAAATAATTTTGTTTAACTTAAGAAGGAGGAAAAAAAAATGAGTAAAGGAGAAGAACTTTTC
Cerulean-rev	GTAGCAGCCTGAGTCGTTATTATTTGTATAGTTCATCCATGCC

5' extension primers:
Color annotations: Promoter   tet operator

5'ext-T7_no-tgt	GATCTTAAGGCTAGAGTACTAATACGACTCACTATAGGGAGACCACAACGGTTTCCCTCTAGAAATAATTTTGTTTAAC
5'ext-T7tet	GATCTTAAGGCTAGAGTACTAATACGACTCACTATAGGGAGATCTCCCTATCAGTGATAGACCTCTAGAAATAATTTTGTTTAAC
5'ext-T3	GATCTTAAGGCTAGAGTACAATTAACACTCACTAAAGGGAGACCTCTAGAAATAATTTTGTTTAAC
5'ext-T3tet	GATCTTAAGGCTAGAGTACTCCCTATCAGTGATAGAATTAACACTCACTAAAGGGAGATCCCTATCAGTGATAGACCTCTAGAAATAATTTTGTTTAAC
5'ext-E.c.lac	GATCTTAAGGCTAGAGTACAATTGTGAGCGGATAACAATTGACATTGTGAGCGGATAACAATATAATATGCGCATCCTCTAGAAATAATTTTGTTTAAC

5'ext-E.c.tet   GATCTTAAGGCTAGAGTAC<mark style="background:red">TCCCTATCAGTGATAGA</mark>GA<mark style="background:green">TTGACA</mark><mark style="background:red">TCCCTAT CAGTGATAGA</mark><mark style="background:green">TATAAT</mark>ATGCGCATCCTCTAGAAATAATTTTGTTTAAC

3' extension primers:
Color annotations: <mark style="background:magenta">Terminator</mark>

3'ext_no-tgt   <mark style="background:magenta">CAAAAAACCCCTCAAGACCCGTTTAGAGGCCCCAAGGGGGTT</mark>ATGCTAGTTT TTTTTTTTTTTTTTTTTTTTTTTTTTTGTAGCAGCCTGAGTCG

3'ext_3'tgt-3   <mark style="background:magenta">CAAAAAACCCCTCAAGACCCGTTTAGAGGCCCCAAGGGGGTT</mark>ATGCTAGTTT TTTTTTTTTTTTTTTTTTTTTTTTTTTTGATAGAGTCCTTCCACGATACCAATGG GCTCAGTTTTTTGTTTTTTGGGTTTTGGTTTTGTTTTCCAGTACACAGGCGTA GCAGCCTGAGTCG

Final amplification primers:

5'final   GATCTTAAGGCTAGAGTAC or /Cy5/GATCTTAAGGCTAGAGTAC

3'final   CAAAAAACCCCTCAAGAC or /Cy5/CAAAAAACCCCTCAAGAC

Specialized primer sets:
Color annotations: <mark style="background:green">Promoter</mark>   <mark style="background:yellow">Ribosomal binding site</mark>

supD:

T7-supD-fwd   GATCTTAAGGCTAGAGTAC<mark style="background:green">TAATACGACTCACTAT</mark>AGGAGAGATGCCGGA GCGGCTGAACGGACCGGTCTC

T3-supD-fwd   GATCTTAAGGCTAGAGTAC<mark style="background:green">AATTAACACTCACTAAA</mark>GGAGAGATGCCGGA GCGGCTGAACGGACCGGTCTC

supD-rev   TGGCGGAGAGAGGGGGATTTGAACCCCCGGTAGAGTTGCCCCTACTCCGGT TTTAGAGACCGGTCCGTTCAGCCG

T7-cr-EGFP:

cr-EGFP-fwd   GGGTATTAA<mark style="background:yellow">AGAGGAGA</mark>AAGGTACCATGTCTAAAGGTGAAGAATTATTCA
(gene specific primer)   C

5'ext-crR12-5'   GATCTTAAGGCTAGAGTAC<mark style="background:green">TAATACGACTCACTAT</mark>AGGGAGAATTCTACCA
(upstream part of 5'ext)   TTCACC

5'ext-crR12-3'   GGTACCTTTCTCCTCTTTAATACCCAAATCCAAGAGGTGAATGGTAGAATT
(downstream part of   CTCCCT
5'ext)

T7-taR12:

T7-taR12-fwd   GATCTTAAGGCTAGAGTAC<mark style="background:green">TAATACGACTCACTAT</mark>AGGACCCAAATCCAGG AGGTGATTGGTAG

taR12-rev   TCTAGAGATATATGGTAGTAGTAAGTTAATTTTCATTAACCACCACTACCA ATCACCTCCTGGATTTG

Table S3.2. DNA template concentrations for experiments in Figure 3.3. All reporter DNA templates contained a target site for binary probes to determine EGFP mRNA concentrations.

Experiment	Regulator DNA	Reporter DNA
Transcriptional activation (Figure 3A)		
by T3 RNA polymerase		
	1nM T7-T3RNAP	5nM T3-EGFP
control	1nM T7-rpoD	5nM T3-EGFP
by sigma factor 70 (rpoD)		
	1nM T7-rpoD	10nM E.c.tet-EGFP
control	1nM T7-T3RNAP	10nM E.c.tet-EGFP
Transcriptional repression by TetR (Figure 3B)		
T7 RNA polymerase promoter		
	1nM T7-tetR	4nM T7tet-EGFP
control	1nM T7-tetR	4nM T7-EGFP
T3 RNA polymerase promoter		
	1nM T7-tetR	4nM T3tet-EGFP
control	1nM T7-tetR	4nM T3-EGFP
E. coli RNA polymerase holoenzyme		
	1nM T7-tetR	4nM E.c.tet-EGFP
control	1nM T7-tetR	4nM E.c.lac-EGFP
Translational activation (Figure 3C)		
by amber suppressor tRNA (supD)		
	20nM T7-supD	10nM T7-amber-EGFP
control	20nM T7-taR12	10nM T7-amber-EGFP
by trans-activator RNA (taR12)		
	20nM T7-taR12	10nM T7-cr-EGFP
control	20nM T7-supD	10nM T7-cr-EGFP
Protein degradation by ClpXP (Figure 3D)		
of EGFP with degradation tag (ssrA)		
	2nM T7-clpX + 2nM T7-clpP	4nM T7-EGFP-ssrA
control	2nM T7-clpX	4nM T7-EGFP-ssrA
control	2nM T7-clpP	4nM T7-EGFP-ssrA
of EGFP without degradation tag		
control	2nM T7-clpX + 2nM T7-clpP	4nM T7-EGFP
control	2nM T7-clpX	4nM T7-EGFP
control	2nM T7-clpP	4nM T7-EGFP
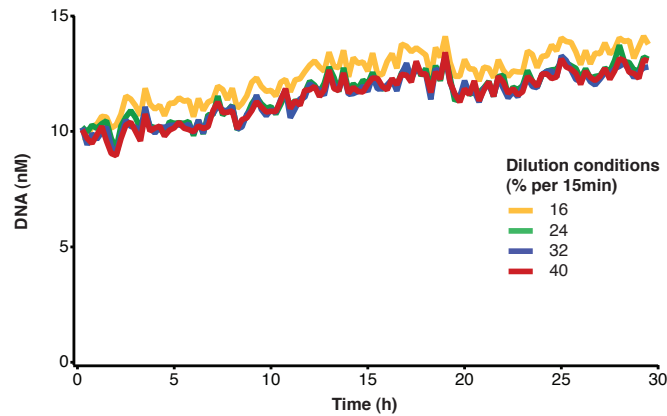
Figure S3.1. DNA concentration during steady state ITT. DNA concentration during the steady state reaction at different dilution rates shown in Fig. 2B was monitored via Cy5 fluorescence of the labeled DNA template.
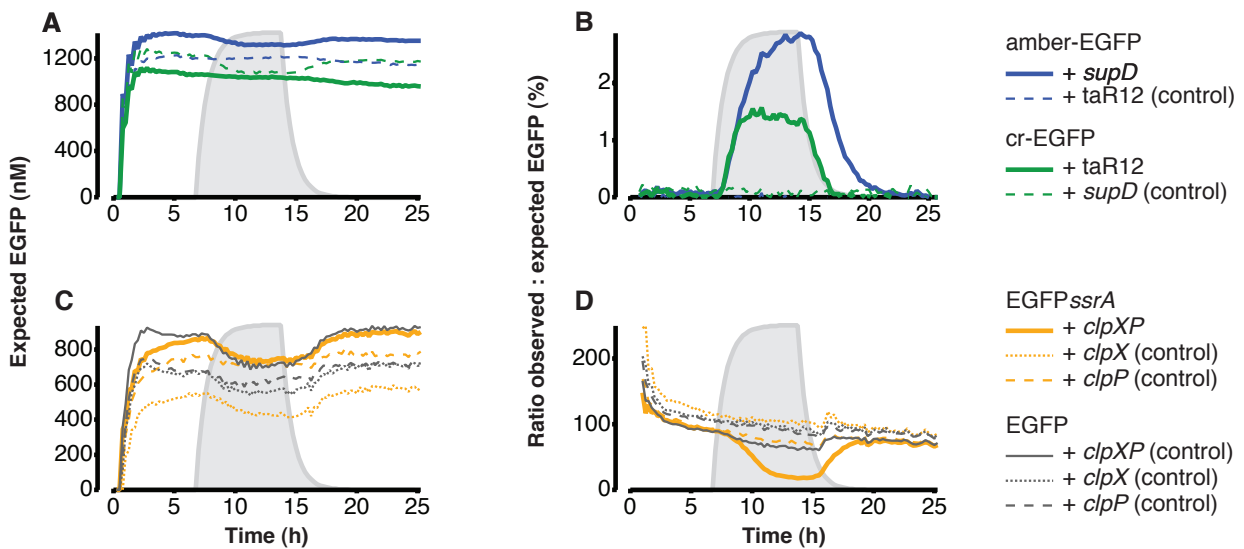
Figure S3.2. Quantitative effects of post-transcriptional regulators. (**A**) Expected EGFP concentration calculated from measured mRNA concentrations for translational activation (Fig. 3C). (**B**) Ratio of observed to expected EGFP concentration, translation efficiency. (**C**) Expected EGFP concentration calculated from measured mRNA concentrations for protein degradation (Fig. 3D). (**D**) Ratio of observed to expected EGFP concentration to quantify the influence of protein degradation.
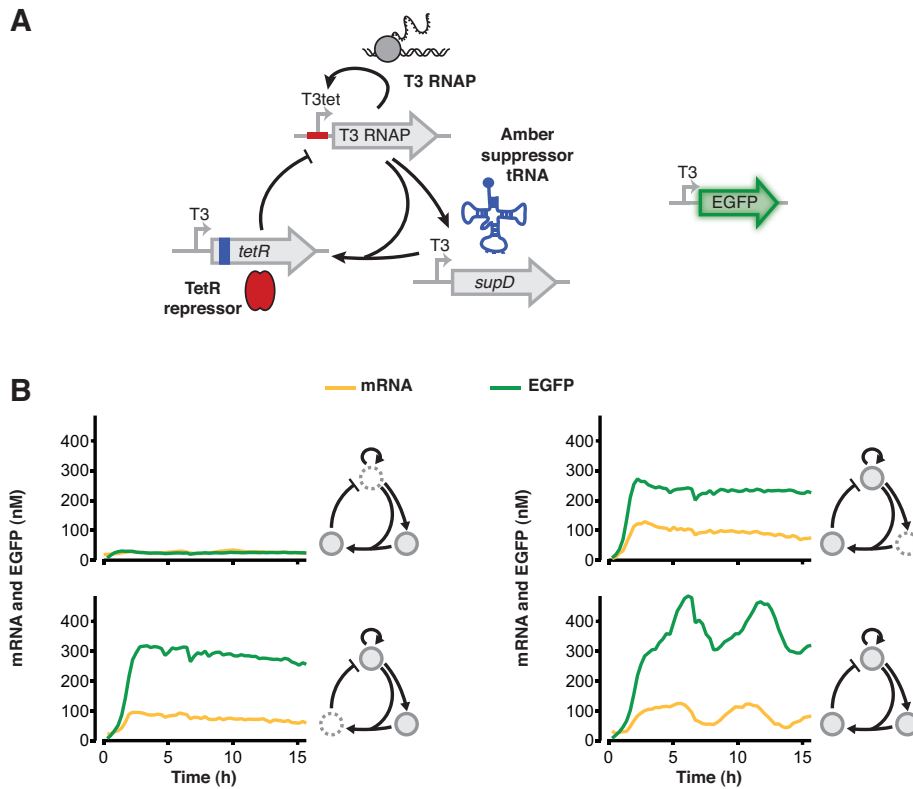
Figure S3.3. Influence of the three oscillator genes. (**A**) Network design of the genetic oscillator. Concentrations of the oscillator DNA templates were 5nM T3tet-T3RNAP, 60nM T3-supD, 10nM T3-amber-tetR. We used the T3-EGFP reporter (5nM) with probe target site to determine mRNA concentration of the reporter during the reaction. (**B**) One network component was omitted at a time to determine if they were necessary to produce oscillations. Reactions were performed with a residence time of 49 min.
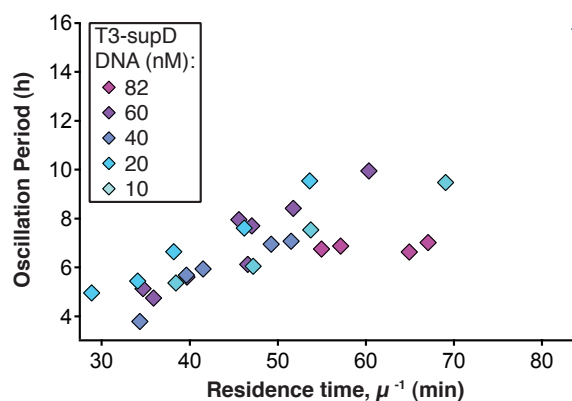
Figure S3.4. Oscillation period versus residence time. Oscillation periods from experiments with different T3-*supD* DNA concentration (Figure 4) were plotted against residence time.

Chapter 4   A cell-free framework for biological systems engineering

Niederholtmeyer H*[1], Sun ZZ*[2], Hori Y[2], Yeung E[2], Verpoorte A[1], Murray RM[2], and Maerkl SJ[1]. (2015) bioRxiv, 018317.

* HN and ZZS contributed equally to this work

[1] Institute of Bioengineering, École Polytechnique Fédérale de Lausanne, Switzerland. [2] Division of Biology and Biological Engineering, California Institute of Technology, Pasadena, United States of America

4.1   Summary

While complex dynamic biological networks control gene expression and metabolism in all living organisms, engineering comparable synthetic networks remains challenging [3,5]. Conducting extensive, quantitative and rapid characterization during the design and implementation process of synthetic networks is currently severely limited due to cumbersome molecular cloning and the difficulties associated with measuring parts, components and systems in cellular hosts. Engineering gene networks in a cell-free environment promises to be an efficient and effective approach to rapidly develop novel biological systems and understand their operating regimes[3,5,90-92]. However, it remains questionable whether complex synthetic networks behave similarly in cells and a cell-free environment, which is critical for *in vitro* approaches to be of significance to biological engineering. Here we show that synthetic dynamic networks can be readily implemented, characterized, and engineered in a cell-free framework and consequently transferred to cellular hosts. We implemented and characterized the "repressilator"[2], a three-node negative feedback oscillator *in vitro*. We then used our cell-free framework to engineer novel three-node, four-node, and five-node negative feedback architectures going from the characterization of circuit components to the rapid analysis of complete networks. We validated our cell-free approach by transferring these novel three-node and five-node oscillators to *Escherichia coli*, resulting in robust and synchronized oscillations reflecting the *in vitro* observation. We demonstrate that comprehensive circuit engineering can be performed in a cell-free system and that the *in vitro* results have direct applicability *in vivo*. Cell-free synthetic biology thus has the potential to drastically speed up design-build-test cycles in biological engineering and enable the quantitative characterization of synthetic and natural networks.

4.2   Results and discussion

A central tenet of engineering involves characterizing and verifying prototypes by conducting rapid design-build-test cycles in a simplified environment. Electronic circuits are tested on a breadboard to verify circuit design and aircraft prototypes are tested in a wind tunnel to characterize their aerodynamics. A simplified environment does not exist for engineering biological systems, nor is accurate software based design possible, requiring design-build-test cycles to be

conducted *in vivo*[5]. To fill the gap between theoretical design and laborious *in vivo* implementation for biological systems we devised a cell-free framework consisting of *E. coli* lysate ("TX-TL")[92,93] and a microfluidic device capable of emulating cellular growth and division[90] (Figure 4.1). Almost all prototyping can be done on linear DNA, which requires less than 8 hours to assemble and test. The cell-free framework provides a simplified and controlled environment that allows us to drastically reduce the design-build-test cycle[33].
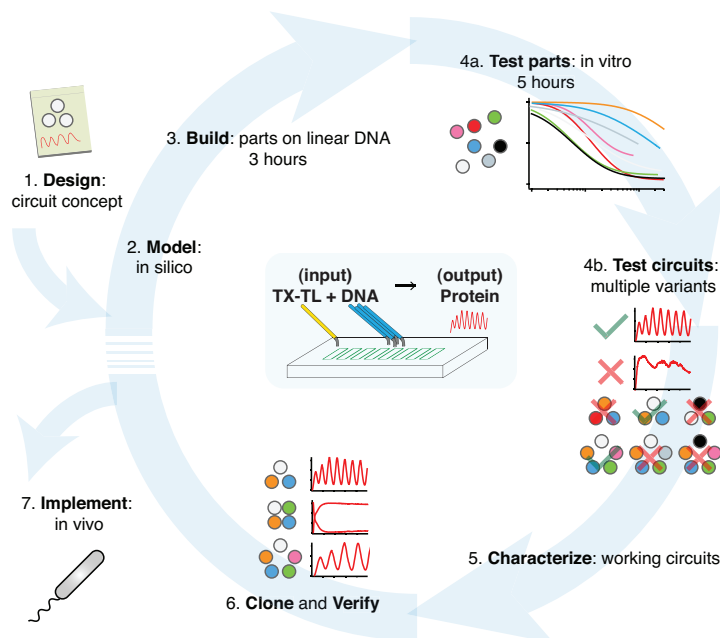
Figure 4.1 Cell-free framework allows for rapid and extensive characterization of biological systems.
Schematic representation of the design-build-test cycle using the cell-free framework. A design is first modeled to obtain intuition about the architecture. Parts are then assembled on linear DNA without cloning, and tested *in vitro*. With functional parts, circuit variants can then be tested and working circuits can be extensively characterized. Final circuits are cloned onto plasmids and implemented *in vivo*. Center shows the microfluidics device used. Input is a circuit encoded by linear or plasmid DNA and TX-TL *in vitro* reagent, which is then translated and transcribed into protein. For a specific example of the cell-free framework applied to engineering a 5-node oscillator network see Fig. S4.3.

We first asked whether our cell-free framework could be used to run and characterize an existing synthetic *in vivo* circuit and chose to test the repressilator[2] as a model circuit. We successfully implemented the original repressilator network in our cell-free framework and observed long-term sustained oscillations with periods matching the *in vivo* study (Figure 4.2). We compared the original repressilator to a modified version containing a point mutation in one of the CI repressor binding sites in the promoter regulating LacI (Figure 4.2**a**). This mutation increases the repressor concentration necessary for half-maximal repression (K_M), and reduces cooperativity[94]. At long dilution times (t_d) both circuits oscillated, but with shifted absolute reporter protein concentrations (Figure 4.2**b**). At decreasing dilution times amplitudes decreased and periods became faster with a linear dependence on t_d. Faster dilution times, however, did not support oscillations for the modified network (Figure 4.2**b-c**). Experimentally, the range of dilution times supporting oscillations can serve as a measure for robust oscillator function, which generally diminishes with decreasing synthesis rates or when binding of one repressor to its promoter is weakened as in the O_R2^* mutant (**Fig. S4.1**). To give another example for an experimental characterization that would be challenging to perform in a cellular environment we analyzed the repressilator network in phase space showing limit cycle oscillations and invariance to initial conditions (Figure 4.2**d**).
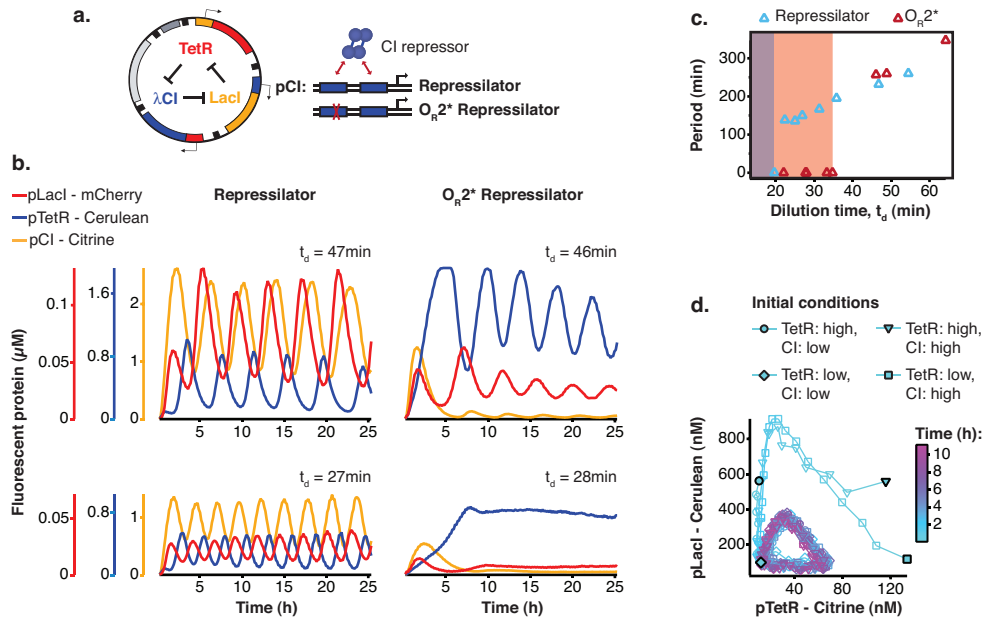
Figure 4.2 Cell-free repressilator characterization.
a, Application of the cell-free framework to characterize the original repressilator[2] and a modified version with a point mutation in the CI promoter (O_R2^*) located in one of the binding sites of the CI repressor. **b,** Expression from the three promoters of the repressilator and the O_R2^* version at different dilution times. **c,** Oscillation periods of the repressilator as a function of dilution time. In the O_R2^* version sustained oscillations were supported in a narrower range of dilution times as compared to the original repressilator network. **d,** Phase portrait of repressilator oscillations starting from different initial TetR and CI repressor concentrations.

The cell-free framework also allows rapid characterization of individual network components. We measured the transfer functions of repressor-promoter pairs in the repressilator network (Figure 4.3, **Fig. S4.2a,b, Table S4.1**) and found that the network is symmetric in terms of transfer functions. In the CI promoter O_R2^* mutant we observed the expected shift in K_M and decreased steepness of the transfer function. We also characterized TetR repressor homologs as building blocks for novel negative feedback circuits (Figure 4.3**a**) and with the exception of QacR observed similar transfer functions as observed *in vivo*[95] (**Fig S4.2c**).

Using three new repressors, BetI, PhlF and SrpR, we constructed a novel 3-node (3n) circuit (3n1) and observed high-amplitude oscillations over a broad range of dilution times with the same dependence of amplitude and period on t_d as for the repressilator (Figure 4.3**b**). In our characterization of the repressilator network and the 3n1 oscillator we found dilution rates to be critical for the existence, period and amplitude of oscillations. Protein degradation is similar to dilution in that it results in removal of repressor proteins. In order to study the effect of degradation we constructed a second 3n network (3n2) using TetR, PhlF and SrpR repressors on linear DNA. One version of the circuit used strong ssrA ClpXP degradation tags, while the second used untagged repressors. We observed oscillations for both circuits (Figure 4.3**c**). However, the circuit without ssrA-tag mediated protein degradation exhibited slower oscillations, which extended to lower dilution times, showing that protein degradation, just like dilution, affects oscillator function and period. Effects of ClpXP-mediated protein degradation, which have been shown to be important for existence and frequency of oscillations *in vivo*[96,97], can thus be emulated in a cell-free environment.

Theory predicts that ring architectures built from an odd number of repressors oscillate, while even-numbered architectures have stable steady states[98,99]. We experimentally built and tested a 4-node circuit from LacI, TetR, PhlF and SrpR on linear DNA. Initial pulses of LacI inducer IPTG or TetR inducer aTc allowed us to switch expression into either one of the two stable steady states (Figure 4.3**d**).

Encouraged by the robust oscillations observed in the 3n networks, we built two 5-node ring oscillators (5n) to test our prototyping environment on a novel synthetic network architecture (Figure 4.3**e**). Despite their considerable complexity both circuits oscillated over a broad range of dilution times with the expected period lengthening, which could be as long as 19h. Comparing all ssrA-tagged 3n and 5n ring architectures, we show that the observed periods could be accurately predicted for all four networks by computational simulations (Figure 4.3**f**). Our cell-free framework allows testing and characterization of complex networks including verifying networks cloned onto a single plasmid, which is the closest approximation to *in vivo* implementation (**Fig. S4.3**).
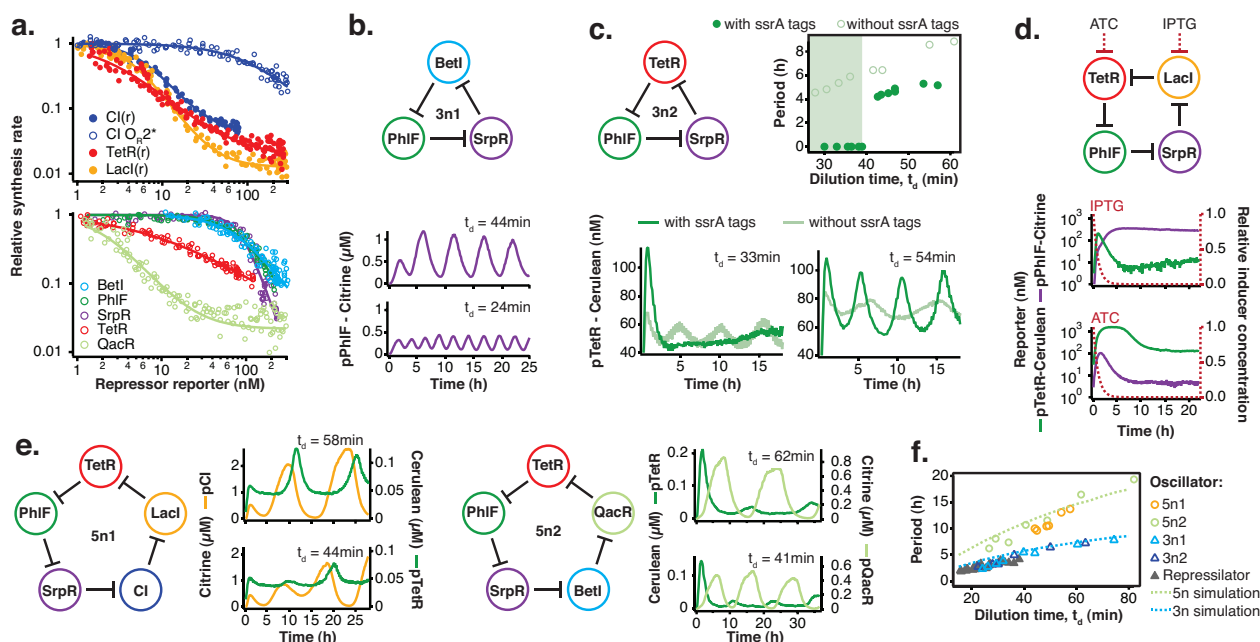
Figure 4.3 Cell-free prototyping and characterization of novel cyclic negative feedback circuits.
a, Transfer functions of the repressilator repressor-promoter pairs (top) and TetR homologs (bottom). The TetR repressor was tested against two different promoters: the promoter used in the repressilator (top panel) and the J23119-TetR promoter [95] (bottom panel). Lines are Hill function fits. **b,** Oscillations of a novel 3-node ring oscillator (3n1) constructed on plasmid DNA. **c,** Two versions of a second 3-node ring oscillator (3n2) on linear DNA were used to study the effect of ClpXP degradation on oscillator function. One version was ssrA-tagged on all repressor genes while the other version did not carry degradation tags on the repressors. The same reporter with a medium-strength degradation tag was used in both versions. **d,** A 4-node cyclic negative feedback network on linear DNA has two stable steady states that depend on the initial conditions. IPTG switched the network into the state where pPhlF was on and pTetR off. An initial pulse of aTc resulted in the opposite stable steady state. **e,** Two 5-node negative feedback architectures oscillated with longer periods than our 3-node networks as predicted by simulations (Supplementary Information) **(f).**

To validate our cell-free approach *in vivo* we cloned the 3n1 and 3n2 networks onto low-copy plasmids and co-transformed each with a medium-copy reporter plasmid into *lacI*- JS006 *E. coli*[80]. When tested on a microfluidic device (mother machine[100]), both 3n oscillators showed regular oscillations with periods of 6 ±1 hours for at least 30 hours (Figure 4.4**a**). Both oscillators were surprisingly robust as all cells undergoing healthy cellular division oscillated (n = 71) (**Fig. S4.4**).

We next tested our 5n oscillators *in vivo*. Due to loading effects[101], 5n1 was not viable when co-transformed with a strong reporter. When tested with a low expression strength reporter both 5n oscillators showed robust oscillations that were maintained for at least 70 hours, and over 95% of all analyzed traps containing healthy cells oscillated (n = 104). In addition, both 5n networks oscillated with similar periods: 8 hours for 5n1, and 9 hours for 5n2 (Figure 4.4**b, Fig. S4.4**).

We also tested both 3n oscillators on a CellASIC system, which allows planar single-layer colony formation. In this system we observed a striking population level synchronization of daughter cells inheriting the oscillator state from their mother cells (Figure 4.4**c**, **Fig. S4.5a**). Synchronization was also apparent when using three different fluorescent reporters simultaneously (**Fig. S4.5b**). We did not observe population level synchronization in the original repressilator, the O_R2^* mutant (**Fig. S4.5c**) nor the 5n networks. Synchronized oscillations were not reported with the original repressilator[2], and have only been observed in oscillators using intercellular communication[102,103]. We hypothesize that the 3n1 and 3n2 synchronization is due to increased repressor concentrations as compared to the original repressilator network (**Fig. S4.5d**), which increases the inheritance of the period phenotype and minimizes the rapid de-synchronization expected from stochastic cellular protein fluctuations[104]. However, a quantitative characterization of the synchronization phenotype requires more in depth understanding of stochastic effects *in vivo*.

Because cells were synchronized, we were able to analyze the population as a whole to make general conclusions of oscillator behavior. We varied dilution time by using different media conditions and media flow rates, and found a direct relationship between division times and period, consistent with the *in vitro* data collected. Oscillation periods of the 5n oscillators were also consistent with our *in vitro* results and showed a similar dependence on doubling time (Figure 4.4**d**).

Finally, we compared 3n1 and 5n2 with weak and strong reporters *in vivo* to analyze the effect of protein degradation on the oscillator period. We theorized that given a constant concentration of ClpXP, stronger reporters would result in more ClpXP loading, thereby slowing the period of oscillation. ClpXP is thought to influence oscillation dynamics *in vivo* in this manner[96]. We found that in the mother machine, both the period distributions of 3n1 and 5n2 showed this characteristic (Figure 4.4**e**), which reflects our *in vitro* findings of differential –ssrA tag dependent period length (Figure 4.3**c**).

We demonstrated the utility of our cell-free framework for biological systems engineering and component characterization. We observed some differences between the *in vitro* and cellular environment, particularly in the difficulty of predicting cellular toxicity and loading effects of the 5n oscillators *in vivo*. While more work is necessary describing and explaining differences between *in vitro* and *in vivo* environments[33,34], the observed behavior of complex networks in our cell-free environment reflected network behavior *in vivo* well. The cell-free framework is thus a powerful emulator of the cellular environment allowing precise control over experimental conditions and enabling studies that are difficult or time consuming to perform in cells. With further developments in cell-free lysate systems and supporting technologies, the *in vitro* approach is posed to play an increasing role in biological systems engineering and provides a unique opportunity to design, build, and analyze biological systems.
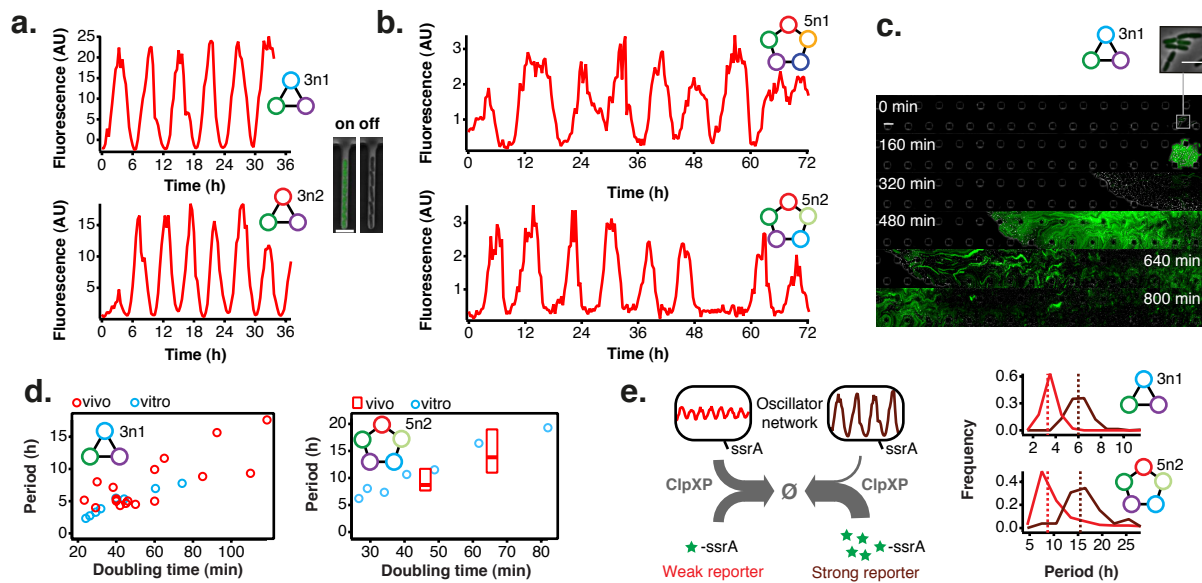
Figure 4.4 Novel 3-node and 5-node ring oscillators *in vivo*.
a, Time series traces of 3-node ring oscillators running in *E. coli* (mother machine). Single trap traces of 3n1 and 3n2 observed for 36 h *in vivo* using a strong pPhlF sfGFP-ssrA reporter and a representative image from an "on" and "off" state of oscillation. Scale bar: 5 µm. **b,** Time series traces of 5-node ring oscillators running in *E. coli* (mother machine). Single trap traces of 5n1 and 5n2 observed for 72 h *in vivo* using a weak pPhlF sfGFP-ssrA reporter. **c,** 3n1 displays phase synchrony *in vivo* (CellASIC). Time series micrographs of 3n1 under a strong pPhlF sfGFP-ssrA reporter every 160 min; inset shows individual cells of the initial microcolony. Scale bar: 10 µm and 5 µm (inset). **d,** Relationship between period and division time *in vivo*. Left, 3n1 *in vivo* under a strong pPhlF sfGFP-ssrA reporter. The *in vitro* data is shown for comparison. Each point in the *in vivo* data corresponds to the period and division time from a CellASIC experiment run under different media type and flow rates. Right, 5n2 *in vivo* under a weak pPhlF sfGFP-ssrA reporter. *In vivo* periods determined at 29ºC and 21ºC growth temperature in mother machine experiments. Boxes represent the inner quartile range with the median. **e,** Influence of reporter concentration on oscillation periods by competing for ClpXP degradation. Left, with constant amounts of ClpXP the reporter concentration affects repressor degradation and thus oscillation period. Histograms of the periods observed with a weak and a strong pPhlF sfGFP-ssrA reporter for both 3n1 and 5n2 run in the mother machine. Dashed lines indicate the medians.

4.3   Methods

DNA and strain construction

DNA was constructed using either Golden Gate Assembly or Isothermal Assembly. For linear DNA, all DNA was constructed using previously published Rapid Assembly protocols on a "v1-1" vector [33]. Linear DNA constructs are summarized in **Table S4.2**. The original repressilator plasmid, pZS1 [2] was used as a template for initial characterization and for construction of the O_R2^* mutant. Transfer function plasmids were constructed by Transcriptic, Inc. For other plasmids, partial sequences were either obtained from Addgene [95] or synthesized on gBlocks or ssDNA annealed oligonucleotides (Integrated DNA Technologies). Specific plasmids required secondary-structure free segments, which were designed by R2oDNA [105]. JS006 [80] was co-transformed with origin-of-replication compatible plasmids to create engineered strains. Specifically, negative-feedback oscillator units were cloned onto pSC101* low copy plasmids (ampR or kanR), while reporters were cloned onto colE1 medium copy plasmids (kanR or cmR) (**Tables S4.3 and S4.4**). To modulate the reporter copy number, all experiments were conducted below 37°C [106]. Strain passage was minimized to avoid plasmid deletions due to the *recA+* nature of JS006 and the high complexity of oscillator plasmids or triple-reporter plasmid. Based on the *in vitro* and *in silico* results, we used strong transcriptional and translational [107] units to maximize gain.

TX-TL reactions

Preparation of TX-TL was conducted as described previously[93], but using strain "JS006" co-transformed with Rosetta2 plasmid and performing a 1:2:1 extract:DNA:buffer ratio. This resulted in extract "eZS4" with: 8.7 mg/mL protein, 10.5 mM Mg-glutamate, 100 mM K-glutamate, 0.25 mM DTT, 0.75 mM each amino acid except leucine, 0.63 mM leucine, 50 mM HEPES, 1.5 mM ATP and GTP, 0.9 mM CTP and UTP, 0.2 mg/mL tRNA, 0.26 mM CoA, 0.33 mM NAD, 0.75 mM cAMP, 0.068 mM folinic acid, 1 mM spermidine, 30 mM 3-PGA, 2% PEG-8000. For experiments utilizing linear DNA GamS was added to a final concentration of 3.5 µM[33].

Steady-state reactions

Experiments were performed in a microfluidic nano-reactor device as described previousely[90,93] with some modifications to optimize the conditions for the lysate-based TX-TL mix. Reaction temperature was 33°C. Lysate was diluted to 2x of the final concentration in 5 mM HEPES 5 mM NaCl buffer (pH 7.2). The reaction buffer mix was combined with template DNA and brought to a final concentration of 2x. For a 24 h experiment 30 µl of these stocks were prepared. During the experiment, lysate and buffer/DNA solutions were kept in separate tubing feeding onto the chip, cooled to approximately 6ºC, and combined on-chip. We ran experiments with dilution rates (μ) between approximately 2.8 and 0.5 h^{-1}, which corresponds to dilution times, $t_d = \ln(2) \mu^{-1}$, between 15 and 85 min. These were achieved with dilution steps exchanging between 7 and 25% of the reactor volume with time intervals of 7 to 10 min, which alternately added fresh lysate stock or fresh buffer/DNA solution into the reactors. Dilution rates were calibrated before each experiment. Initial conditions for the limit cycle analysis of the repressilator network were set by adding pre-synthesized repressor protein at the beginning of each experiment. For this, CI repressor (together with Citrine reporter) and TetR repressor (together with Cerulean reporter) were expressed for 2.5h in batch. On chip the initial reaction was mixed to be composed of 25% pre-synthesis reaction and 75% fresh TX-TL mix and repressilator template DNA. Then, the experiment was performed at a t_d of 19.2 ± 0.3 min. Initial conditions for the 4-node experiment were 2.5µM aTc or 250µM IPTG, and the experiment was performed at a t_d of 44.5 ± 0.9 min. DNA template concentrations used in steady-state reactions are listed in **Table S4.5**. Arbitrary fluorescence values were converted to absolute concentrations from a calibration using purified Citrine, Cerulean, and mCherry, which were prepared using previously published protocols utilizing a His6 purification method followed by size-exclusion chromatography and a Bradford assay to determine protein concentration[33].

Transfer function measurement

Transfer functions of the repressor – promoter pairs were determined in the nano-reactor device at a minimum of two different dilution times (**Fig. S4.2**). All tested promoters were cloned into a plasmid in front of a BCD7 ribosomal binding site and the Citrine open reading frame. A non-saturating concentration of 1nM plasmid was used in the experiment. The repressors were expressed from linear templates carrying the J23151 promoter and the BCD7 ribosomal binding site with time-varying concentrations, which were increased from 0 to 2.5nM and decreased back to 0 during the course of the experiment[90]. Simultaneousely we expressed Cerulean as a reporter for the repressor concentration from a linear template at an identical concentration as the repressor template. From the concentration of the Citrine reporter we calculated the synthesis rate of the fluorescent protein over time using a model of steady state protein synthesis in the nano-reactor device[90],

(1) $\qquad P_d(t + \Delta t) = P_d(t) + syn(t) \cdot \Delta t - mat \cdot P_d(t) \cdot \Delta t - dil \cdot P_d(t)$

(2) $\qquad P_f(t + \Delta t) = P_f(t) + mat \cdot P_d(t) \cdot \Delta t - dil \cdot P_f(t)$

where P_d and P_f are dark and fluorescent reporter concentration respectively, t is time, Δt is the time interval between dilution steps, *dil* is the volume fraction replaced per dilution step, which was determined during the calibration of the device, and *mat* is maturation rate of the fluorescent protein. Maturation times of Citrine and Cerulean were determined as described previously[90] and were 15 ±4 min for Cerulean and 29 ±3 min for Citrine. Dark fluorescent protein was calculated from equation (2):

(3) $\qquad P_d(t) = \dfrac{P_f(t + \Delta t) - P_f(t) + dil \cdot P_f(t)}{mat \cdot \Delta t}$

and the synthesis rate was calculated from equation (1):

(4) $\qquad syn(t) = P_d(t + \Delta t) - P_d(t) + mat \cdot P_d(t) \cdot \Delta t + dil \cdot P_d(t)$.

We used the sum of measured fluorescent Cerulean concentration and equation (3) for dark Cerulean as a measure of the total repressor protein present at any time during the experiment.

The synthesis rates were normalized to their respective maximal values (v_{max}) and plotted against the concentration of the repressor reporter using only repressor concentrations higher than 1nM. The transfer curves were then fit to a Hill function

(5) $\qquad y = f(x) = y_{min} + (1 - y_{min}) \dfrac{K_M^{\,n}}{K_M^{\,n} + x^n}$

where y is the synthesis rate, y_{min} is the minimum synthesis rate, *n* is the Hill coefficient and K_M is the Michaelis Menten constant for half maximal promoter activity. The fitting was performed in Igor Pro using orthogonal distance regression with ODRPACK95 assuming a 9% error in the measurements of Citrine and Cerulean fluorescence.

V_{max} measurements

Relative promoter strengths (v_{max} values) were determined using the transfer function promoter plasmids. *In vitro* strengths were determined in 5 µl TX-TL reactions at a DNA template concentration of 1nM. Reactions were assembled in 384-well plates, overlaid with 35 µl Chill-Out Liquid wax (BioRad) and analyzed using a Biotek SynergyMx plate reader set to 33ºC reaction temperature, and reading Citrine fluorescence with Exc:510±9nm and Em:540±9nm. For comparison, Citrine fluorescence at 6h was normalized to the value of pLacI.

In vivo strengths were determined using *E. coli* JS006 transformed with the same plasmids. Cells were grown at 29ºC in MOPS medium supplemented with 0.4% glycerol and 0.2% casaminoacids. For each strain, three independent overnight cultures were diluted 1:50 and grown to mid-log phase. They were then diluted to a starting OD_{600} of 0.15 into 100 µl growth medium in a 96-well plate and grown in the plate reader at 29ºC with periodic shaking measuring Citrine fluorescence. Fluorescence values were normalized to OD resulting in steady state values after 2 h. Average steady state values were normalized to pLacI for comparison with the *in vitro* measurement.

***In vivo* experiments**

Mother machine[100] experiments were conducted with custom-made microfluidic chips (mold courtesy of M. Delincé and J. McKinney, EPFL). *E. coli* cells were trapped in channels of 30 μm length, 2 μm width and 1.2 μm height. Before loading onto the device, cells were grown from a frozen stock to stationery phase. Cells were then concentrated 10-fold and loaded onto the chip. Experiments were performed using LB medium supplemented with 0.075% Tween-20 at a flow rate of 400 μl/h. Oscillation traces were collected from single mother machine traps using the background subtracted average fluorescence intensity of the entire trap.

CellASIC experiments were conducted using B04A plates (Merck Millipore, Darmstadt Germany). Flow rates were varied between 0.25 psi – 2 psi. Cells were grown from frozen stock in media at running temperature to stationery phase. Cells were then diluted 1:100 for 2 hours, and loaded on a equilibrated plate at 1:1000 or less to achieve single-cell loading efficiencies per chamber. To vary cellular doubling times, different growth media were used: LB (BD Biosciences), M9CA (Sigma Aldrich) with 0.2% glucose, 2xYT (MP Bio), MOPS EZ Rich (Teknova).

Cells were imaged in time series every 10-20 min using a 100x phase objective minimizing both lamp intensity (12% Xcite 120, Excelitas Inc. Waltam MA or 1-2% CoolLED pE-2, Custom interconnected Ltd., UK) and exposure times (<500ms) to limit photo-toxicity.

Analysis of *in vivo* data

Images were processed and stitched[108], if necessary, using Fiji/ImageJ[109]. Fluorescence traces of cell populations with synchronized oscillations were extracted from CellASIC movies using background corrected mean fluorescence intensity from the entire field of view. For cells that were not synchronized over the complete field of view, we tracked regions of oscillating sister cells at the edge of the microcolony. We used ImageJ to define polygonal regions around those cells and manually shifted the polygonal region to track the front of growing cells. Periods were determined from fluorescence traces derived from mother machine and CellASIC movies by measuring the time from one oscillation peak to the next peak. Doubling times were estimated by averaging over the doubling times of at least ten individual cells.

Model

We consider an *n*-node negative cyclic feedback biocircuit and denote the genes, mRNAs and proteins by $G_1, G_2, ..., G_n$, and $M_1, M_2, ..., M_n$ and $P_1, P_2, ..., P_n$, respectively. Let $r_i(t)$ and $p_i(t)$ denote the concentrations of mRNA M_i and protein P_i, respectively. For example, the novel 3-node ring oscillator in Figure 4.3**b** is defined by $n = 3$, $r_1(t) = $ [BetI mRNA], $r_2(t) = $ [PhlF mRNA], $r_3(t) = $ [SrpR mRNA], $p_1(t) = $ [BetI protein], $p_2(t) = $ [PhlF protein], $p_3(t) = $ [SrpR protein].

Our mathematical model considers transcription, translation and degradation of mRNA and protein molecules as summarized in the box below, where a_i and b_i represent the degradation rates of M_i and P_i, respectively, and c_i and β_i are the translation and transcription rates. The constants K_{i-1} and v_i are the Michaelis-Menten constant and the Hill coefficient associated with the protein P_{i-1} and the corresponding promoter on gene G_i. We hereafter use subscripts 0 and $n+1$ as the substitutes of n and 1, respectively, to avoid notational clutter.

Using the law of mass action and the quasi-steady state approximation, the dynamics of the mRNA and protein concentrations can be modeled by the following ordinary differential equations (ODE)

$$\dot{r}_i(t) = -(a_i + \mu)r_i(t) + \beta_i g \frac{K_{i-1}^{v_i}}{K_{i-1}^{v_i} + p_{i-1}^{v_i}(t)},$$ (1)

$$\dot{p}_i(t) = -(b_i + \mu)p_i(t) + c_i r_i(t),$$

where $i = 1, 2, \ldots, n$, and g is the concentration of the circuit plasmid. The constant μ is the dilution rate of mRNA and proteins by the microfluidic device. The dilution time of the microfluidic device is defined by

$$T_d := \frac{\ln(2)}{\mu}.$$ (2)

Stoichiometry and reaction rates:

Description	Reaction	Reaction rate
Transcription of M_i	$G_i + P_{i-1} \rightarrow G_i + P_{i-1} + M_i$	$\beta_i \dfrac{K_{i-1}^{v_i}}{K_{i-1}^{v_i} + p_{i-1}^{v_i}}$
Translation of M_i	$M_i \rightarrow M_i + P_i$	$c_i r_i$
Degradation of M_i	$M_i \rightarrow \emptyset$	$a_i r_i$
Degradation of P_i	$P_i \rightarrow \emptyset$	$b_i p_i$

The ODE model (1) was numerically simulated using ode45 solver of MATLAB R2013b to obtain qualitative insight into the period as well as the oscillatory parameter regime (Figure 4.3f and Fig. S4.1b). The parameters summarized in the following table were used for the simulations.

Parameters used for simulations:

	Description	Parameter value
a_i	Degradation rate of mRNAs (min^{-1})	ln(2)/8 (half-life time: 8 minutes)
b_i	Degradation rate of proteins (min^{-1})	ln(2)/90 (half-life time: 90 minutes)
β_i	Transcription rate (nM • min^{-1} • plasmid concentration^{-1})	0.4
c_i	Translation rate (nM • min^{-1} • mRNA concentration^{-1})	0.5
K_i	Michaelis-Menten constant (nM)	5.0
v_i	Hill-coefficient	2.0

The plasmid concentration g was set as $g = 5.0$ nM for Figure 4.3f. The initial concentrations for the simulations were $r_1(0) = 30$, $p_1(0) = 0$ and $r_i(0) = p_i(0) = 0$ for $i = 2, 3, \ldots, n$.

The period of oscillations was calculated based on the autocorrelation of the simulated protein concentration $p_1(t)$. More specifically, let

$$R(\tau) := \int_{T_1}^{T_2} p_1(t + \tau)p_1(t)dt,$$ (3)

where T_1 is a positive constant such that $p_1(t)$ is steady state at $t = T_1$, and T_2 is a sufficiently large constant compared to the period of oscillations. The period of oscillations T_{period} was determined by $T_{\text{period}} = \min_{\tau > 0} \text{argmax}_\tau R(\tau)$. The

simulation result is also consistent with the analytic estimation of the oscillation period in Hori et al. [99] in that the period increases monotonically with the dilution time T_d.

The parameter region for oscillations (Fig. S4.1a) was obtained based on the analysis result (Theorem 3) by Hori et al. [110]. Since parameter values do not depend on the subscript i as shown in the parameters table above, we remove the subscript i and define $a := a_1 (= a_2 = \ldots a_n)$. In the same way, we define b, c, β, K and v.

It was shown that the protein concentrations p_i ($i = 1, 2, \ldots, n$) oscillate if both of the following inequalities are satisfied[110].

$$v > W(n, Q), \tag{4}$$

$$c\beta > \left(\frac{W(n,Q)}{v - W(n,Q)}\right)^{\frac{1}{v}} \left(\frac{v}{v - W(n,Q)}\right) K(a + d)(b + d), \tag{5}$$

where

$$W(n, Q) := \frac{2\left(-\cos\left(\frac{\pi}{n}\right) + \sqrt{\cos^2\left(\frac{\pi}{n}\right) + Q^2 \sin^2\left(\frac{\pi}{n}\right)}\right)}{Q^2 \sin^2\left(\frac{\pi}{n}\right)}, \text{ and } Q := \frac{\sqrt{(a+d)(b+d)}}{(a+b+2d)/2}.$$

To obtain the parameter region in Fig. S4.1a, we substituted $n = 3$ and the parameters shown in the table above into the right-hand side of the inequality condition (5), then we varied $T_d (= \ln(2)/\mu)$ between 5 to 80. The inequality (4) was always satisfied for these parameters.

The parameter region of Fig. S4.1c was obtained by the local stability analysis of the model (1). The previous theoretical result [110] showed that the model (1) has a unique equilibrium point and the protein concentrations p_i ($i = 1, 2, \ldots, n$) show stable oscillations if the Jacobian matrix evaluated at the equilibrium point has an eigenvalue in the open right-half complex plane. Based on this result, we computed the Jacobian eigenvalues with varying K_3, which we denote by K_{cI}, and T_d. The values in the parameters table above were used for the other parameters. The plasmid concentration was set as $g = 5.0$ nM in the computation.

4.4 Supplementary Information
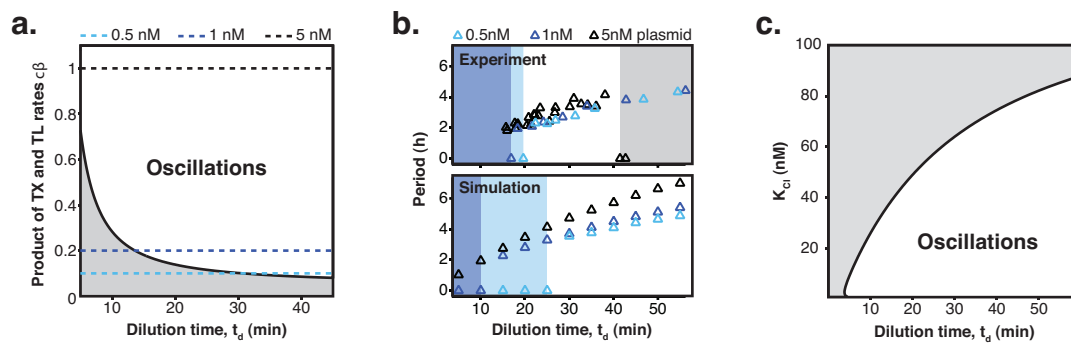
Figure S4.1 Oscillation parameter regime for a 3-node repressilator network in terms of dilution time.
a, Transcription (TX) and translation (TL) rates supporting oscillations at different dilution times for a 3-node repressilator network. **b,** We experimentally studied the effect of varying transcription rates on the WT repressilator by measuring the range of dilution times that supported sustained oscillations. Transcription rates could be rapidly adjusted by varying DNA template concentrations of the repressilator plasmid. For different DNA template concentrations, oscillations occurred in different ranges of dilution times. Markers at a period of 0 h indicate a stable steady state, and shaded regions highlight dilution times that did not support oscillations for a specific DNA template concentration. A simulation of the repressilator network produced similar results but did not capture loading effects on the biosynthetic machinery for high DNA template concentrations. **c,** Increasing the K_M value of one repressor, as for CI repressor in the O_R2^* repressilator version, reduces the range of dilution rates that support oscillations as indicated by our experimental results (**Fig. 2c**) (see Materials and Methods for details on model).
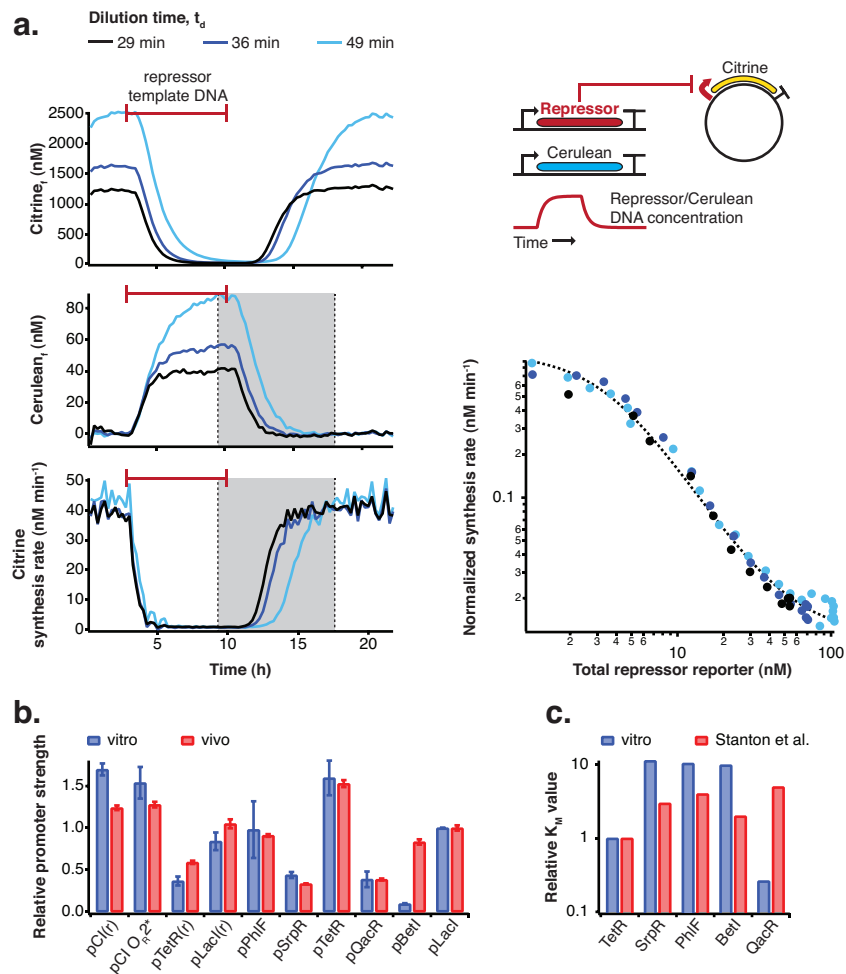
Figure S4.2 Repressor characterization.
a, Transfer functions of the repressor – promoter pairs were determined using the cell-free framework as described in the Methods. Shown are experimental results and analysis using LacI - pLacI(r) as an example. Synthesis rates from the promoter of interest could be followed by Citrine fluorescence. Varying repressor template DNA concentration over time allowed us to determine synthesis rates at different repressor concentrations. Cerulean was co-expressed with the repressor and served as reporter for repressor concentration. Transfer functions were obtained by plotting Citrine synthesis rates from highest to lowest repressor concentration (grey shaded area) against total Cerulean concentration and were identical for different dilution times set in the nano-reactor device. **b,** Comparison of relative promoter strengths (v_{max}), determined *in vitro* and *in vivo*. pCI(r), pTetR(r), and pLacI(r) are from[2]; pTetR is from[95] and pLacI from[111]. Error bars indicate standard deviations of three replicates. **c,** Comparison of K_M values measured *in vitro* in this study with K_M values determined *in vivo* by Stanton et al.[95]. K_M values were normalized to the K_M of TetR.
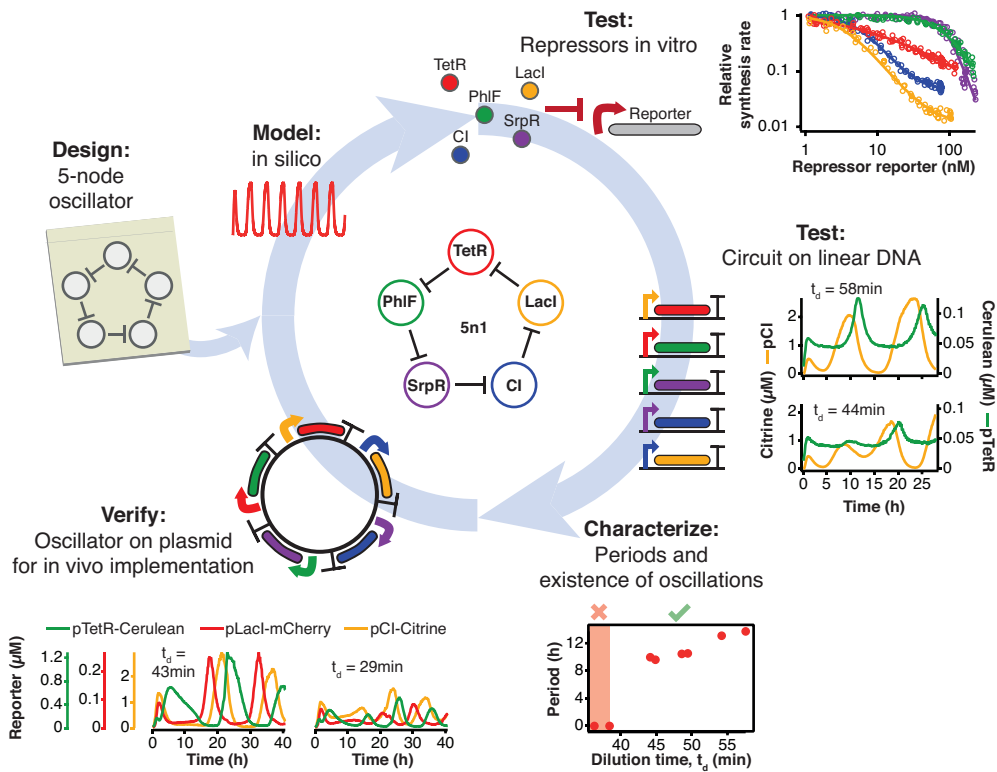
Figure S4.3 Engineering a 5-node negative feedback oscillator using the cell-free framework.
A novel network architecture, which shows the intended behavior *in silico* is first assembled on linear DNA using *in vitro* characterized parts. Initial circuit testing on linear DNA is advantageous because: i) linear DNA can be synthesized in a few hours, ii) it allows rapid testing of multiple circuit variants, iii) and allows expression strengths of network components to be easily tuned by varying their relative concentrations. A functional circuit can then be further characterized to identify parameter ranges that support the desired behavior and to experimentally test hypotheses. If an *in vivo* implementation is intended, the cloned plasmids are verified for correct function *in vitro* before *in vivo* implementation.
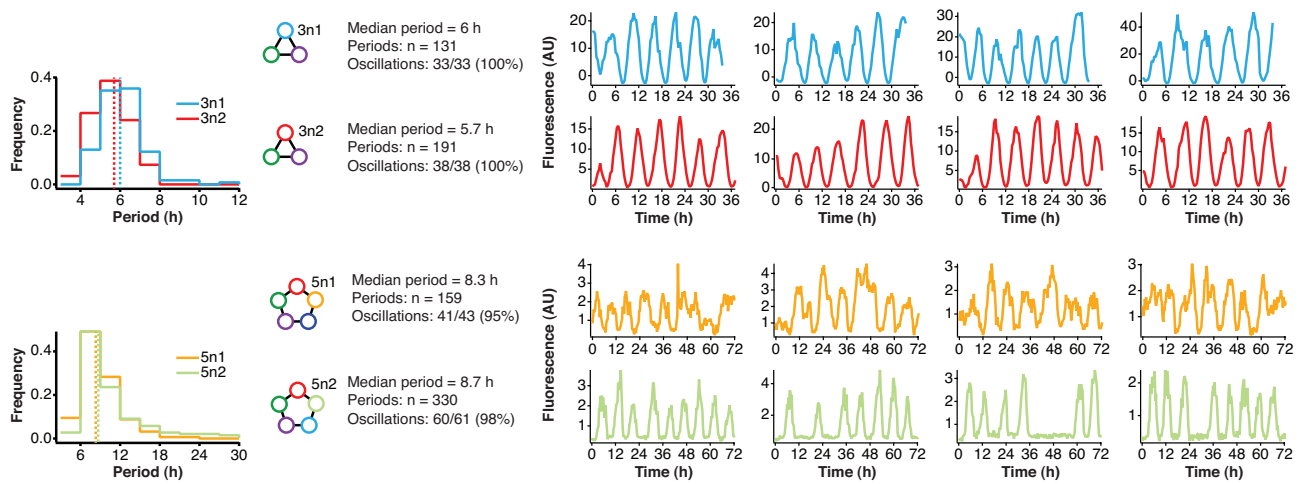
Figure S4.4 Robust oscillations of 3-node and 5-node oscillators *in vivo*.
3-node (top) and 5-node networks (bottom) oscillate with periods that depend on the network size *in vivo*. Shown are the distributions of observed period lengths with medians indicated by dashed lines. Both 3-node and 5-node networks exhibited robust oscillation with all growing cells oscillating for the 3-node networks and more than 95% of growing cells oscillating for the 5-node networks (defined as at least two distinct oscillation peaks per trace). Shown are four example traces for all oscillators in addition to the ones shown in **Fig. 4a-b**. Both 3-node networks were analyzed using a strong pPhlF sfGFP-ssrA reporter and the two 5-node networks were analyzed using a weak pPhlF sfGFP-ssrA reporter.
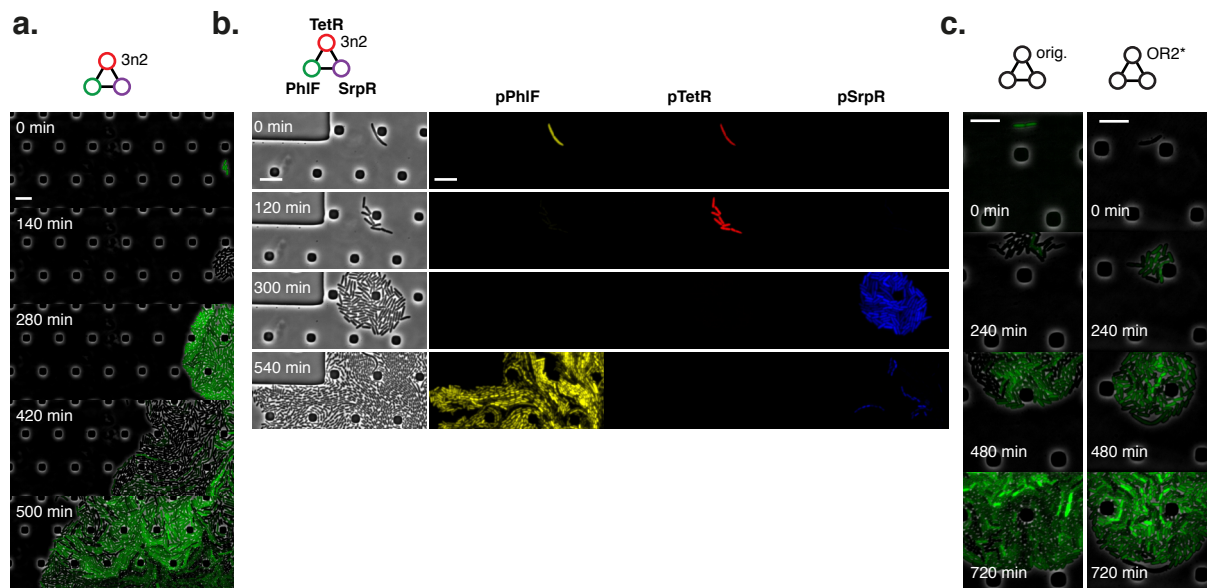
Figure S4.5 Population level synchronization of 3-node oscillators *in vivo*.
a, 3n2 oscillator displays phase synchrony *in vivo*. 3n2 is run under a strong pPhlF sfGFP-ssrA reporter in the CellASIC microfluidic device. **b,** 3n2 displays phase synchrony observing 3 reporters simultaneously. Reporters are a strong pPhlF Citrine-ssrA, pTetR mCherry-ssrA, and pSrpR Cerulean-ssrA. Shown is one oscillation cycle. **c,** Original repressilator and O_R2^* repressilator do not show phase synchrony. These are run under pTetR(r)-eGFP(ASV) in M9 minimal media; oscillations were not supported in LB. All scale bars: 10 μm.

Table S4.1 Transfer function parameters. Parameter values of repressor – promoter pairs were determined by fitting to the Hill equation as described in the Methods.

Name	K_M	n	y_{min}
CI – pCI[2]	5.9	1.9	0.04
CI – pCI(O$_R$2*)[94]	103	1.2	0
LacI – pLacI(r)[2]	4.1	1.9	0.01
TetR – pTetR(r)[2]	2.3	1.2	0.02
LacI – pLacI[111]	3.6	1.7	0.01
SrpR – pSrpR[95]	86	3.6	0
PhlF – pPhlF[95]	79	2	0
TetR – pTetR[95]	7.6	0.8	0
BetI – pBetI[95]	75.4	1.7	0
QacR – pQacR[95]	2.0	1.6	0.02

Table S4.2. Linear DNAs used in this study.

Name	Description	Notes
pJ23119-tetO-BCD2-phlF-ssrA(LAA)	# 3n2, 5n1, 4n	
pLacI-BCD2-tetR-ssrA(LAA)	& 5n1, 4n	
pLambdaCI-BCD2-lacI-ssrA(LAA)	% 5n1	
pPhlF-BCD2-srpR-ssrA(LAA)	# 3n2, 5n1, 4n	
pSprR-BCD2-lambdaCI-ssrA(LAA)	# 5n1	
pSrpR-BCD2-tetR-ssrA(LAA)	# 3n2	
pPhlF-BCD2-srpR	# 3n2/no-ssrA	
pSrpR-BCD2-tetR	# 3n2/no-ssrA	
pTetR-BCD2-phlF	# 3n2/no-ssrA	
pSrpR-BCD2-lacI-ssrA(LAA)	# 4n	
pBetI-BCD7-QacR-ssrA(LAA)	# 5n2	
pPhlF-BCD7-srpR-ssrA(LAA)	# 5n2	
pQacR-BCD7-tetR-ssrA(LAA)	# 5n2	
PSrpR-BCD7-BetI-ssrA(LAA)	# 5n2	
pTetR-BCD7-phlF-ssrA(LAA)	# 5n2	
pJ23151-BCD7-betI	$ transfer fxns	
pJ23151-BCD7-lacI	$ transfer fxns	
pJ23151-BCD7-lambdaCI	$ transfer fxns	
pJ23151-BCD7-phlF	$ transfer fxns	
pJ23151-BCD7-qacR	$ transfer fxns	
pJ23151-BCD7-srpR	$ transfer fxns	
pJ23151-BCD7-tetR	$ transfer fxns	
pLacI-BCD2-sfGFP-ssrA(LAA)	& test reporter	
pLambdaCI-BCD2-sfGFP-ssrA(LAA)	% test reporter	
pPhlF-BCD2-sfGFP-ssrA(LAA)	# test reporter	
pSrpR-BCD2-sfGFP-ssrA(LAA)	# test reporter	
pTetR-BCD2-sfGFP-ssrA(LAA)	# test reporter	

\# Promoter from Stanton et al. (2014)[95]
\$ Promoter from Anderson promoter panel
% Promoter from Elowitz and Leibler (2000)[2]
& Promoter from Lutz and Bujard (1997)[111]

Table S4.3. Plasmids used in this study.

Name	Description	Resistance	Copy number	Notes
pZS1	% Original repressilator plasmid	ampR	pSC101	
pZS1 w/ OR2* mutation	%	ampR	pSC101	minimize passages
pZE21-GFP(AAV)	% Original repressilator reporter (pTetO1)	kanR	colE1	
pZE21-eGFP(ASV)	% pZE21-GFPAAV with eGFP replacement	kanR	colE1	
pET21a(+)-Histag-Cerulean	Expression vector for Cerulean purification	ampR	colE1	c. Transcriptic Inc.
pET21a(+)-Histag-Citrine	Expression vector for Citrine purification	ampR	colE1	c. Transcriptic Inc.
pET21a(+)-Histag-mCherry	Expression vector for mCherry purification	ampR	colE1	c. Transcriptic Inc.
pTetR(r)-BCD7-Citrine	% transfer fxns	kanR	pSC101*	
pTetR-BCD7-Citrine	# transfer fxns	kanR	pSC101*	c. Transcriptic Inc.
pSrpR-BCD7-Citrine	# transfer fxns	kanR	pSC101*	c. Transcriptic Inc.
pQacR-BCD7-Citrine	# transfer fxns, in vitro reporter	kanR	pSC101*	c. Transcriptic Inc.
pPhlF-BCD7-Citrine	# transfer fxns, in vitro reporter	kanR	pSC101*	c. Transcriptic Inc.
pLacI-BCD7-Citrine	& transfer fxns	kanR	pSC101*	c. Transcriptic Inc.
pLacI(r)-BCD7-Citrine	% transfer fxns	kanR	pSC101*	
pCI(OR2*)-BCD7-Citrine	* transfer fxns	kanR	pSC101*	
pCI-BCD7-Citrine	% transfer fxns	kanR	pSC101*	
pBetI-BCD7-Citrine	# transfer fxns	kanR	pSC101*	c. Transcriptic Inc.
3n1	oscillator plasmid	kanR	pSC101*	minimize passages
3n2	oscillator plasmid	kanR	pSC101*	minimize passages
5n1	oscillator plasmid	kanR	pSC101*	minimize passages
5n2	oscillator plasmid	kanR	pSC101*	minimize passages
pBetI-BCD7-phlF-ssrA(LAA)	# for building 3n1	ampR	pSC101*	
pBetI-BCD7-qacR-ssrA(LAA)	# for building 5n2	ampR	pSC101*	
pLacO1-BCD7-tetR-ssrA(LAA)	& for building 5n1	ampR	colE1	amplify in lacI repressor strain
pLambdaCI-BCD7-lacI-ssrA(LAA)	% for building 5n1	ampR	colE1	amplify in lambdaCI repressor strain
pPhlF-BCD7-srpR-ssrA(LAA)	# for building 3n1, 3n2, 5n1, 5n2	ampR	pSC101*	
pQacR-BCD7-tetR-ssrA(LAA)	# for building 5n2	ampR	pSC101*	
pSrpR-BCD7-betI-ssrA(LAA)	# for building 3n1, 5n2	ampR	pSC101*	
pSrpR-BCD7-lambdaCI-ssrA(LAA)	# for building 5n1	ampR	pSC101*	
pSrpR-BCD7-tetR-ssrA(LAA)	# for building 3n2	ampR	pSC101*	
pTetR-BCD7-phlF-ssrA(LAA)	# for building 3n2, 5n1, 5n2	ampR	colE1	amplify in tetR repressor strain
pPhlF-BCD20-sfGFP-ssrA(LAA)	# 1 color strong reporter used in study	ampR	colE1	
pPhlF-BCD22-sfGFP-ssrA(LAA)	# 1 color weak reporter used in study	ampR	colE1	

pPhlF-BCD20-Citrine-ssrA(LAA)	# for building 3-color reporter plasmid	ampR	colE1	
pSrpR-BCD20-Cerulean-ssrA(LAA)	# for building 3-color reporter plasmid	ampR	colE1	
pTetR-BCD20-mCherry-ssrA(LAA)	# for building 3-color reporter plasmid	ampR	colE1	
3-color BCD20 reporter, pPhlF/pSrpR/pJ23119-tetO	3 color reporter plasmid	cmR	colE1	minimize passages
pTetR(r)-Citrine(ASV)	% in vitro reporter	kanR	colE1	
pTetR(r)-Cerulean(ASV)	% in vitro reporter	kanR	colE1	
pLacI(r)-mCherry(ASV)	% in vitro reporter	kanR	colE1	
pLacI(r)-Cerulean(ASV)	% in vitro reporter	kanR	colE1	
pCI-Citrine-(ASV)	% in vitro reporter	kanR	colE1	
pLacI(r)TetR(ASV)	% for initial conditions experiment	kanR	colE1	
pTetR(r)-CI(ASV)	% for initial conditions experiment	kanR	colE1	

Promoter from Stanton et al. (2014)[95]
$ Promoter from Anderson promoter panel
%   Promoter from Elowitz and Leibler (2000)[2]
&   Promoter from Lutz and Bujard (1997)[111]
*   Promoter from Rosenfeld et al. (2005)[94]

Table S4.4. Strains used in this study.

Name	*E. coli* type	Resistance	Notes
Rosetta2	JS006	cmR	
pZS1 + pZE21-GFP(AAV)	JS006	kanR ampR	
pET21a(+)-Histag-Citrine	BL21-DE3	ampR	
pET21a(+)-Histag-Cerulean	BL21-DE3	ampR	
pET21a(+)-Histag-mCherry	BL21-DE3	ampR	
3n1 + pPhlF-BCD20-sfGFP-ssrA(LAA)	JS006	kanR ampR	minimize passages
3n1 + pPhlF-BCD22-sfGFP-ssrA(LAA)	JS006	kanR ampR	minimize passages
3n2 + pPhlF-BCD20-sfGFP-ssrA(LAA)	JS006	kanR ampR	minimize passages
3n2 + pPhlF-BCD22-sfGFP-ssrA(LAA)	JS006	kanR ampR	minimize passages
5n1 + pPhlF-BCD20-sfGFP-ssrA(LAA)	JS006	kanR ampR	cells unhealthy, minimize passages
5n1 + pPhlF-BCD22-sfGFP-ssrA(LAA)	JS006	kanR ampR	minimize passages
5n2 + pPhlF-BCD20-sfGFP-ssrA(LAA)	JS006	kanR ampR	minimize passages
5n2 + pPhlF-BCD22-sfGFP-ssrA(LAA)	JS006	kanR ampR	minimize passages
3n2 + 3-color BCD20 reporter, pPhlF/pSrpR/pJ23119-tetO	JS006	kanR cmR	minimize passages
pZS1 + pZE21-eGFP(ASV)	JS006	kanR ampR	
pZS1 w/ OR2* mutation + pZS21-eGFP(ASV)	JS006	kanR ampR	

Table S5. DNA concentrations used in experiments.

Experiment	DNA and concentration	Type of DNA
Repressilator orig./O$_R$2*, 3color	Repressilator pZS1 or pZS1 w/ O$_R$2* mutation, 0.5 nM (if not otherwise indicated)	Plasmid
	pTetR(r)-Cerulean(ASV), 5 nM	Plasmid
	pLacI(r)-mCherry(ASV), 5 nM	Plasmid
	pCI-Citrine(ASV), 5 nM	Plasmid
Repressilator, initial conditions	**Reaction in nano-reactor:**	
	Repressilator pZS1, 5 nM	Plasmid
	pLacI(r)-Cerulean(ASV), 5 nM	Plasmid
	pTetR(r)-Citrine-(ASV), 5 nM	Plasmid
	Pre-synthesis reaction (CI):	
	pTetR(r)-Citrine(ASV), 5 nM	Plasmid
	pTetR(r)-CI(ASV), 5 nM	Plasmid
	Pre-synthesis reaction (TetR):	
	pLacI(r)-Cerulean(ASV), 5 nM	Plasmid
	pLacI(r)TetR(ASV), 5 nM	Plasmid
Response curve measurements	Promoter plasmid: pXXX-BCD7-Citrine, 1 nM	Plasmid
	Repressor template: pJ23151-BCD7-XXX, 0-2.5 nM	Linear
	Repressor reporter: pJ23151-BCD7-Cerulean, 0-2.5 nM	Linear
3n1	3n1 oscillator plasmid, 5 nM	Plasmid
	pPhlF-BCD7-Citrine, 2.5 nM	Plasmid
3n2	pJ23119-tetO-BCD2-phlF-ssrA(LAA), 1.5 nM	Linear
	pPhlF-BCD2-srpR-ssrA(LAA), 12 nM	Linear
	pSrpR-BCD2-tetR-ssrA(LAA), 24 nM	Linear
	pTetR(r)-Cerulean(ASV), 5 nM	Plasmid
3n2/no-ssrA	pJ23119-tetO-BCD2-phlF, 1.5 nM	Linear
	pPhlF-BCD2-srpR, 12 nM	Linear
	pSrpR-BCD2-tetR, 24 nM	Linear
	pTetR(r)-Cerulean(ASV), 5 nM	Plasmid
4n	pJ23119-tetO-BCD2-phlF-ssrA(LAA), 0.75 nM	Linear
	pLacI-BCD2-tetR-ssrA(LAA), 6 nM	Linear
	pPhlF-BCD2-srpR-ssrA(LAA), 6 nM	Linear
	pSrpR-BCD2-lacI-ssrA(LAA), 12 nM	Linear
	pTetR(r)-Cerulean(ASV), 2.5 nM	Plasmid

	pLacI(r)-mCherry(ASV), 2.5 nM	Plasmid
	pPhlF-BCD7-Citrine, 2.5 nM	Plasmid
5n1	pJ23119-tetO-BCD2-phlF-ssrA(LAA), 1.1 nM	Linear
	pLacI-BCD2-tetR-ssrA(LAA), 16.8 nM	Linear
	pLambdaCI-BCD2-lacI-ssrA(LAA), 1.4 nM	Linear
	pPhlF-BCD2-srpR-ssrA(LAA), 5.6 nM	Linear
	pSprR-BCD2-lambdaCI-ssrA(LAA), 11.2 nM	Linear
	pCI-Citrine(ASV), 3 nM	Plasmid
	pTetR(r)-Cerulean(ASV), 2.5 nM	Plasmid
5n1, plasmid DNA	5n1 oscillator plasmid, 5 nM	Plasmid
	pTetR(r)-Cerulean(ASV), 5 nM	Plasmid
	pLacI(r)-mCherry(ASV), 5 nM	Plasmid
	pCI-Citrine(ASV), 5 nM	Plasmid
5n2	pBetI-BCD7-QacR-ssrA(LAA), 1 nM	Linear
	pPhlF-BCD7-srpR-ssrA(LAA), 12 nM	Linear
	pQacR-BCD7-tetR-ssrA(LAA), 4 nM	Linear
	pSrpR-BCD7-BetI-ssrA(LAA), 24 nM	Linear
	pTetR-BCD7-phlF-ssrA(LAA), 4 nM	Linear
	pTetR(r)-Cerulean(ASV), 2.5 nM	Plasmid
	pQacR-BCD7-Citrine, 2.5 nM	Plasmid

Chapter 5   Conclusions and outlook

The work presented in this thesis shows that cell-free environments are powerful systems to engineer and to quantitatively and extensively characterize complex dynamic genetic networks. This section will briefly summarize the results, and discuss limitations and future steps. While the research presented here was conducted, enormous progress has been made in the field of cell-free synthetic biology, and in this section I will also compare our results and solutions with those of others.

As shown in chapter 2, we designed fluorescent binary FRET probes and a complementary mRNA target sequence to measure mRNA concentrations in the defined PURE transcription and translation system, and used them to develop a quantitative model of mRNA dynamics. As most regulators used in genetic circuits act on the initiation of transcription, it is important to be able to determine mRNA concentrations during TX-TL reactions. We used the probes we developed both in batch reactions on the plate reader and in continuous reactions in the microfluidic nano-reactor device to understand the kinetics of the TX-TL reaction, and the effects of various genetic regulators. As the probe target site is located in the 3' untranslated region of the mRNA, the target site can be used to measure the concentration of any mRNA of interest. The main limitation of our binary probes is that the detection limit for mRNA is relatively high (concentrations below 10nM become problematic). To solve this it would theoretically be possible to place multiple target sites on one mRNA to increase the signal. We have not tested the binary probes in a lysate-based TX-TL system. It is likely that the DNA oligonucleotides would need to be modified to prevent degradation by nucleases for use in cell extracts. We observed that binding kinetics can limit the temporal resolution but binding of probes to our optimized target site was sufficiently fast for the analysis of mRNA dynamics in the PURE mix. Other methods to measure mRNA concentrations in TX-TL reactions were recently developed including molecular beacons[11,112] and Spinach aptamers[113], but these techniques suffer from similar limitations for binding kinetics and detection limits.

For the successful implementation of complex dynamic networks in TX-TL reactions it is critical to maintain far-from-equilibrium conditions. As shown in chapter 3, we developed a microfluidic nano-reactor device that allows us to run continuous TX-TL reactions for over 30h with transcription and translation rates at constant steady state levels. Advantages of this system are the low volume of reagents that is needed for long experiments (about 50μl TX-TL reagents for eight simultaneous 30h experiments) and the high level of control over dilution rates and other experimental conditions our microfluidic setup allows. In this system we implemented a novel genetic oscillator, which was the first oscillating genetic network in a TX-TL reaction. This showed that dynamic genetic networks could indeed be implemented and characterized *in vitro*. The microfluidic chip we developed is very flexible. It can be used to run up to eight different experiments at the same time, for example, at different dilution rates or using different template DNAs. These parameters can also be changed over the course of an experiment, allowing us to switch DNA concentrations, add or remove inducers, and vary dilution rates over time. This flexibility somewhat limits the throughput, however, as the fluid manipulations take time and have to be integrated into a program that maintains (close to) continuous reaction

conditions. Another limitation is that both TX-TL reagents and DNA flow through the reactor. This makes it necessary to prepare rather large amounts of template DNA (either by PCR for linear templates or by extracting plasmids from *E. coli*), which is time consuming and probably as costly as the TX-TL reagents. Roy Bar-Ziv and co-workers have developed a different microfluidic device allowing continuous TX-TL reactions and the implementation of dynamic genetic networks[91]. In their device, dilution rates are "hard wired" into the chip by varying capillary lengths connecting the reaction chambers to the flow channel, and template DNA is attached to the surface, so that only TX-TL reagents need to be flowed. This simpler chip layout would allow a higher throughput but the process of attaching DNA to the chip surface is not straightforward.

Finally, in chapter 4 we demonstrate that cell-free systems can be used for rapid prototyping of dynamic genetic networks. Combining custom prepared lysate-based TX-TL reagents with steady state reaction conditions provides the opportunity to test networks in a simplified environment, which is however similar enough to *in vivo* conditions to produce relevant results. Using this cell-free framework, we were the first to show the successful implementation of a synthetic *in vivo* oscillator in an *in vitro* system. We then engineered novel 3-, 4- and 5-node cyclic negative feedback architectures using *in vitro* characterized parts and showed that the novel oscillators functioned similarly *in vivo* as in the cell-free environment. These results indicate that cell-free synthetic biology has the potential to drastically speed up design-build-test cycles in biological engineering and enable the quantitative and more complete characterization of synthetic and natural networks. The main limitation, when porting networks from the cell-free environment to *E. coli*, were toxic effects that the strongly expressing synthetic circuit imposed on the cells. It would be useful to develop a sensor that could indicate strong resource usage already in the cell-free framework. Apart from toxicity, we also observed some differences in the behavior of parts and networks between the *in vitro* and the *in vivo* system. For example, promoter expression strengths did not always compare as had been reported before[33,34]. Comparing the K_d values with the values from *in vivo* studies, we found that fold-differences were generally higher *in vitro* than *in vivo*[94,95] but the order of repressor strengths was preserved with the exception of QacR, which was a much stronger repressor *in vitro* than *in vivo*. The majority of *in vitro* and *in vivo* results, however, compared surprisingly well. It will be interesting to explore why discrepancies exist in some isolated cases, which might reveal new insights about natural *in vivo* processes. With its large volume compared to the volume of an *E. coli* cell, our reactor-based approach cannot capture stochastic processes that influence the behavior of genetic networks in cells. It is, however, also an advantage to characterize networks in a more controlled and deterministic system because results are not obscured by noise and the variability that is inevitable when working with living cells.

Further work will be necessary to determine how complex *in vitro* systems can get and whether fundamental differences to cellular systems exist. We have shown that results between *in vivo* and *in vitro* systems compare well for molecular ring oscillators. If this is true for other genetic network classes remains to be shown. For prototyping applications, it would be interesting to increase the throughput of the microfluidic chip, for example to screen large numbers of different network variants. To increase throughput, the microfluidic chip could be re-designed to include a larger number of reactors, but this would likely decrease flexibility in other experimental parameters. Also, in its current implementation our setup only allows interrogation of the reaction by fluorescent readouts. It would however be extremely interesting to couple the system with a mass-spectrometer to be able to also quantify metabolites in real-time. This would allow the analysis of dynamic metabolic networks coupled to genetic circuits. Expression of metabolic pathways could be applied to genomic mining or to develop a metabolism for an artificial cell. In fact, for artificial cell research continuous TX-TL reactions could be extremely powerful because they would allow the testing of separate

fundamental sub-processes that would have to be implemented in an artificial cell such as DNA replication and ribosome biogenesis. To conclude, cell-free, continuous reaction environments will be useful for fundamental research in characterizing genetic network architectures, artificial cell research and rapid prototyping to speed up design-build-test cycles in synthetic biology.

Bibliography

1. Gardner, T. S., Cantor, C. R. & Collins, J. J. Construction of a genetic toggle switch in Escherichia coli. *Nature* **403,** 339–342 (2000).
2. Elowitz, M. B. & Leibler, S. A synthetic oscillatory network of transcriptional regulators. *Nature* **403,** 335–338 (2000).
3. Lu, T. K., Khalil, A. S. & Collins, J. J. Next-generation synthetic gene networks. *Nat Biotechnol* **27,** 1139–1150 (2009).
4. Purnick, P. & Weiss, R. The second wave of synthetic biology: from modules to systems. *Nat Rev Mol Cell Biol* **10,** 410–422 (2009).
5. Kwok, R. Five hard truths for synthetic biology. *Nature* **463,** 288–290 (2010).
6. Loose, M., Fischer-Friedrich, E., Ries, J., Kruse, K. & Schwille, P. Spatial Regulators for Bacterial Cell Division Self-Organize into Surface Waves in Vitro. *Science* **320,** 789–792 (2008).
7. Asahara, H. & Chong, S. In vitro genetic reconstruction of bacterial transcription initiation by coupled synthesis and detection of RNA polymerase holoenzyme. *Nucleic Acids Res.* **38,** e141 (2010).
8. Shimizu, Y. *et al.* Cell-free translation reconstituted with purified components. *Nat Biotechnol* **19,** 751–755 (2001).
9. Bujara, M., Schümperli, M., Pellaux, R., Heinemann, M. & Panke, S. Optimization of a blueprint for in vitro glycolysis by metabolic real-time analysis. *Nature Chemical Biology* **7,** 271–277 (2011).
10. Karzbrun, E., Shin, J., Bar-Ziv, R. H. & Noireaux, V. Coarse-grained dynamics of protein synthesis in a cell-free system. *Phys. Rev. Lett.* **106,** 48104 (2011).
11. Stögbauer, T., Windhager, L., Zimmer, R. & Rädler, J. O. Experiment and mathematical modeling of gene expression dynamics in a cell-free system. *Integr Biol (Camb)* **4,** 494–501 (2012).
12. Kim, J. & Winfree, E. Synthetic in vitro transcriptional oscillators. *Mol Syst Biol* **7,** 1–15 (2011).
13. Montagne, K., Plasson, R., Sakai, Y., Fujii, T. & Rondelez, Y. Programming an in vitro DNA oscillator using a molecular networking strategy. *Mol Syst Biol* **7,** 1–7 (2011).
14. Padirac, A., Fujii, T., Estévez-Torres, A. & Rondelez, Y. Spatial waves in synthetic biochemical networks. *J Am Chem Soc* **135,** 14586–14592 (2013).
15. Padirac, A., Fujii, T. & Rondelez, Y. Bottom-up construction of in vitro switchable memories. *Proc Natl Acad Sci USA* **109,** E3212–E3220 (2012).
16. Isalan, M., Lemerle, C. & Serrano, L. Engineering gene networks to emulate Drosophila embryonic pattern formation. *PLoS Biol* **3,** e64 (2005).
17. Merkle, D., Kahya, N. & Schwille, P. Reconstitution and Anchoring of Cytoskeleton inside Giant Unilamellar Vesicles. *ChemBioChem* **9,** 2673–2681 (2008).
18. Osawa, M., Anderson, D. E. & Erickson, H. P. Reconstitution of Contractile FtsZ Rings in Liposomes. *Science* **320,** 792–794 (2008).
19. Keber, F. C. *et al.* Topology and dynamics of active nematic vesicles. *Science* **345,** 1135–1139 (2014).
20. Forster, A. C. & Church, G. M. Towards synthesis of a minimal cell. *Mol Syst Biol* **2,** 45 (2006).
21. Fujiwara, K., Katayama, T. & Shin-ichiro, M. N. Cooperative working of bacterial chromosome replication proteins generated by a reconstituted protein expression system. *Nucleic Acids Res.* **41,** 7176–7183 (2013).
22. Jewett, M. C., Calhoun, K. A., Voloshin, A., Wuu, J. J. & Swartz, J. R. An integrated cell-free metabolic platform for protein production and synthetic biology. *Mol Syst Biol* **4,** 220 (2008).
23. Schwille, P. & Diez, S. Synthetic biology of minimal systems. *Critical Reviews in Biochemistry and Molecular Biology* **44,** 223–242 (2009).
24. Fessner, W. & Walter, C. 'Artificial Metabolisms' for the Asymmetric One-Pot Synthesis of Branched-Chain Saccharides. *Angewandte Chemie International Edition in English* **31,** 614–616 (1992).
25. Schultheisz, H. L., Szymczyna, B. R., Scott, L. G. & Williamson, J. R. Pathway Engineered Enzymatic de NovoPurine Nucleotide Synthesis. *ACS Chem Biol* **3,** 499–511 (2008).
26. Bujara, M., Schümperli, M., Billerbeck, S., Heinemann, M. & Panke, S. Exploiting cell-free systems: Implementation and debugging of a system of biotransformations. *Biotechnology and bioengineering* **106,** 376–389 (2010).
27. Harper, A. D., Bailey, C. B., Edwards, A. D., Detelich, J. F. & Keatinge-Clay, A. T. Preparative, in Vitro

Biocatalysis of Triketide Lactone Chiral Building Blocks. *ChemBioChem* **13,** 2200–2203 (2012).

28. Loscha, K. V. *et al.* Multiple-Site Labeling of Proteins with Unnatural Amino Acids. *Angew. Chem. Int. Ed.* **51,** 2243–2246 (2012).
29. Zawada, J. F. *et al.* Microscale to manufacturing scale-up of cell-free cytokine production-a new approach for shortening protein production development timelines. *Biotechnology and bioengineering* **108,** 1570–1578 (2011).
30. Goerke, A. R. & Swartz, J. R. Development of cell-free protein synthesis platforms for disulfide bonded proteins. *Biotechnology and bioengineering* **99,** 351–367 (2007).
31. Woodrow, K. A. & Swartz, J. R. A sequential expression system for high-throughput functional genomic analysis. *Proteomics* **7,** 3870–3879 (2007).
32. Lui, B. H., Cochran, J. R. & Swartz, J. R. Discovery of Improved EGF Agonists Using a Novel In Vitro Screening Platform. *J Mol Biol* **413,** 406–415 (2011).
33. Sun, Z. Z., Yeung, E., Hayes, C. A., Noireaux, V. & Murray, R. M. Linear DNA for rapid prototyping of synthetic biological circuits in an Escherichia coli based TX-TL cell-free system. *ACS Synth. Biol.* **3,** 387–397 (2013).
34. Chappell, J., Jensen, K. & Freemont, P. S. Validation of an entirely in vitro approach for rapid prototyping of DNA regulatory elements for synthetic biology. *Nucleic Acids Res.* **41,** 3471–3481 (2013).
35. Karig, D. K., Iyer, S., Simpson, M. L. & Doktycz, M. J. Expression optimization and synthetic gene networks in cell-free systems. *Nucleic Acids Res.* **40,** 3763–3774 (2012).
36. Burrill, D. R. & Silver, P. A. Making Cellular Memories. *Cell* **140,** 13–18 (2010).
37. Kim, J., Khetarpal, I., Sen, S. & Murray, R. M. Synthetic circuit for exact adaptation and fold-change detection. *Nucleic Acids Res.* **42,** 6078–6089 (2014).
38. Zadorin, A. S., Rondelez, Y., Galas, J.-C. & Estévez-Torres, A. Synthesis of Programmable Reaction-Diffusion Fronts Using DNA Catalyzers. *Phys. Rev. Lett.* **114,** 068301 (2015).
39. Novák, B. & Tyson, J. J. Design principles of biochemical oscillators. *Nat Rev Mol Cell Biol* **9,** 981–991 (2008).
40. Franco, E. *et al.* Timing molecular motion and production with a synthetic transcriptional clock. *Proceedings of the National Academy of Sciences* **108,** E784–93 (2011).
41. Kim, J., White, K. S. & Winfree, E. Construction of an in vitro bistable circuit from synthetic transcriptional switches. *Mol Syst Biol* **2,** 68 (2006).
42. Baccouche, A., Montagne, K., Padirac, A., Fujii, T. & Rondelez, Y. Dynamic DNA-toolbox reaction circuits: A walkthrough. *Methods* 1–16 (2014). doi:10.1016/j.ymeth.2014.01.015
43. Katzen, F., Chang, G. & Kudlicki, W. The past, present and future of cell-free protein synthesis. *Trends Biotechnol* **23,** 150–156 (2005).
44. Shin, J. & Noireaux, V. Efficient cell-free expression with the endogenous E. Coli RNA polymerase and sigma factor 70. *J. Biol. Eng.* **4,** 8 (2010).
45. Shin, J. & Noireaux, V. An E. coli cell-free expression toolbox: application to synthetic gene circuits and artificial cells. *ACS Synth. Biol.* **1,** 29–41 (2012).
46. Noireaux, V., Bar-Ziv, R. & Libchaber, A. Principles of cell-free genetic circuit assembly. *Proc Natl Acad Sci USA* **100,** 12672–12677 (2003).
47. Ishikawa, K., Sato, K., Shima, Y., Urabe, I. & Yomo, T. Expression of a cascading genetic network within liposomes. *FEBS Lett* **576,** 387–390 (2004).
48. Xie, Z., Liu, S. J., Bleris, L. & Benenson, Y. Logic integration of mRNA signals by an RNAi-based molecular computer. *Nucleic Acids Res.* **38,** 2692–2701 (2010).
49. Davidson, E. A., Meyer, A. J., Ellefson, J. W., Levy, M. & Ellington, A. D. An in vitro Autogene. *ACS Synth. Biol.* **1,** 190–196 (2012).
50. Shin, J. & Noireaux, V. Study of messenger RNA inactivation and protein degradation in an Escherichia coli cell-free expression system. *J. Biol. Eng.* **4,** 9 (2010).
51. Spirin, A. S., Baranov, V. I., Ryabova, L. A., Ovodov, S. Y. & Alakhov, Y. B. A continuous cell-free translation system capable of producing polypeptides in high yield. *Science* **242,** 1162–1164 (1988).
52. Spirin, A. S. High-throughput cell-free systems for synthesis of functionally active proteins. *Trends Biotechnol* **22,** 538–545 (2004).
53. Khnouf, R., Beebe, D. J. & Fan, Z. H. Cell-free protein expression in a microchannel array with passive pumping. *Lab Chip* **9,** 56 (2009).
54. Siuti, P., Retterer, S. T. & Doktycz, M. J. Continuous protein production in nanoporous, picolitre volume containers. *Lab Chip* **11,** 3523–3529 (2011).
55. Noireaux, V. & Libchaber, A. A vesicle bioreactor as a step toward an artificial cell assembly. *Proc Natl Acad Sci USA* **101,** 17669–17674 (2004).
56. Shin, J., Jardine, P. & Noireaux, V. Genome Replication, Synthesis, and Assembly of the Bacteriophage T7 in a Single Cell-Free Reaction. *ACS Synth. Biol.* **1,** 408–413 (2012).
57. Maeda, Y. T. *et al.* Assembly of MreB Filaments on Liposome Membranes: A Synthetic Biology Approach.

ACS Synth. Biol. **1,** 53–59 (2011).

58.   Paige, J. S., Wu, K. Y. & Jaffrey, S. R. RNA Mimics of Green Fluorescent Protein. *Science* **333,** 642–646 (2011).

59.   Didenko, V. V. DNA probes using fluorescence resonance energy transfer (FRET): designs and applications. *Biotechniques* **31,** 1106–1121 (2001).

60.   Marras, S. A. E., Tyagi, S. & Kramer, F. R. Real-time assays with molecular beacons and other fluorescent nucleic acid hybridization probes. *Clin Chim Acta* **363,** 48–60 (2006).

61.   Sei-Iida, Y., Koshimoto, H., Kondo, S. & Tsuji, A. Real-time monitoring of in vitro transcriptional RNA synthesis using fluorescence resonance energy transfer. *Nucleic Acids Res.* **28,** e59 (2000).

62.   Tsourkas, A., Behlke, M. A., Xu, Y. & Bao, G. Spectroscopic features of dual fluorescence/luminescence resonance energy-transfer molecular beacons. *Anal. Chem.* **75,** 3697–3703 (2003).

63.   Calhoun, K. A. & Swartz, J. R. Energy systems for ATP regeneration in cell-free protein synthesis reactions. *Methods Mol. Biol.* **375,** 3–17 (2007).

64.   Yao, C., Luo, J., Hsiao, C.-H. C., Donelson, J. E. & Wilson, M. E. Leishmania chagasi: a tetracycline-inducible cell line driven by T7 RNA polymerase. *Exp. Parasitol.* **116,** 205–213 (2007).

65.   Kamionka, A., Bogdanska-Urbaniak, J., Scholz, O. & Hillen, W. Two mutations in the tetracycline repressor change the inducer anhydrotetracycline to a corepressor. *Nucleic Acids Res.* **32,** 842–847 (2004).

66.   Lopez, P. J., Guillerez, J., Sousa, R. & Dreyfus, M. On the mechanism of inhibition of phage T7 RNA polymerase by lac repressor. *J Mol Biol* **276,** 861–875 (1998).

67.   Dubendorff, J. W. & Studier, F. W. Controlling basal expression in an inducible T7 expression system by blocking the target T7 promoter with lac repressor. *J Mol Biol* **219,** 45–59 (1991).

68.   Giordano, T. J., Deuschle, U., Bujard, H. & McAllister, W. T. Regulation of coliphage T3 and T7 RNA polymerases by the lac repressor-operator system. *Gene* **84,** 209–219 (1989).

69.   Geertz, M., Rockel, S. & Maerkl, S. J. A high-throughput microfluidic method for generating and characterizing transcription factor mutant libraries. *Methods Mol. Biol.* **813,** 107–123 (2012).

70.   Sheff, M. A. & Thorn, K. S. Optimized cassettes for fluorescent protein tagging in Saccharomyces cerevisiae. *Yeast* **21,** 661–670 (2004).

71.   Zuker, M. Mfold web server for nucleic acid folding and hybridization prediction. *Nucleic Acids Res.* **31,** 3406–3415 (2003).

72.   Aranda, P. S., LaJoie, D. M. & Jorcyk, C. L. Bleach gel: a simple agarose gel for analyzing RNA quality. *Electrophoresis* **33,** 366–369 (2012).

73.   Hansen, C. L., Sommer, M. O. A. & Quake, S. R. Systematic investigation of protein phase behavior with a microfluidic formulator. *Proc Natl Acad Sci USA* **101,** 14431–14436 (2004).

74.   Ridgeway, W. K., Seitaridou, E., Phillips, R. & Williamson, J. R. RNA-protein binding kinetics in an automated microfluidic reactor. *Nucleic Acids Res.* **37,** e142–e142 (2009).

75.   Galas, J.-C., Haghiri-Gosnet, A.-M. & Estévez-Torres, A. A nanoliter-scale open chemical reactor. *Lab Chip* **13,** 415–423 (2013).

76.   Niederholtmeyer, H., Xu, L. & Maerkl, S. J. Real-Time mRNA Measurement during an in Vitro Transcription and Translation Reaction Using Binary Probes. *ACS Synth. Biol.* **2,** 411–417 (2012).

77.   Isaacs, F. J. *et al.* Engineered riboregulators enable post-transcriptional control of gene expression. *Nat Biotechnol* **22,** 841–847 (2004).

78.   Anderson, J. C., Voigt, C. A. & Arkin, A. P. Environmental signal integration by a modular AND gate. *Mol Syst Biol* **3,** 133 (2007).

79.   Banecki, B., Wawrzynow, A., Puzewicz, J., Georgopoulos, C. & Zylicz, M. Structure-function analysis of the zinc-binding region of the Clpx molecular chaperone. *J. Biol. Chem.* **276,** 18843–18848 (2001).

80.   Stricker, J. *et al.* A fast, robust and tunable synthetic gene oscillator. *Nature* **456,** 516–519 (2008).

81.   Heyman, Y., Buxboim, A., Wolf, S. G., Daube, S. S. & Bar-Ziv, R. H. Cell-free protein synthesis and assembly on a biochip. *Nature Nanotechnology* **7,** 374–378 (2012).

82.   Mendell, J. E., Clements, K. D., Choat, J. H. & Angert, E. R. Extreme polyploidy in a large bacterium. *Proc Natl Acad Sci USA* **105,** 6730–6734 (2008).

83.   Karig, D. K., Jung, S.-Y., Srijanto, B., Collier, C. P. & Simpson, M. L. Probing cell-free gene expression noise in femtoliter volumes. *ACS Synth. Biol.* **2,** 497–505 (2013).

84.   Thorsen, T., Maerkl, S. J. & Quake, S. R. Microfluidic large-scale integration. *Science* **298,** 580–584 (2002).

85.   Garcia-Cordero, J. L., Nembrini, C., Stano, A., Hubbell, J. A. & Maerkl, S. J. A high-throughput nanoimmunoassay chip applied to large-scale vaccine adjuvant screening. *Integr Biol (Camb)* **5,** 650–658 (2013).

86.   Rockel, S., Geertz, M., Hens, K., Deplancke, B. & Maerkl, S. J. iSLIM: a comprehensive approach to mapping and characterizing gene regulatory networks. *Nucleic Acids Res.* **41,** e52 (2013).

87.   Tian, J. *et al.* Accurate multiplex gene synthesis from programmable DNA microchips. *Nature* **432,** 1050–1054 (2004).

88.   Unger, M. A., Chou, H. P., Thorsen, T., Scherer, A. & Quake, S. R. Monolithic microfabricated valves and

89.   Andersen, J. B. *et al.* New unstable variants of green fluorescent protein for studies of transient gene expression in bacteria. *Appl Environ Microbiol* **64,** 2240–2246 (1998).

90.   Niederholtmeyer, H., Stepanova, V. & Maerkl, S. J. Implementation of cell-free biological networks at steady state. *Proceedings of the National Academy of Sciences* **110,** 15985–15990 (2013).

91.   Karzbrun, E., Tayar, A. M., Noireaux, V. & Bar-Ziv, R. H. Programmable on-chip DNA compartments as artificial cells. *Science* **345,** 829–832 (2014).

92.   Shin, J. & Noireaux, V. An E. coliCell-Free Expression Toolbox: Application to Synthetic Gene Circuits and Artificial Cells. *ACS Synth. Biol.* **1,** 29–41 (2012).

93.   Sun, Z. Z. *et al.* Protocols for implementing an Escherichia coli based TX-TL cell-free expression system for synthetic biology. *J Vis Exp* e50762 (2013). doi:10.3791/50762

94.   Rosenfeld, N., Young, J., Alon, U., Swain, P. & Elowitz, M. Gene Regulation at the Single-Cell Level. *Science* **307,** 1962–1965 (2005).

95.   Stanton, B. C. *et al.* Genomic mining of prokaryotic repressors for orthogonal logic gates. *Nature Chemical Biology* **10,** 99–105 (2014).

96.   Cookson, N. A. *et al.* Queueing up for enzymatic processing: correlated signaling through coupled degradation. *Mol Syst Biol* **7,** 561 (2011).

97.   Prindle, A. *et al.* Rapid and tunable post-translational coupling of genetic circuits. *Nature* **508,** 387–391 (2014).

98.   Smith, H. Oscillations and multiple steady states in a cyclic gene model with repression. *Journal of mathematical biology* **25,** 169–190 (1987).

99.   Hori, Y., Takada, M. & Hara, S. Biochemical oscillations in delayed negative cyclic feedback: Existence and profiles. *Automatica* **49,** 2581–2590 (2013).

100.   Wang, P. *et al.* Robust Growth of Escherichia coli. *Current Biology* **20,** 1099–1103 (2010).

101.   Ceroni, F., Algar, R., Stan, G.-B. & Ellis, T. Quantifying cellular capacity identifies gene expression designs with reduced burden. *Nat Meth* (2015). doi:10.1038/nmeth.3339

102.   Danino, T., Mondragón-Palomino, O., Tsimring, L. & Hasty, J. A synchronized quorum of genetic clocks. *Nature* **463,** 326–330 (2010).

103.   Prindle, A. *et al.* A sensing array of radically coupled genetic 'biopixels'. *Nature* **481,** 39–44 (2011).

104.   Kiviet, D. J. *et al.* nature13582. *Nature* **514,** 376–379 (2014).

105.   Casini, A. *et al.* R2oDNA Designer: Computational Design of Biologically Neutral Synthetic DNA Sequences. *ACS Synth. Biol.* **3,** 525–528 (2014).

106.   Fitzwater, T., Zhang, X. Y., Elble, R. & Polisky, B. Conditional high copy number ColE1 mutants: resistance to RNA1 inhibition in vivo and in vitro. *The EMBO Journal* **7,** 3289 (1988).

107.   Mutalik, V. K. *et al.* Precise and reliable gene expression via standard transcription and translation initiation elements. *Nat Meth* **10,** 354–360 (2013).

108.   Preibisch, S., Saalfeld, S. & Tomancak, P. Globally optimal stitching of tiled 3D microscopic image acquisitions. *Bioinformatics* **25,** 1463–1465 (2009).

109.   Schindelin, J. *et al.* Fiji: an open-source platform for biological-image analysis. **9,** 676–682 (2012).

110.   Hori, Y., Kim, T.-H. & Hara, S. Existence criteria of periodic oscillations in cyclic gene regulatory networks. *Automatica* **47,** 1203–1209 (2011).

111.   Lutz, R. & Bujard, H. Independent and tight regulation of transcriptional units in Escherichia coli via the LacR/O, the TetR/O and AraC/I1-I2 regulatory elements. *Nucleic Acids Res.* **25,** 1203–1210 (1997).

112.   Sokolova, E. *et al.* Enhanced transcription rates in membrane-free protocells formed by coacervation of cell lysate. *Proc Natl Acad Sci USA* **110,** 11692–11697 (2013).

113.   van Nies, P. *et al.* Unbiased Tracking of the Progression of mRNA and Protein Synthesis in Bulk and in Liposome-Confined Reactions. *ChemBioChem* **14,** 1963–1966 (2013).

pumps by multilayer soft lithography. *Science* **288,** 113–116 (2000).

Curriculum vitae

Henrike Niederholtmeyer

EDUCATION

- **Ph.D., Biotechnology and Bioengineering**, École Polytechnique Fédérale de Lausanne, Switzerland (May 2015).

- **M.Sc., Biotechnology**, Westfälische Wilhelms-Universität Münster, Germany (1/2010).

- **B.Sc., Biology**, Westfälische Wilhelms-Universität Münster, Germany (9/2007).

RESEARCH EXPERIENCE

- **Department of Bioengineering, EPF Lausanne, Switzerland.**
  Doctoral assistant, April 2010 – present.
  Advisor: Dr. Sebastian Maerkl.
  PhD thesis: Implementation and Characterization of Dynamic Genetic Networks in Vitro.

    - Developed a microfluidic platform to perform in vitro transcription and translation reactions in miniaturized flow-reactors allowing synthesis at steady state.

    - Engineered and implemented various genetic networks (mainly oscillators).

- **Department of Systems Biology, Harvard Medical School, USA.**
  Visiting Masters student, January 2009 – December 2009.
  Advisor: Dr. Pamela Silver.
  Masters thesis: Synthetic Biology Approaches to Metabolic Engineering.

    - Engineered cyanobacteria to secrete sugars.

    - Worked on synthetic symbiosis engineering cyanobacteria to become artificial chloroplasts in vertebrate cells.

- **Institute of Microbiology, University of Münster, Germany.**
  Undergraduate researcher, March 2007 – August 2007.
  Advisor: Dr. Volker Wendisch.
  Bachelor thesis: Experimental characterization of the polyphosphate metabolism in *Corynebacterium glutamicum* – Role of the putative polyphosphate dependent NAD kinase PPNK.

    - Purified enzyme and characterized enzyme activity.

    - Molecular biology in *Corynebacterium glutamicum*.

AWARDS AND SCHOLARSHIPS

- Best Poster Prize, "New Frontiers in Synthetic Life" meeting at Radboud University Nijmegen, The Netherlands (11/2013).

- Fellowship for studies in the US, German National Academic Foundation (1/2009 -12/2009).

- Scholar of the German National Academic Foundation (10/2007 – 1/2010).

PUBLICATIONS AND PATENTS

1. Niederholtmeyer H*, Sun ZZ*, Hori Y, Yeung E, Verpoorte A, Murray RM, and Maerkl SJ. (2015) A cell-free framework for biological systems engineering. **bioRxiv**, 018317.

2. Niederholtmeyer H, Stepanova V, and Maerkl SJ (2013). Implementation of cell-free biological networks at steady state. **Proceedings of the National Academy of Sciences** 110, 15985–15990.

3. Niederholtmeyer H, Xu L, and Maerkl SJ (2012). Real-Time mRNA Measurement during an in Vitro Transcription and Translation Reaction Using Binary Probes. **ACS Synthetic Biology** 2, 411–417.

4. Bonacci W, Teng PK, Afonso B, Niederholtmeyer H, Grob P, Silver PA, and Savage DF (2012) Modularity of a carbon-fixing protein organelle. **Proceedings of the National Academy of Sciences** 109, 478–483.

5. Agapakis CM, Niederholtmeyer H, Noche RR, Lieberman TD, Megason SG, Way JC, and Silver PA (2011). Towards a synthetic chloroplast. **PLoS ONE** 6, e18877.

6. Niederholtmeyer H*, Wolfstädter BT*, Savage DF, Silver PA, and Way JC (2010). Engineering cyanobacteria to synthesize and export hydrophilic products. **Applied and Environmental Microbiology** 76, 3462–3466.

7. Lindner SN*, Niederholtmeyer H*, Schmitz K, Schoberth SM, and Wendisch VF (2010). Polyphosphate/ATP-dependent NAD kinase of Corynebacterium glutamicum: biochemical properties and impact of ppnK overexpression on lysine production. **Applied Microbiology and Biotechnology** 87, 583–593.

8. Way JC, Niederholtmeyer H, and Wolfstaedter B. "Production of Secreted Bioproducts from Photosynthetic Microbes". **WO Patent** 2,011,029,013. **EP Patent** 2,473,597.

*Contributed equally.